2002

Ground State Properties of Newly Discovered Superconductor :MgB2 : an ab initio Hartree-Fock,and Density Functional Studies

Islam, Mr.Fakir Nazrul

University of Rajshahi

GROUND STATE PROPERTIES OF NEWLY DISCOVERED SUPERCONDUCTOR MgB_2 : AN *AB INITIO* HARTREE-FOCK AND DENSITY FUNCTIONAL STUDIES

A Dissertation
Submitted to the University of Rajshahi in Fulfilment of the Requirements for the Degree of Doctor of Philosophy

in
Physics

By
Fakir Nazrul Islam
B.Sc. (Honours), M.Sc.(Thesis)

May 2002

Condensed Matter Physics Laboratory
Department of Physics
University of Rajshahi, Rajshahi
BANGLADESH

Dedicated to my beloved
Daughter
Nazifa Ifrit Islam

Declaration

I do hereby declare that the entire research work embodied in this thesis entitled "Ground State Properties of Newly Discovered Superconductor MgB_2 : an ab initio Hartree-Fock and Density Functional Studies", submitted to the University of Rajshahi, Rajshahi, Bangladesh, for the degree of Doctor of Philosophy, is the result of my own investigations. No part of this research work in any form has been submitted to any other University or Institution for any degree or award.

Candidate

14.05.02

(Fakir Nazrul Islam)
Assistant Professor, Department of Physics
University of Rajshahi, Rajshahi 6205
Bangladesh

Prof. A K M Azharul Islam
Ph.D(Lond), D.I.C (Lond), C.Phys.
Former Chairman, Dept. of Physics
Former Dean, Faculty of Science
Fellow, Bangladesh Academy of Sciences
Fellow, Institute of Physics (London)

Tel: +88 0721 750980 (Res)
Fax: +88 0721 750064 (off)
e-mail: azharislam46@yahoo.com
Department of Physics
Rajshahi University
Rajshahi 6205, Bangladesh

Certificate

I hereby certify that the thesis entitled "Ground State Properties of Newly Discovered Superconductor MgB_2 : an ab initio Hartree-Fock and Density Functional Studies", submitted by Mr. Fakir Nazrul Islam, Assistant Professor, Department of Physics, University of Rajshahi, Rajshahi, Bangladesh, has been completed under my direct supervision. This is a bona fide record of the research carried out by the candidate.

To the best of my knowledge, this thesis has not been submitted for the award of any degree or award elsewhere.

Supervisor

১৪.৫.২০০২

(A K M Azharul Islam)

ACKNOWLEDGEMENT

First of all, I express my gratefulness to Almighty Allah for successful completion of this Ph.D. research work.

I express my sincerest gratitude to my honorable supervisor Professor A K M Azharul Islam, Department of Physics, University of Rajshahi, Bangladesh, for his constant direction, constructive criticism and inspiration in pursuing the whole investigations of the present study. Words are always insufficient to express his working capacities and unending enthusiasm for scientific rigorousness for innovative investigations. This always becomes the everlasting source of inspiration for his students.

I wish to thanks Professor Shamsunnar Islam, Chairman, Department of Physics, University of Rajshahi, for her support in different phases of academic and administrative affairs related to this work.

I like to express my gratitude to Professor M. Nazrul Islam for his cooperation and valuable suggestions for my study.

It is a pleasure for me to extend my thanks to the members of our Condensed Matter Physics Research Group, Professor M. Enamul Haque, Associate Professor Md. Abdul Wahed and Mr. Rezaul Islam Molla for their cooperation and positive attitude to create a research environment in the Laboratory.

I must extend my appreciation and special thanks to Mr. M. Rezaul Islam, Associate Professor, Department of Applied Physics, University of Rajshahi, for his help and advice regarding computer programming.

I express my sincere thanks to all of my teachers and colleagues for their encouragement to complete my work. I also gratefully acknowledge the wishes of my relatives, well-wishers and innumerable friends.

I will be ever grateful to my wife Shakila Islam and my only daughter Nazifa Ifrit for their sacrifice, encouragement and inspiration for me over the years spent on this research work. My debt to them can never be compensated.

The Author

Fakir Nazrul Islam

ABSTRACT

The ground state properties of magnesium diboride (MgB_2), a binary compound known since 1950s but very recently discovered as a superconductor, are investigated in the present study. We use here *ab initio* Hartree-Fock Linear Combination of Atomic Orbitals (HF-LCAO) method. Hartree-Fock (HF) and density functional theory (DFT) options of the method have been applied for the study of energy, elastic constants, bulk modulus, band structure, density of states (DOS) and electric field gradient (EFG) for MgB_2 both in equilibrium and under pressure. The zero pressure bulk modulus, pressure derivative of bulk modulus and their in- and out-of-plane linear values are calculated and analyzed. The analysis of the evaluated parameters reveals the diversity in bonding interactions. The diboride is found to be characterized by moderately sizable anisotropy of compressibilities, which is smaller than cuprates, but larger than many other related diborides. The anisotropic compression is expected to induce different pressure effects on different phonon modes and also to influence the electronic structure at Fermi energy.

The five different elastic constants of the new superconducting MgB_2 are calculated by *ab initio* method using a DFT Hamiltonian with both correlation and exchange potentials. The results are compared with those from a recent FPLMTO calculation. The fully relaxed and isotropic bulk moduli are also estimated and the implication of their comparison is made, e.g., MgB_2 is less anisotropic than one would otherwise suppose on the basis of its 'planar' crystal structure.

The electronic band structure and electric field gradient (EFG) for MgB_2 are also studied here as a function of pressure. The band structure calculations are in good agreement with other recent calculations. The superconductivity in MgB_2 is related to and dominated by the existence of boron σ $p_{x,y}$-band holes at the Γ-point, with negligible contribution from the Mg ions. The character of the σ band is unchanged even after application of pressure, although there is a shift of position and an increase of dispersion. The calculated density of states decreases with pressure that, in conjunction with the Bardeen-Cooper-Schrieffer (BCS) theory, agrees with the trend of the experimental T_c versus pressure data. The broad bump in $T_c(P)$ data observed by Tissen et al. near 9 GPa is not indicated in the present band structure study. The EFG at B site is nearly constant as a function of pressure and that of Mg changes by ~ 34% over the pressure range considered. The present result indicates that the B electronic system does not change much under pressure up to ~38 GPa which confirms one reported study but disagrees with the other.

Ph.D. Thesis Title:

Ground State Properties of Newly Discovered Superconductor MgB_2: an *ab initio* Hartree-Fock and Density Functional Studies

CONTENTS

CHAPTER 3

BASIS-SETS FOR MgB_2 13-19

CHAPTER 4

METHODS OF CALCULATION 20-45

LIST OF PUBLICATIONS FROM THE PRESENT Ph.D. WORK

No.	Title of the Article	Journal
1.	**F N Islam,** A K M A Islam and M N Islam; Electronic structure and electric field gradient in superconducting MgB2 under pressure: an *ab initio* study.	J. Phys.: Condens. Matter, **13** (2001) 11661-11667
2.	A K M A Islam and **F N Islam**; *Ab Initio* Investigation of Elastic Constants of Superconducting MgB_2.	Physica C **363** (2001) 189-193.
3.	A K M A Islam, **F N Islam** and S Kabir; *Ab Initio* Investigation of Mechanical Behaviour of MgB_2 Superconductor under Pressure.	J. Phys.: Condens. Matter. **13** (2001) L641-L645.
4.	A K M A Islam and **F N Islam**; Properties of Newly Discovered MgB_2 Superconductor under Pressure.	Physica B (2002) *in press.*

LIST OF FIGURES

Figure Captions	**Page No.**

LIST OF TABLES

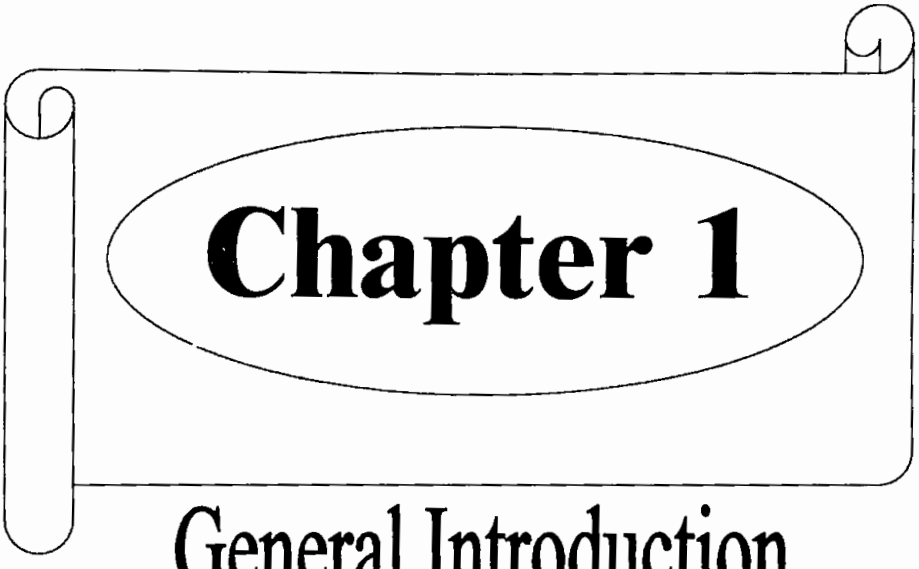

Chapter 1

General Introduction

CHAPTER 1

GENERAL INTRODUCTION

Magnesium diboride (MgB_2) is a binary compound. It is now known as a material with very simple crystal structure, high T_c=40K, large coherence length (ξ), high critical current density (J_c) and critical fields. The more current a superconductor can carry at a certain temperature, the greater its potential for everyday use. Many high temperature superconductors are complex metal oxides, which behave like ceramic – they are granular and brittle. It is therefore difficult to send current through these types of wires. The grain boundaries are weak connections for the electric current and hinder practical application. With MgB_2, the grain boundaries do not form weak connections. The material (MgB_2) gets another problem out of the way common to many superconductors – it is not that sensitive to an applied magnetic field. So, it has become a material of high potential for large-scale applications. The present study was under taken from the early stage when the material has just been discovered as a superconducting material. Since magnesium diboride is known since 1950s, but the recent discovery of superconductivity in January, 2001 at a much higher T_c=40K [1,2] in this non-cuprate intermetallic compound has triggered tremendous research interest in the structural and electronic properties of the material. A variety of experimental [3-15] and theoretical [16-35] research has been carried out till date to understand the structural, elastic and electronic properties and to determine the underlying mechanism of superconductivity in MgB_2. A few of these works involve both theoretical and experimental studies.

On 10th January 2001, Akimitsu's research group reported the superconductivity of MgB_2 at a conference entitled 'Symposium on Transition Metal Oxides, 2001' in Sendai, Japan [2]. This latest achievement of the critical temperature (T_c) in MgB_2 has drawn a remarkable attention of the international scientific community towards investigations into it or similar binary compounds for searching more new properties or thrilling information which will further accelerate the scientists to open up a new horizon in the sky of superconductivity. As a result, a lot of theoretical ideas and experimental data are being accumulated very rapidly.

The condensed matter physics community has actually been surprised with curiosity and enthusiasm by the sudden announcement of the discovery of MgB_2 superconductor (10th January 2001) after 15 years of the discovery of superconductivity in cuprates. During this long period (15 years) the scientists of this field tried their best to unfold many non-conventional features of superconductivity in the cuprates. Unfortunately, so far no fundamental and generally agreed upon understanding of the mechanism leading to the superconductivity of cuprates has been achieved. The only feature, which is generally agreed upon, is that high T_c cuprates are not conventional BCS-electron-phonon driven superconductors [21]. The discovery of superconductivity in MgB_2 has given an opportunity to the scientists to rethink and to make real progress in the understanding of superconductivity. The material possesses a hexagonal crystal structure. One thus expects anisotropy in its physical properties.

After the Sendai declaration, enormous research works on MgB_2 have been carried out among many research groups of the world to unfold the mystery

of origin of the superconducting mechanism in MgB_2. The present [16-20] and other studies [3-15, 21-35] using various methods are very important way of forecasting the unrevealed properties or new superconducting mechanism of this burning materials or similar other compounds. These researches no doubt did a lot in the field of the superconductivity. We emphasized on those properties of MgB_2, which were totally left out or lightly touched by aforesaid studies. Thus our present investigations on MgB_2 are one of such attempts to fill up these gaps and to keep some contributions to the progress of the latest development.

The present thesis is organized as the following chapters: The first chapter is general introductory, stressing the special need to carry out research on MgB_2 superconducting material. The second chapter is devoted to a description of the crystal structure of the superconductor under present study. The third chapter deals with the basis sets. Chapter four describes the methods of calculation used to study of MgB_2. Chapter five contains the results of various investigations of the study and a brief discussion of the research findings. A summary of the present investigation is illustrated in chapter six.

In appendix-A, a list of acronyms is presented while appendix-B lists the published research articles in different International Journals from the present Ph.D. work.

Chapter 2

Crystal Structure of MgB_2

CHAPTER 2

CRYSTAL STRUCTURE OF MgB_2

2.1 Introduction

The crystal structure of MgB_2 is described in the present chapter. The structural geometry of the superconducting MgB_2 crystal is illustrated with figures in two and three dimensions. The aim of this chapter is to give a transparent and appropriate understanding of the structure of MgB_2 superconductor. The coordination number and the relative positions of the constituent atoms are also pointed out in the study. A comparison of these parameters (calculated in the present study) with other available theoretical and experimental data are given on chapter 5.

2.2 The Crystal Structure

The discovery of superconductivity in magnesium diboride has initiated a lot of research activities on MgB_2. Magnesium diboride is the first binary compound found to occupy an intermediate place between low- and high-temperature superconductors [36]. It has a very simple hexagonal closed packed crystal structure. It is very similar to graphite both crystallographically and electronically. The boron atoms are arranged in layers with layers of Mg interleaved between them (Figure 2.2). The structure of each boron layer is the same as that of a graphite structure. Thus MgB_2 is composed of two layers of boron and magnesium along the c axis in the hexagonal structure (Figures 2.3 and 2.4).

In the chemical point of view, the electronic charge transfer takes place between magnesium and boron atoms when they form MgB_2 crystal according to the following rule. Although this point will be discussed later on there is nearly complete 2e charge transfer from Mg to the boron sub system: $MgB_2 \equiv Mg^{++} (B^-)_2$. Each boron acquires one electron and hence acquires the electron configuration of a carbon atom [22],

$$B^-(2s^2p^2) \equiv C(2s^2sp^2)$$

Thus the B- sheets are electronically like graphite sheets.

The interlayer interaction in this diboride is strong even though the Mg layers alternate with the B layers in its crystal structure. The boron (B) atoms lie on the corners of hexagons with three nearest neighbour B atoms in each plane while the magnesium (Mg) atoms are situated in the centers of each boron hexagon, but midway between adjacent boron layers (Figures 2.3 and 2.4). In the crystal structure of MgB_2 the hexagonal Mg layers and plane graphite like sheets of B are staked in the order . . . MgBMgB . . . [37-41]. It has the structure similar to AlB_2. Figure 2.1 shows the two dimensional crystal structure of MgB_2 while figures 2.2, 2.3 and 2.4 display its three dimensional structure. In all of these figures, the large spheres represent the magnesium and small spheres represent the boron atoms. According to International Hermann-Mauguin symbolism the space group of magnesium diboride is P6/mmm. The corresponding sequential number of the space group is 191. The structural arrangement of MgB_2 can also be described as the alternate stacking of planes of boron atoms forming a honeycomb lattice and planes of magnesium atoms forming a triangular one [42]. Each Mg atom is at the center of a hexagonal prism made of boron atoms.

2.2.1 Lattice Parameter

The crystallographic axes **a**, **b** and **c** of any crystal system drawn from one of the lattice points determine the size and shape of a unit cell. The angles α, β and γ denote the angles between the vectors **b** and **c**, **c** and **a**, and **a** and **b**, respectively. The lengths a, b and c and angles α, β and γ are collectively known as **lattice parameters** or **lattice constants** of the unit cell. In MgB_2 the lattice parameter a = b and the angles $\alpha = \beta = 90^0$ and $\gamma = 120^0$. The experimental values of the lattice parameters of MgB_2 are, a = 3.086 Å and c = 3.524 Å [1]. The ratio c/a of the lattice parameter is 1.1419. For other binary compounds or diborides the values of c/a are found to be different to a significant extent [36].

2.2.2 Coordination Numbers and Polyhedra

The coordination number (C.N.) and the coordination polyhedra serve to characterize the immediate surroundings of an atom. The coordination number specifies the number of coordinated atoms; these are the closest neighbouring atoms [43]. The Mg atoms have twelve nearest neighbours B atoms at a distance of 2.510 Å, six nearest neighbours in plane Mg atoms at 3.089 Å. On the other hand, the B atoms have six nearest neighbours Mg atoms at a distance of 2.510 Å and three nearest neighbours in plane B atoms at 1.783 Å. The coordination numbers are shown in figures 2.3 and 2.4. There is one formula unit per primitive cell [44]. The coordination polyhedron results when the centers of mutually adjacent coordinated atoms are connected with one another. For every coordination number typical coordination polyhedra exist. The coordination polyhedra of Mg atoms and that of B atoms are $[MgB_{12}Mg_8]$ and $[BMg_6B_3]$, respectively (Figure 2.4).

2.3 Primitive Cell

A primitive cell is a type of cell or unit cell having minimum volume. There are many ways of choosing unit or primitive cell for a given crystal system. The number of atoms per unit cell must be the same for a particular crystal structure i.e. the number of atoms in a unit cell is independent of the process by which the unit cell is chosen. By repetition of the unit cell with suitable symmetry operations the full structure of the crystal can be obtained. Thus we can define unit cell as the fundamental structural unit or building block of the crystal. A unit cell is marked in the crystal structure of MgB_2 in figure 2.4, wherein all the atom positions in the crystal can be generated by translations of the unit cell integral distances along each of its edges. The unit cell of MgB_2 has three atoms – two borons (2B) and one magnesium (1Mg) atoms. Each unit cell contains a total of 22 electrons. The number of symmetry operators for MgB_2 crystal system is 24. The positions of atoms in the unit cell are: Mg atom is at (0,0,0) and the 2B atoms are at (1/3,2/3,1/2) and (2/3,1/3,1/2). Each boron atom here is equidistance from three other boron atoms. The unit cell parameters of MgB_2 and of some other isostructural phases MX_2 ($CaGa_2$, $ZrBe_2$, $HfBe_2$, AgB_2, AuB_2) are shown in Table 2.1.

Table 2.1. The unit cell parameters of MgB_2 and of some other isostructural phases MX_2.

Compound (TMB_2)	Calc./ Expt. a(Å)	Calc./ Expt. c(Å)	Volume (Å^3)	TM-B (Å)	B-B (Å)	Reference
MgB_2	3.0889	3.5337	29.199	2.510	1.783	Present
	3.086	3.524	29.064	2.504	1.781	[1, 30]
TiB_2	3.070	3.262	26.625	2.409	1.773	
	3.038	3.220	25.737	-	-	
VB_2	2.983	3.047	23.481	2.297	1.722	
	2.998	3.056	23.787	-	-	
CrB_2	2.949	3.045	22.933	2.284	1.703	
	2.969	3.066	23.406	-	-	
MnB_2	2.924	2.950	21.843	2.242	1.688	
	3.009	3.039	23.829	-	-	[44]
FeB_2	2.931	2.921	21.732	2.235	1.674	
	3.045	3.035	24.370	-	-	
YB_2	3.314	3.855	36.666	2.716	1.914	
	3.290	3.835	35.949	-	-	
ZrB_2	3.197	3.561	31.520	2.564	1.846	
	3.170	3.533	30.746	-	-	
TaB_2	3.115	3.244	27.260	2.421	1.799	
	3.294	3.886	29.199	-	-	
AgB_2	3.000	3.240	29.064	2.372	1.732	[36]

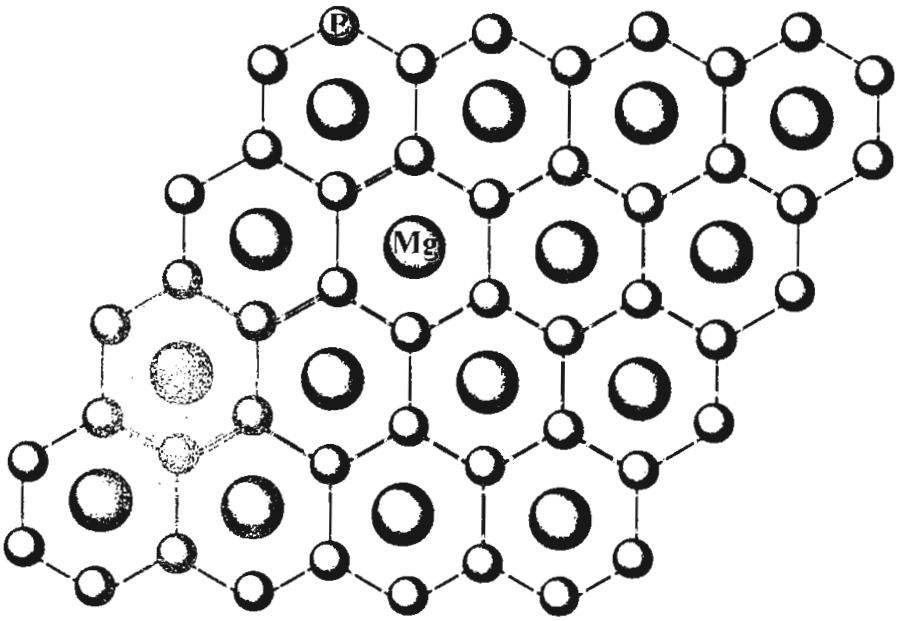

Figure 2.1. The crystal lattice structure of MgB_2 (two dimensional view). Large spheres indicate magnesium and small spheres indicate boron atoms.

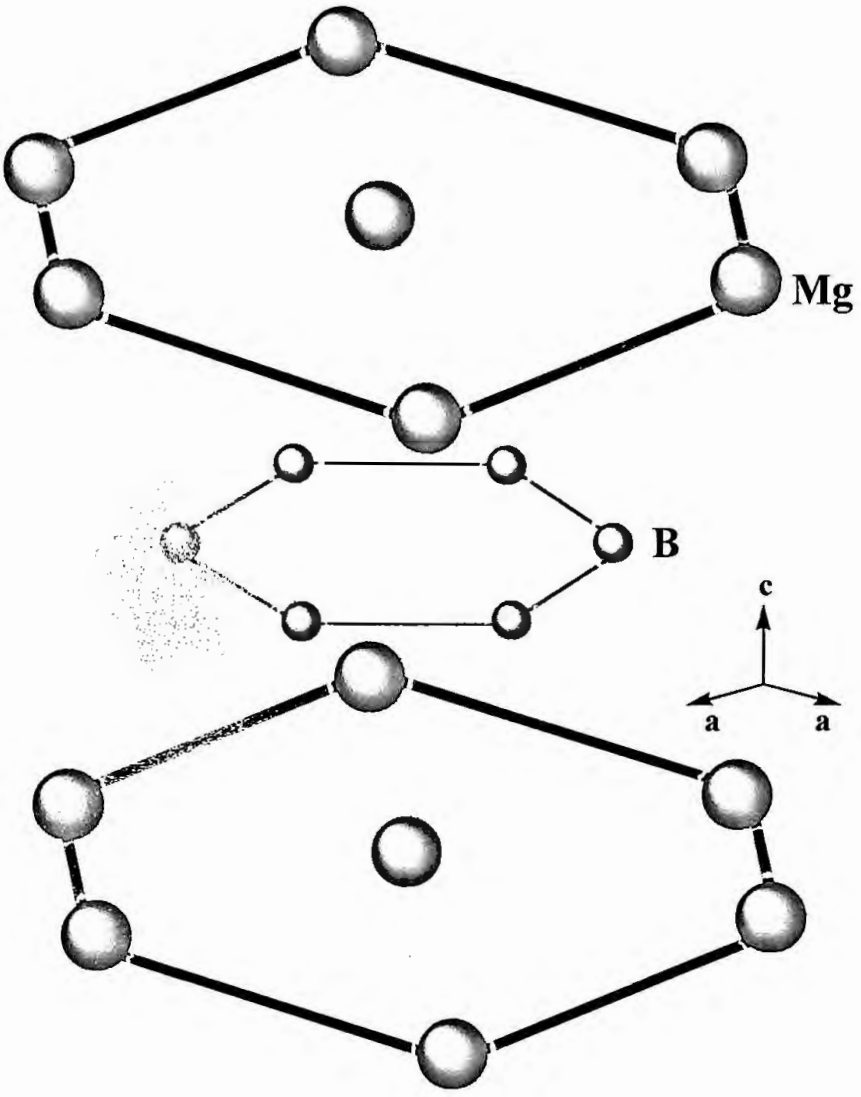

Figure 2.2. Physical picture of MgB_2 superconductor. The layered structure seems to play a significant role for the superconductivity.

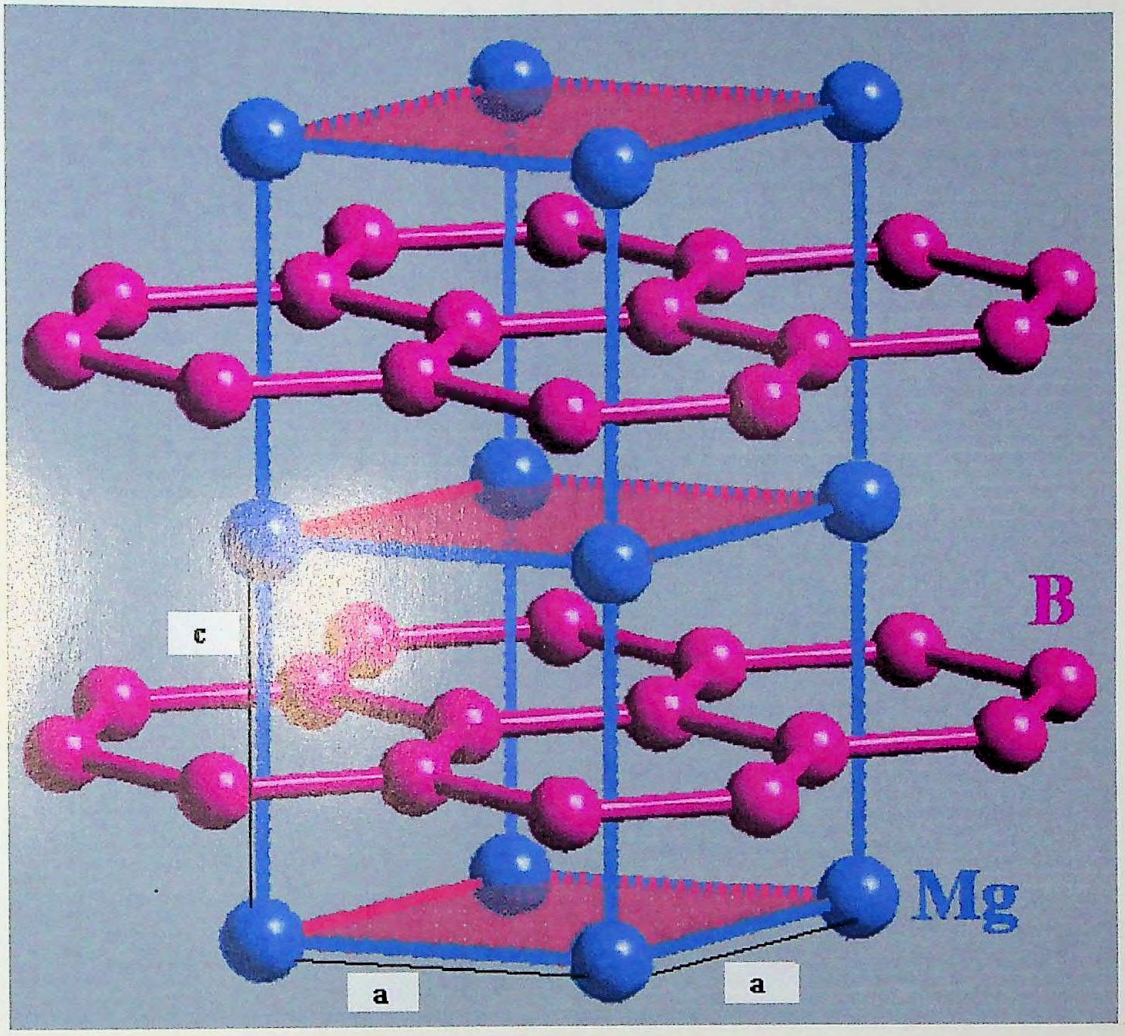

Figure 2.3. The crystal structure of MgB_2 (three dimensional view) superconductor.

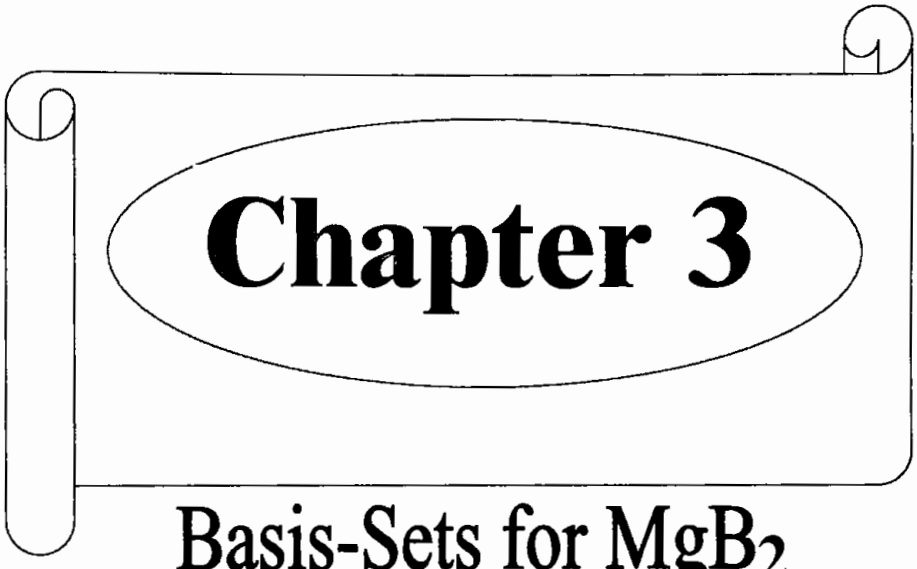

Chapter 3

Basis-Sets for MgB_2

integrals occurring in the calculation. This speed of evaluation of the integrals mainly depends on the basis-sets of the atoms. Two types of all electron basis-sets are included in CRYSTAL98 (a computer programme). CRYSTAL98 is used to calculate the different properties of molecules and crystals by solving embedded equations. Gaussian type orbitals are commonly used in the *ab initio* calculations because they are well documented and able to provide quite reasonable optimized geometries with minimum CPU time.

3.3 Gaussian Functions

The basis function comprises of Slater-type orbitals (STOs) and Gaussian-type orbitals (GTOs). They are both the product of spherical harmonics $Y_{lm}(\theta, \phi)$ and a radial function R(r). The basic form of the radial function is $R(r) = r^n \exp(-\alpha r^2)$, where α is the exponent. Gaussian type orbitals have been used in our study. GTOs have some advantages over STOs for which its applications are frequent rather than the former. A few important characteristics of GTOs are as follows:

(a) In molecular applications, GTOs are usually constructed as a linear combination of Gaussian primitives $g_j(\mathbf{r})$, characterized by the same centre, the same angular numbers but different exponents [46]:

$$\varphi_\mu(\mathbf{r}) = \sum_{j=1}^{p_\mu} d_j g_j(\mathbf{r}); \quad g_j(\mathbf{r}) \equiv g(\mathbf{r};\alpha,\ell,\mathrm{m}) = r^l Y_{lm}(\theta,\phi)\exp\left(-\alpha_j r^2\right) \qquad (3.1)$$

where α_j represents exponents and d_j contraction coefficients. These combinations are called contracted Gaussians.

(b) In solid state applications, finite number (p) of GTOs are attributed to the various atoms in the reference zero cell ($\mathbf{A}_\mu$ will denote the coordinate of the nucleus on which φ_μ is centered); the same GTOs are then associated with all translationally equivalent atoms in the crystal. In total, we have Np GTOs, from which we can construct Np Gaussian-type Bloch-orbitals:

$$\varphi_\mu(r;\kappa) = \sum_g \varphi_\mu(r - A_\mu - g)\exp(ik.g) \quad (\mu = 1,..p;\ \kappa = 1,..N) \qquad (3.2)$$

(c) For the crystalline system, very diffuse primitives are avoided because, (i) the number of integrals to be explicitly calculated increases explosively, (ii) the accuracy of the calculation must be particularly high in order to avoid pseudo-linear dependence catastrophes, and (iii) diffuse functions are not of much use in densely packed crystals, because their tails are founding regions where there is large variational freedom associated with functions on other atoms.

(d) The contracted GTOs are quite able to describe accurately the electronic distributions both in valence and in the core region with a limited number of basis functions.

(e) An additional advantage of GTOs is due to the fact that their Fourier transform is another Gaussian and their use in combination with plane wave (PW) techniques is therefore easy [47].

(f) A given set of GTOs associated with atomic positions, usually performs better when the atoms are close to each other than if they are far apart. The region between two atoms is better described if use is made of functions centered on both atoms. There is then an over-estimation of binding energies, which is called basis-sets superposition error (BSSE).

BSSE can be very important with poor basis-sets; the counterpoise technique for estimating this error gives usually reasonable results [48].

3.4 Basis-Sets for MgB_2

In previous section we have mentioned that the accuracy of different calculations largely depend on the appropriate selection of the basis-sets. So, a special care was taken to choose the basis-sets for MgB_2. In our present *ab initio* calculation, all-electron general GTOs free basis-sets (given in the input; Table 3.1 and 3.2) have been used for MgB_2 superconductor. The basis-sets used for B and Mg are 6-21G* [49] and 8-61G [48], respectively. The magnesium basis-sets are presented in Table 3.1 while Table 3.2 displays the boron basis-sets. The basis-sets used for Mg contain 15 functions, a contraction of 8, 6 and 1 Gaussian type functions for 1s, 2sp and 3sp shells, respectively. On the other hand, 9 functions are used for B (6, 2, and 1 contracted Gaussian type functions for 1s, 2sp and 3sp shells, respectively). The addition of d-type polarization functions on boron atom gives its basis-set as 6-21G*. The basis-sets have been optimized for equilibrium or minimum energy at the least cycles of SCF convergence. Optimizing value of the outer exponent of the boron sp shell is 0.1820 a.u.

The core shells of Mg atom have been described as a linear combination of eight Gaussians while the valence shells contain six and one Gaussians. Similarly, the linear combination of Gaussians for core and valence shells of boron atom is shown in the Table 3.2. Contraction coefficients have been optimized variationally for isolated atoms. The best exponent of the outer sp shell for boron was found to 0.1820.

When free basis-sets (BS) are chosen, two points should be taken into account:

i) From the point of view of the CPU time, basis-sets with sp shell (s and p functions sharing the same set of exponents) can give rise a saving factor as large as 4, in comparison with basis-sets where s and p have different exponents [46].

ii) As a rule, extended atomic basis-sets should be avoided. One should not forget that the real basis functions are Bloch functions.

Table 3.1. The magnesium basis-sets. Exponents (a.u.) and coefficients of the s, p and d Gaussian functions.

Shell	Type	Gaussian	Exponent (α_j)	Coefficient (d_j)		
				s	p	d
1	s	1	68371.875000	0.0002226		
		2	9699.340090	0.0018982		
		3	2041.176786	0.0110451		
		4	529.862906	0.0500627		
		5	159.186000	0.1691230		
		6	54.684800	0.3670310		
		7	21.235700	0.4004100		
		8	8.746040	0.1498700		
2	sp	1	156.795	-0.00624	0.00772	
		2	31.0339	-0.07882	0.06427	
		3	9.6453	-0.07992	0.21040	
		4	3.7109	0.29063	0.34314	
		5	1.61164	0.57164	0.37350	
		6	0.64294	0.30664	0.23286	
3	sp	1	0.4	1.0	1.0	

Table 3.2. The boron basis-sets. Exponents (a.u.) and coefficients of the s, p and d Gaussian functions.

Shell	Type	Gaussian	Exponent (α)	Coefficient (d_j)		
				s	p	d
1	s	1	2082.000	0.00185		
		2	312.300	0.01413		
		3	70.890	0.06927		
		4	19.850	0.2324		
		5	6.292	0.4702		
		6	2.129	0.3603		
2	sp	1	2.2820	-0.3687	0.2312	
		2	0.4652	1.1990	0.8668	
3	sp	1	0.1243	1.0	1.0	
3	d	1	0.8			1.0

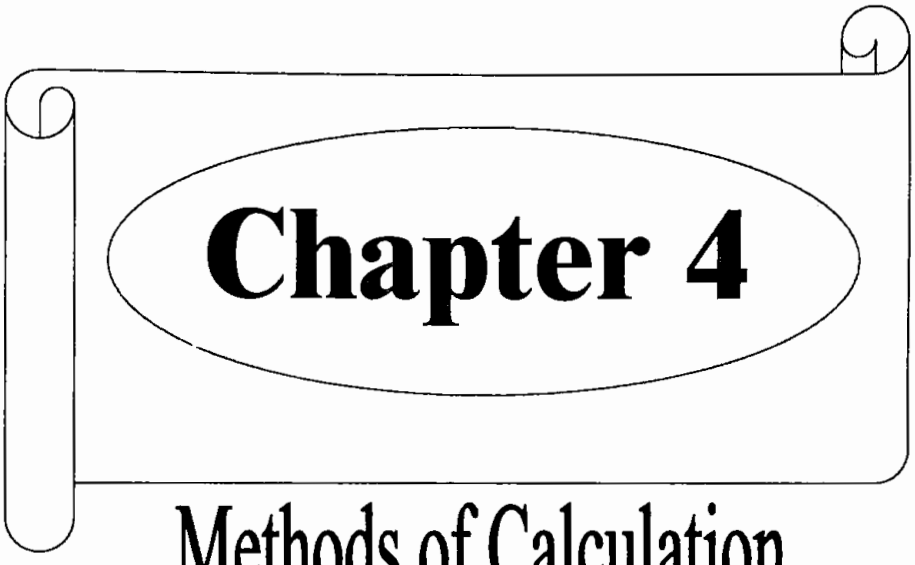

Chapter 4

Methods of Calculation

CHAPTER 4

METHODS OF CALCULATION

4.1 Introduction

The basic models of condensed matter physics have been refined so as to describe more and more accurately, a wide spectrum of observable quantities of real physical systems. The traditional schemes have been reformulated so as to assume a first principle (*ab initio*) parameter free character. In the new formulation the various schemes have been improved quite substantively by raising the level of approximations [50]. The corresponding basic equation is now solved with unprecedented numerical accuracy because of the availability of high-speed computers.

The present chapter provides a general overview of the methods used in the calculation. The computational tools, adopted for the present study of the physical and electrical properties of magnesium diboride MgB_2 superconductor, is the first principle *ab initio* quantum mechanical technique. The all-electron *ab initio* self-consistent-field (SCF) Hartree-Fock linear combination of atomic orbitals, (HF-LCAO) method (implemented in crystal98) has been used in the present investigations. A detailed description of the HF-LCAO method is given in reference [50]. The density functional theory (DFT) and Hartree-Fock (HF) approaches are presented here very concisely. To calculate the ground state total energy of MgB_2, the Coulomb and exchange series for one and two electron integrals are approximated and evaluated in the present method. Integrals between non-overlapping distributions are also approximated. In some cases,

numbers of terms of the Coulomb series are aggregated to reduce the integrals to be calculated.

The contributions to the energy per electron for the homogeneous electron gas, as a function of Wigner-seitz radius (r_s) is shown schematically in figure 4.1. The importance of exchange and correlation contributions to the total energy can be understood from this figure.

The structure and sequence of functioning of the source code are also explained very precisely by means of flow chart and diagram in section 4.6 of this chapter.

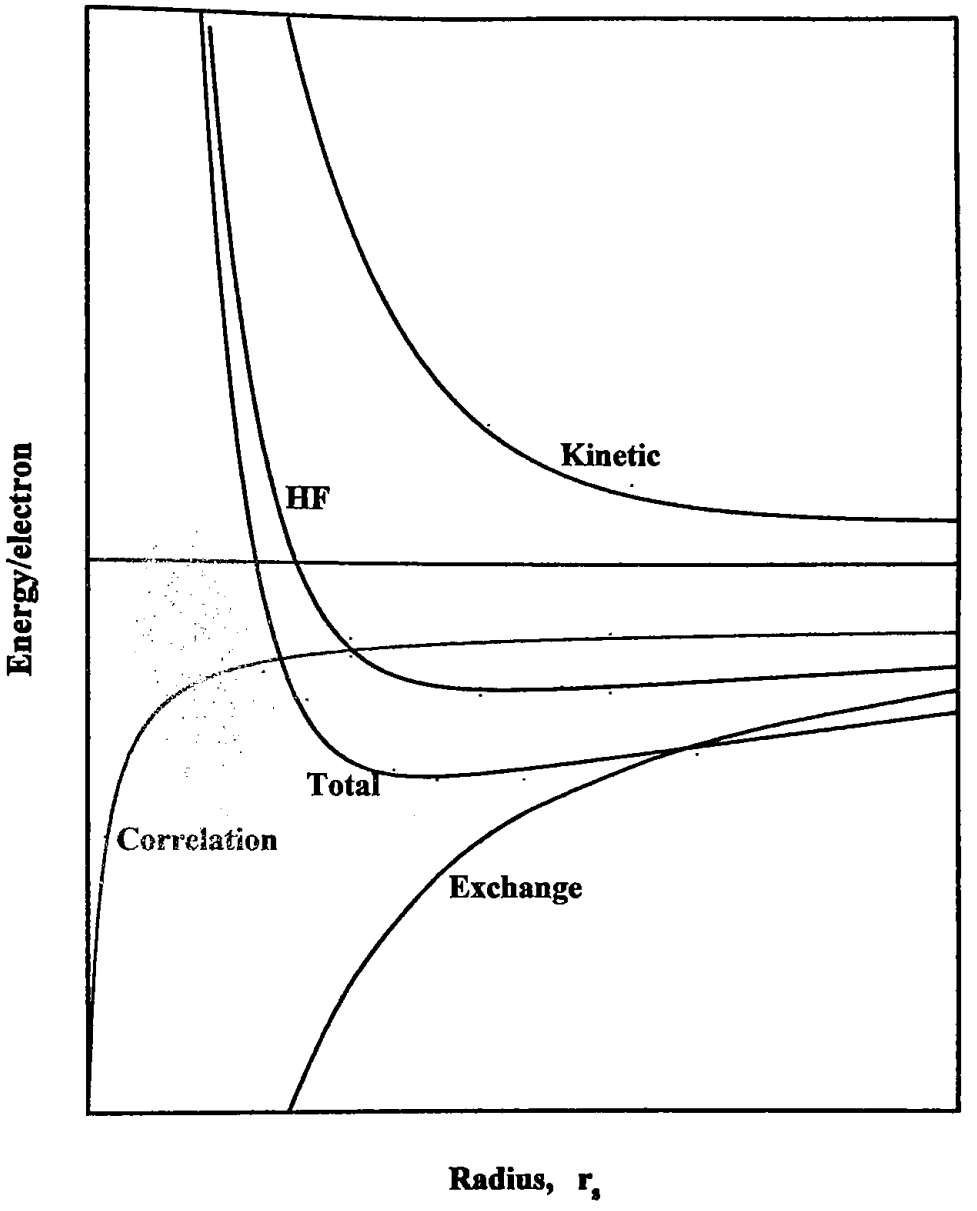

Figure 4.1. Schematic picture for the contributions to the total energy per electron as a function of the Wigner-Seitz radius.

4.2 *Ab initio* Method

The most widespread method for calculating the ground state properties of periodic systems is the *ab initio* technique. The term *'ab initio'* means 'from the beginning'. The *ab initio* approach begins with the non-relativistic Hamiltonian and requires no inputs of empirical information. With a given crystalline structure and chemical composition for any periodic system, the *ab initio* method is used to calculate the physical and chemical properties of the system as accurately as possible without any need for an *a priori* information. In this method, the fundamental approximation made is the expansion of the single particle wave functions (Crystalline Orbital, CO) as a linear combination of Bloch functions (BF) defined in terms of local functions (Atomic Orbital, AO). The local functions are, in turn, linear combinations of Gaussian type functions (GTF) whose exponents and coefficients are defined by input [45]. The derivation of the *ab initio* methods, Hartree-Fock (HF) and Density Functional Theory (DFT) adopted in the present study, are illustrated in the following subsections.

4.2.1 Hartree-Fock (HF) Method

The Hartree-Fock (HF) method is also known as self-consistent-field (SCF) method. It is an important approximation method introduced by Douglas R Hartree. The goal of this method is similar to that of the variational method. The method treats the problem of many-electron system in which the eigenfunction for the system is represented as the product of Z single-electron wave functions. Each one of these wave functions is determined as a solution of Schrödinger equation (SE) in the field of the nucleus and of the total average charge distribution of the electrons in the other wave

functions. The field of the average electron distribution derived from the wave functions must be the same as the field used in evaluating these wave functions. This aspect led to the term "SCF" for the atomic field so determined.

We are concerned with those electronic properties that depend on the electronic structure of the crystal. This, in turn, is a function of the geometry and the electric charge of the nuclei, which will be taken as fixed and arranged according to a crystalline lattice. The first thing that is important to start any *ab initio* study of electronic structure is the choice of the Hamiltonian. The non-relativistic Hamiltonian ($\hat{H}$) for any electronic system can be expressed as [46]:

$$\hat{H} = -\sum_{i}\left(\nabla_i^2/2\right) - \sum_{i,A} Z_A/r_{i,A} + \sum_{i>j} 1/r_{ij} + \sum_{A>B} Z_A Z_B/r_{AB} \qquad (4.1)$$

In the Hamiltonian expression of equation (4.1), the first, second, third and forth terms are respectively the kinetic energy of electrons, coulomb interaction with nuclei and electrons, coulomb interaction among electrons and electrostatic interaction between nuclei. The electronic structure of a system can be easily understood when the Hamiltonian and the total number of electrons of that system is known. The ground state electronic structure (GSES) governs the properties of any system in condensed matter physics. So, the calculation of ground state energy and some other properties associated to the energy are the main objectives of our interest. The GSES of a given system can be determined by solving the Schrödinger equation (SE):

$$\hat{H}\psi_0 = E_0\psi_0 \qquad (4.2)$$

where E_0 is the ground state energy of the system. It is the lowest energy eigenvalue for the nuclear configuration. In the solution procedure of equation (4.2), the complexity and problems arise due to the inter-electronic interaction term, $\sum_{i>j} 1/r_{ij}$. The factorization of the problems of many electrons into individual electron is prevented mainly by the inter-electronic interaction. In order to overcome this problem, a simplified form is suggested by introducing an effective potential [46] for each electron in the field of the others and substituting a sum of one-electron Hamiltonian ($\hat{H} \approx \sum_i \hat{h}_i$). Some higher order terms are neglected in the process of simplification.

$$\Rightarrow \underset{\text{nuclear motion}}{(\text{fixed nuclei})} \Rightarrow \underset{\text{relativistic effects}}{\hat{H}} \Rightarrow \underset{\text{higher order effects}}{\{\hat{h}_i\}} \Rightarrow \underset{\text{excited states}}{\text{GSES}}$$

4.2.2 Density Functional Theory (DFT)

The Density Functional Theory (DFT) was introduced by Hohenberg and Kohn [51]. They showed that the total energy is a functional of the electron density. This means that one does not need to know the complicated many-electron wave function, but only the electron density $\rho(\mathbf{r})$, which is the key quantity in density functional theory. DFT techniques are based on two theorems. The first theorem states that a given ground states electron density, $\rho_0(\mathbf{r})$ exits only when the two external potentials differ by a constant. The second theorem establishes a variational criterion for determining $\rho_0(\mathbf{r})$ and E_0 together for a given external potential created by a

set of nuclear charge, e.g. $V(\mathbf{r}) = -\Sigma_A Z_A / |\mathbf{r} - \mathbf{r}_A|$. E_0 is found by minimizing an expression of the form [46]:

$$\begin{aligned} E[\rho(\mathbf{r})] &= \int \rho(\mathbf{r}) V(\mathbf{r}) d\mathbf{r} + \frac{1}{2} \iint [\rho(\mathbf{r})\rho(\mathbf{r}')] / |\mathbf{r} - \mathbf{r}'| \, d\mathbf{r} \, d\mathbf{r}' \\ &+ \int \rho(\mathbf{r}) g(\mathbf{r}; [\rho]) d\mathbf{r} + \sum_{A>B} Z_A Z_B / r_{AB} \\ &= E_{ext} + E_J + E_{kxc} + E_{RepNuc} \end{aligned} \tag{4.3}$$

with respect to an arbitrary function, $\rho(\mathbf{r})$, which represents an n-electron density. In equation (4.3), the first term is the interaction energy with the external potential; the second term gives the classical-self-interaction of the charge density $\rho(\mathbf{r})$. The third term contains the $g(\mathbf{r})$ function, which may be represented as a density of kinetic, exchange and correlation energy per unit electron density at $\mathbf{r}$ while the last term is the usual internuclear repulsion. The minimum is obtained in correspondence to $\rho_0(\mathbf{r})$. $g(\mathbf{r})$ is a functional of density ρ. Its analytic form is not known. So, different approximations like LDA (Local Density Approximation) and GGA (Generalized Gradient Approximation) are used. A short description of LDA and GGA are given in the following sub-sections. Now we draw our attention to find out the ground state energy of the system. Within the Kohn and Sham (KS) method the ground state energy is calculated according to the self-consistent-field (SCF) procedure as follows:

1. The n/2 lowest eigenvalues and the corresponding eigenvectors are found out for one-electron effective Hamiltonian,

$$\hat{h}_{eff} \, \psi_i(\mathbf{r}) \equiv \left[-\frac{1}{2} \nabla^2 + V_{eff}(\mathbf{r}) \right] \psi_i(\mathbf{r}) = \varepsilon_i \, \psi_i(\mathbf{r}) \tag{4.4}$$

2. Calculation of density, $\rho(\mathbf{r})$;

$$\rho(\mathbf{r}) = 2\sum_i |\psi_i(\mathbf{r})|^2 \tag{4.5}$$

3. Re-calculation of effective potential, $V_{eff}(\mathbf{r})$ as a functional of the density, $\rho(\mathbf{r})$;

$$V_{eff}(\mathbf{r}) = V(\mathbf{r}) + \int \rho(\mathbf{r}')/|\mathbf{r} - \mathbf{r}'|\, d\mathbf{r}' + \mu_{xc}(\mathbf{r};[\rho]) \tag{4.6}$$

where $\mu_{xc}(\mathbf{r};[\rho])$ is the effective exchange-correlation potential

4. If self-consistency is not reached, go to step 1.

5. At self-consistency, $\rho(\mathbf{r}) = \rho_0(\mathbf{r})$ (GS density) and the ground state total energy can be calculated by the following equation (4.7),

$$E_0 = E_{kps} + \int \rho_0(\mathbf{r}) V(\mathbf{r}) d\mathbf{r} + 1/2 \int [\rho_0(\mathbf{r})\rho_0(\mathbf{r}')]/|\mathbf{r} - \mathbf{r}'|\, d\mathbf{r}\, d\mathbf{r}' + E_{xc} + E_{RepNuc} \tag{4.7}$$

where the pseudo-kinetic energy, E_{kps} is defined by,

$$E_{kps} = \sum_i \int \psi_i(\mathbf{r})^* \left(-\tfrac{1}{2}\nabla^2\right) \psi_i(\mathbf{r}) d\mathbf{r} \tag{4.8}$$

and the exchange-correlation energy, E_{xc} is expressed as,

$$E_{xc} = \int \rho_0(\mathbf{r}) \varepsilon_{xc}(\mathbf{r};[\rho_0]) d\mathbf{r} \tag{4.9}$$

The application of the DFT method has become a powerful technique to study the electronic structure of crystals. The ground state properties of a system of electrons and ions are determined by calculating GS energy from the electron density using equation (4.7).

4.2.2(a) Local Density Approximation (LDA)

The exchange-correlation energy for a homogenous electron gas is expressed by the following equation given by Kohn and Sham [52],

$$E_{xc}^{LDA}[\rho] = \int \rho(r)\,\varepsilon_{xc}[\rho(r)]\,dr \qquad (4.10)$$

They [52] also introduced the local spin density approximation (LSDA) where spin polarization is allowed and the exchange-correlation energy becomes a functional of the local electron-spin densities, $\rho_\uparrow$ and $\rho_\downarrow$:

$$E_{xc}^{LSDA}[\rho_\uparrow, \rho_\downarrow] = \int \rho(r)\,\varepsilon_{xc}[\rho_\uparrow(r)\,\rho_\downarrow(r)]\,dr \qquad (4.11)$$

By writing E_{tot} in this form and applying the variational principle one-electron KS equations maybe derived in the following form:

$$\left\{-\frac{1}{2}\nabla^2 + V_{ext}(r) + V_c[\rho(r)] + \mu_{xc}[\rho(r)]\right\}\psi_i(r) = \varepsilon_i\psi(r) \qquad (4.12)$$

where μ_{xc} is the fictional derivative of E_{xc} with respect to density. Thus the many-body-problem can be solved in this method by replacing a set of effective one electron KS equations and the electron density is obtained by summing over all occupied states i.e. $\rho(r) = \sum_{i\ \text{occupied}} |\psi_i(r)|^2$.

4.2.2(b) Generalized Gradient Approximation (GGA)

The generalized gradient approximation (GGA) is more efficient than local density approximation (LDA). Gradient corrections are included in this new approximation. It is also applicable to the system of inhomogeneous electron gas. Thus it is able to yield the more appropriate results and the

exchange-correlation energy E_{xc} is a function of the spin density and their gradients [46]:

$$E_{xc}^{GGA}[\rho_{\uparrow},\rho_{\downarrow}] = \int [\rho_{\uparrow}(r),\rho_{\downarrow}(r),\nabla\rho_{\uparrow}(r),\nabla\rho_{\downarrow}(r),]\,dr \qquad (4.13)$$

The purpose of introduction of GGA is to improve the quality of LDA results significantly.

4.3 Basic Equations Embedded in the Programme

In this section, the fundamental equations of the HF-LCAO method are given. The Crystalline Orbital (CO) ψ_i (**r;k**), is a linear combination of Bloch functions (BF), ϕ_μ (**r;k**). The Bloch functions are expressed in terms of the local functions φ_μ (**r**), which is also known as atomic orbitals (AOs). The mathematical expression for these relations are given as below:

$$\psi_i(\mathbf{r};\mathbf{k}) = \sum_{\mu} a_{\mu,i}(\mathbf{k})\ \phi_\mu(\mathbf{r};\mathbf{k}) \qquad (4.14)$$

$$\varphi_\mu(\mathbf{r};\mathbf{k}) = \sum_{\mathbf{g}} \varphi_\mu(\mathbf{r}-\mathbf{A_\mu}-\mathbf{g})e^{\mathbf{ik.g}} \qquad (4.15)$$

Where $\mathbf{A}_\mu$ denotes the coordinates of the nucleus in the zero reference cell on which φ_μ is centered, and the $\sum_g$ is extended to the set of all lattice vectors **g**. The local functions are expressed as a linear combination of a certain number, n_G, of individually normalized Gaussian type functions (GTF) with fixed coefficients, d_j and exponents, α_j, defined in the input [45,46]:

$$\varphi_\mu(\mathbf{r}-\mathbf{A_\mu}-\mathbf{g}) = \sum_{j}^{n_G} d_j\, G(\alpha_j;\mathbf{r}-\mathbf{A_\mu}-\mathbf{g}) \qquad (4.16)$$

The AOs belonging to a given atom are grouped into shells. The shell can contain all AOs with the same quantum numbers, n and ℓ (e.g. 3s, 2p, 3d shells) or all the AOs with the same principal quantum number, n, if the number of GTPs and the corresponding exponents are the same for all of them (mainly sp shells). The α exponent is the smallest of the α_j exponents of the Gaussian in the contraction. The adjoined Gaussian (G) is used to estimate the AO overlap and select the level of approximation to be adopted for the evaluation of the integrals.

The expansion coefficients of the Bloch function, $\alpha_{\mu,i}$ (**k**), are calculated by solving the matrix equation for each reciprocal lattice vector, **k**;

$$\mathbf{F(k)\ A(k) = S(k)\ A(k)E(k)} \tag{4.17}$$

in which **S(k)** is the overlap matrix over the Bloch functions, **E(k)** is the diagonal energy matrix and **F(k)** is the Fock matrix in reciprocal space;

$$F(\mathbf{k}) = \sum_{g} F^{g} e^{i\mathbf{k}.\mathbf{g}} \tag{4.18}$$

Now the matrix element of the Fock matrix (F^g) in direct space can be written as a sum of one-electron and two-electron contributions in the basis-sets of the AOs;

$$F_{12}^{g} = H_{12}^{g} + B_{12}^{g} \tag{4.19}$$

Again the one-electron contribution is the sum of the kinetic and the nuclear attraction terms,

$$H_{12}^{g} = T_{12}^{g} + Z_{12}^{g} = \left\langle \varphi_1^0 \middle| \hat{\mathbf{T}} \middle| \varphi_2^g \right\rangle + \left\langle \varphi_1^0 \middle| \hat{\mathbf{Z}} \middle| \varphi_2^g \right\rangle \tag{4.20}$$

and the two-electron term is the sum of the Coulomb and exchange contributions,

$$B_{12}^{g} = C_{12}^{g} + X_{12}^{g}$$
$$= \sum_{3,4}\sum_{n} P_{3,4}^{n} \sum_{h}\left[\left(\varphi_1^0\,\varphi_2^g \middle| \varphi_3^h\,\varphi_4^{h+n}\right) - \frac{1}{2}\left(\varphi_1^0\,\varphi_3^h \middle| \varphi_2^g\,\varphi_4^{h+n}\right)\right] \tag{4.21}$$

The density matrix elements P^n in the AOs basis-sets are computed by integration over the volume of the Brillouin zone (BZ),

$$P_{3,4}^{n} = 2\int_{BZ} d\mathbf{k}\; e^{i\mathbf{k}.\mathbf{n}} \sum_{n} \alpha_{3n}^{*}(\mathbf{k})\;\alpha_{4n}(\mathbf{k})\,\theta(\varepsilon_F - \varepsilon_n(\mathbf{k})) \tag{4.22}$$

where a_{in} denotes the i-th component of the n-th eigenvector, θ is the step function, ε_F, the Fermi energy and ε_n, the n-th eigen value. The total electronic energy per unit cell is given by,

$$E^{elec} = \sum_{1,2}\sum_{g} P_{12}^{g}\left(H_{12}^{g} + B_{12}^{g}\right) \tag{4.23}$$

4.3.1 The Coulomb Series

The appropriate coupling between electron-nucleus and electron-electron is very important for the evaluation of the Coulomb contributions to the total energy and Fock matrix. The computational technique for doing so was presented Dovesi et al. [53] and by Saunders et al. [54]. A very short description is given here.

The Coulomb bielectronic contribution to the Fock matrix (C_{12}^{g}) and to the total energy is given by,

$$E_{ee}^{coul} = \frac{1}{2}\sum_{12}\;\sum_{g} P_{12}^{g}\sum_{3,4}\;\sum_{t} P_{3,4}^{n}\sum_{h}\left[\left(\varphi_1^0\;\varphi_2^g \,\middle|\, \varphi_3^h\;\varphi_4^{h+n}\;\right)\right] \tag{4.24}$$

Seven indices are involved in equation (18); four of them (1,2,3 and 4) refer to the AOs of the unit cell, the other three (**g, n** and **h**) span the infinite set

of translation vectors. By the symbol φ_2^g we mean AO number 2 in cell g. P is the density matrix. The electron-electron and electron-nuclei series (C^*_{12} and Z^*_{12}) can be rearranged as follows [45]:

The Coulomb and nuclear attraction terms are expressed as,

$$C_{12}^{g} + Z_{12}^{g} = \sum_{\lambda}\sum_{h} \int d\mathbf{r}\, d\mathbf{r}'\, \varphi_1^0(\mathbf{r})\varphi_2^g(\mathbf{r}) |\mathbf{r} - \mathbf{r}' - \mathbf{h}|^{-1} \rho_\lambda (\mathbf{r}' - \mathbf{h}) \tag{4.25}$$

For a given shell λ, there is a finite set B_λ of **h** vectors for which the two interacting distributions overlap. In the bielectronic zone (B_λ), all the bielectronic integrals are evaluated explicitly. In the infinite region (monoelectronic zone, M_λ), ρ_λ is expanded and evaluated to infinity analytically [54]. The final expression for the Coulomb contribution to the Fock matrix is

$$\begin{aligned} C_{12}^{g} + Z_{12}^{g} \;=\; & \sum_{\lambda}\Bigg\{ \sum_{h}^{B_\lambda}\Bigg[\sum_{3\varepsilon\lambda}\sum_{4}\sum_{n} P_{34}^{n} \left(\varphi_1^0 \varphi_2^g \,\middle|\, \varphi_3^h \varphi_4^{h+n}\right) \\ & - \sum_{\ell,m} \gamma_\ell^m (\mathbf{A}_\lambda ; \{\lambda\}\, \varphi_\ell^m (\mathbf{12g}; \mathbf{A}_\lambda + \mathbf{h}) \Bigg] \\ & + \sum_{h}\sum_{\ell,m} \gamma_\ell^m (\mathbf{A}_\lambda ; \{\lambda\}' \,)\, \varphi_\ell^m (\mathbf{12g}; \mathbf{A}_\lambda + \mathbf{h}) \Bigg\} \end{aligned} \tag{4.26}$$

where $\gamma_\ell^m (\mathbf{A}_\lambda ; \{\lambda\} = \int d\mathbf{r}\, \rho_\lambda (\mathbf{r} - \mathbf{A}_\lambda) N_\ell^m X_\ell^m (\mathbf{r} - \mathbf{A}_\lambda)$ and

$$\begin{aligned} & \varphi_\ell^m (\mathbf{12\,g}; \mathbf{A}_\lambda + \mathbf{h}) \\ & = \int d\mathbf{r}\, \varphi_1^0(\mathbf{r}) \varphi_2^g(\mathbf{r}) X_\ell^m (\mathbf{r} - \mathbf{A}_\lambda - \mathbf{h}) |\mathbf{r} - \mathbf{A}_\lambda - \mathbf{h}|^{-2\ell - 1} \end{aligned}$$

The advantage of applying equation (4.26) is that many long-range integrals can be replaced by fewer three-centre integrals.

4.3.2 The Exchange Series

The exchange series demand a careful selection of the terms that contributes to the Fock matrix and then to the total energy [55]. The exchange contribution to the total energy can be written as,

$$E^{exch} = \frac{1}{2}\sum_{12}\sum_{g} P_{12}^{g}\left[-\frac{1}{2}\sum_{34}\sum_{n} P_{3,4}^{n}\sum_{h}\left(\varphi_1^0\varphi_3^h\middle|\varphi_2^g\varphi_4^{h+n}\right)\right] \qquad (4.27)$$

where the terms in the square brackets is the exchange contribution to the 12g element of direct space Fock matrix. Exchange energy converges itself because it has no counterpart of opposite sign as the Coulomb term.

4.4 The Role of Symmetry in *ab initio* Calculation

Translational symmetry allows the factorization of the eigenvalue problem in periodic calculations, because the Bloch functions are a basis for irreducible representations of the translational group. Point symmetry plays a vital role to reduce the number of points for which the matrix equations are to be solved. Point symmetry is also explicitly used in the reconstruction of Hamiltonian, which is totally symmetric with respect to the point group operators of the system.

In the HF-CO-LCAO scheme, the very extensive use of point symmetry allows us to evaluate bielectronic and monoelectronic integrals with saving factors as large as h in the number of bielectronic integrals to be computed or h^2 in the number of those to be stored for the SCF part of the calculation, where h is the order of the point group. The different steps of the procedure are explained in the literature [56].

4.5 Integration in Reciprocal Space

The integration in reciprocal space is an important aspect of *ab initio* calculations for the periodic systems. The problem arise at each stage of the self-consistence procedure, when determining the Fermi energy, ε_F, when reconstructing the one-electron density matrix and, after self consistency is reached, when calculating the density of states (DOS) and a number of observable quantities [46]. The P matrix in direct space is computed following equation (4.22). The technique adopted to compute ε_F and the P matrix in SCF step is described in reference [51]. The Fourier-Legendre technique is used to calculate the total and projected DOS [52]. The integral of equation (4.22) and the Fermi energy are evaluated from a certain set of sampling points {k} in the reciprocal space.

4.6 The CRYSTAL98 Code

The CRYSTAL98 source code is written in the FORTRAN language. It consists of several programmes, which are based on FORTRAN90 [57] standard and FORTRAN77 [58] standard. A group of researchers (The Theoretical Chemistry Group of the University of Torino) initially developed the code [51,52]. The development of the present version (CRYSTAL98) [45] of the code has been assisted by the constant support and interest of C. Pisani, and a lot of contributions were made by M. Causa, N. M. Harrison, E. Apra and R. Orlando. Calculation of wave function and properties of any crystalline system can be performed by this program using the Hartree-Fock Linear Combination of Atomic Orbitals (LCAO) method with HF and DFT approximations.

4.6.1 The CRYSTAL98 Code Structure

The structure of the code is generally divided into three parts. Part-I contains the input routines, which includes geometry, basis-sets and computational parameters. The symmetry analysis, infinite lattice generation, monoelectronic and bielectronic integrals are evaluated in this section. The SCF (self consistent field) calculations are performed in part-II. There are four steps in each SCF cycle : α, β, γ & δ [50]. In α step, the Fock matrix is generated from the combination of direct density matrix and the integrals. In order to have the block diagonal structure the Fourier transformation of the Fock matrix is made in β. In γ the Fock matrices $F(\mathbf{k})$ in the reciprocal space are diagonalized. The eigenvalues are used to calculate the Fermi surface and the eigenvectors to compute the direct density matrix at the final step δ. Part-III finally computes the ground state properties, starting from the conversed solution. A complete SCF cycle is illustrated diagrammatically in figure 4.3.

4.6.2 The Flow Chart of the Code Operation

The functionality of the various programmes and their links are illustrated in figure 4.2. Unformatted Sequential data sets have been used in the present calculations. The s, p and d shells of the GTF can be used. The sp shell (s and p shell) can also be used. The advantage of using sp shell is to save the CPU time. A common filing system maintains all types of programme communication.

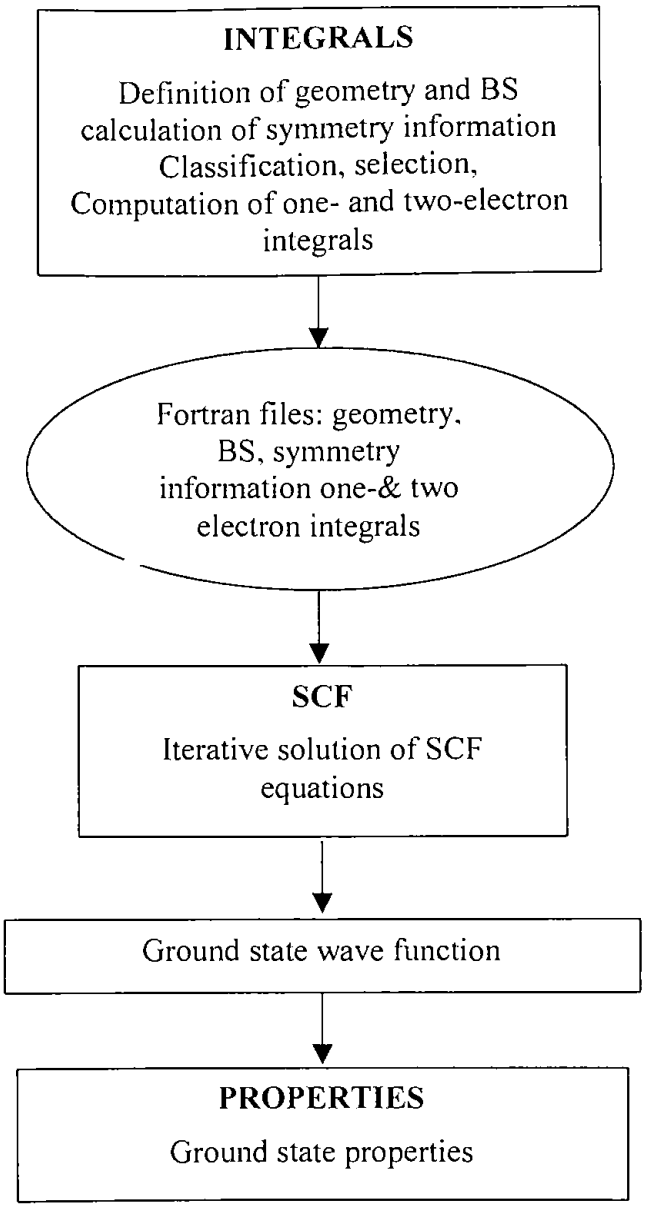

Figure 4.2. The flow chart of the functionality executed by the code is presented in the diagram.

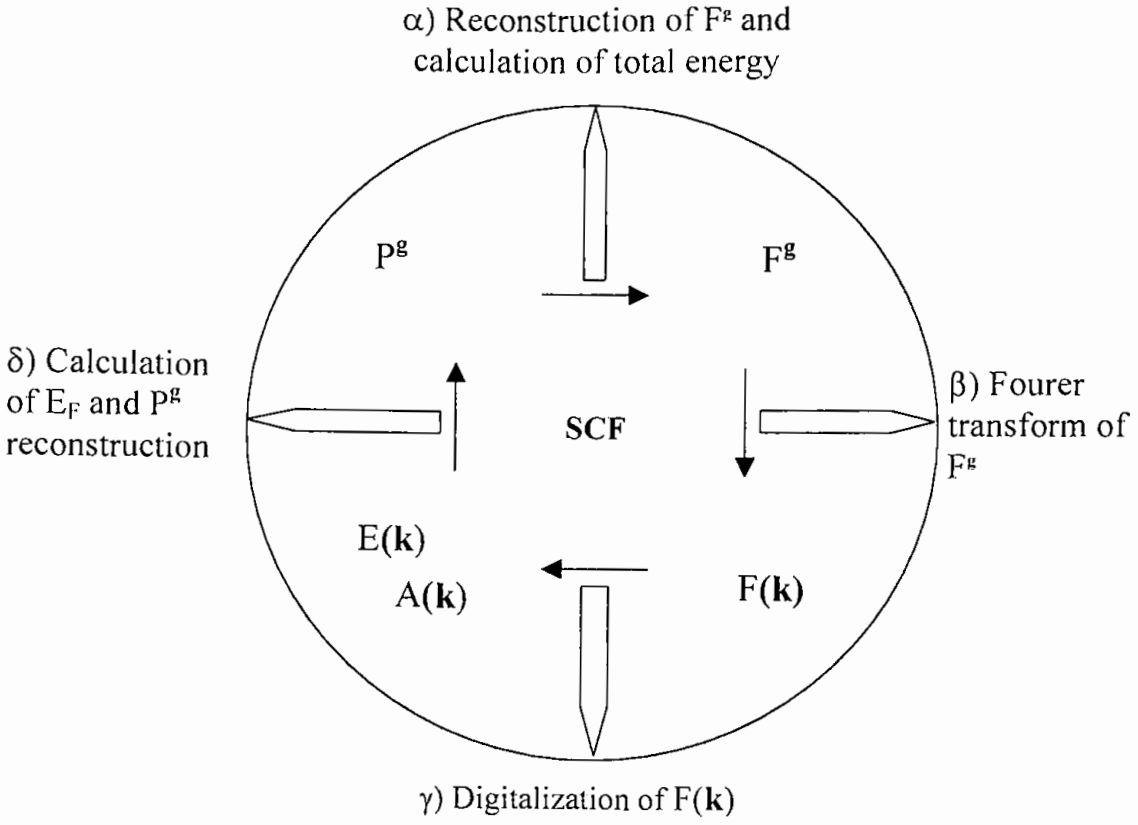

Figure 4.3. Illustration of different functions executed in each step of an SCF cycle.

4.7 Computation of Different Properties of MgB_2

The present investigations for various properties of MgB_2 were based on *ab initio* self-consistent-field linear combination of atomic orbitals (SCF-LCAO) computer programme CRYSTAL98 [45, 46, 50] with Hartree-Fock (HF) and density functional theory (DFT) options. The DFT Hamiltonian was used where the electronic correlation (BECKE) and the exchange (PWGGA) potential are chosen according to functionals proposed in the literature [59-62]. The integrations over the Brillouin zone (BZ) were performed using the Monkhorst-Pack scheme [63]. We simply remark here that CRYSTAL98 is a general program for the treatment of crystalline compounds of any space group, which has been applied to the study of semiconductors, crystals, slabs and polymers.

The basis-sets used are 6-21G* for B and 8-61G for Mg which are presented and described in chapter 3 (Tables 3.1 and 3.2). It is also explained in our paper [16]. The unit cell of MgB_2 consists of three atoms. Eleven shells and thirty seven atomic orbitals have been used for the ground state energy calculation of MgB_2. Each atomic orbital is a linear combination of Gaussian-type functions (GTF), which are the product of a radial Gaussian times a real solid harmonic function (see chapter 3). The exponents and coefficients of the inner shells were optimized in the study of MgB_2. The exponents of the most diffuse sp and d shells for each atom have been optimized by searching for the minimum crystalline energy. The present basis-sets appear adequate to provide a high quality description of the ground state properties of MgB_2.

The quality of the calculation depends on the density of points with which the Brillouin zone (BZ) is sampled. The integrations over the BZ were performed using the Monkhorst-Pack scheme [63]. The accuracy of the infinite Coulomb and exchange series evaluation was increased by introducing tight tolerances of the order of 10^{-7} for coulomb overlapping and penetration. To achieve SCF convergence with greater accuracy during the Brillouin zone (BZ) integration very tight condition was set for the calculation of energy eigenvalues (convergence on eigenvalue 10^{-7}) and ground state energy (convergence on energy 10^{-5}). The accuracy of the integration (mono- and bi-electron integrals) also depends on the number of sampling points in the reciprocal space. A dense Monkhorst [63] and Gilat net [64] were defined with a total of 133 and 793 k-points in the reciprocal space, respectively, corresponding to the shrinking factors of 12 and 24. But for the calculation of the elastic constants a Gilat net was defined with a total of 150 k-points in the reciprocal space, corresponding to a shrinking factor of 8. In order to achieve the convergence, we had to use this smaller k-points net in the later case.

4.7.1 Total Energy

The total energy E of MgB_2 has been calculated at different primitive cell volume and it was minimized as a function of the c/a ratio for selected values of volume. Then the energy was plotted as a function of normalized volume V_n ($=V/V_0$) for HF and DFT approaches, respectively.

The zero pressure bulk modulus B_0 and its pressure derivative B_0'($=dB_0/dP$) were determined by fitting Murnaghan equation of state, equation (4.28), as detailed elsewhere [65]:

$$\Delta E(V) = E - E_0 = B_0 V_0 \left[\frac{V_n}{B_0'} + \frac{1}{1 - B_0'} - \frac{V_n^{1-B_0'}}{B_0'(B_0' - 1)} \right] \tag{4.28}$$

where E_0 is the equilibrium energy. The pressure was then obtained from normalized primitive-cell volume, V_n (=V/V_0, V_0 being the equilibrium volume) through the thermodynamic relationship:

$$P = -\frac{dE}{dV} = \frac{B_0}{B_0'} \left[V_n^{-B_0'} - 1 \right] \tag{4.29}$$

The normalized cell volume (V_n) is then plotted as a function of the calculated pressure. The pressure dependence of the lattice parameters of MgB_2 are also tested and the linear bulk modulus (B_{a0} and B_{c0}) and their respective pressure derivatives (B_{a0}' and B_{c0}') by fitting Murnaghan equation of state, equation (4.29), with the calculated data of the present work.

4.7.2 Elastic Constants, C_{ij}

The elastic constants are defined as the second derivatives of the ground state energy with respect to strain components ($\partial \varepsilon_i$). Mathematically it can be generally written as,

$$C_{ij} = 1/V \cdot \frac{\partial^2 E}{\partial \varepsilon_i \partial \varepsilon_j} \tag{4.30}$$

where E and V are the energy and volume of the unit cell.

There are five independent components of the elasticity tensor for MgB_2, instead of three as in the cubic case. These elastic constants are usually denoted by C_{11}, C_{12}, C_{13}, C_{33} and C_{44} (or C_{55}). It is very difficult to calculate the elastic constants for hexagonal systems because of its low symmetry rather than the cube systems. The elastic constants are defined by means of a Taylor expansion of the total energy of the system E(V,δ), with respect to

a small strain δ of the lattice of volume V. The Bravais lattice spanned by three vectors are written in a form R = ($\sqrt{3}/2$ -1/2 0; 0 1 0; 0 0 c/a). We can express the energy of a strained system [66]:

$$E(V,\delta) = E(V_0,0) + V_0\left[\sum_i \tau_i \xi_i \delta_i + \frac{1}{2}\sum_{ij} C_{ij}\delta_i \xi_j \delta_j\right] \qquad (4.31)$$

where $E(V_0,0)$ = energy of the unstrained system with volume V_0. τ_i is an element in the stress tensor, ξ_i is a factor to take care of Voigt index [66].

Now we concentrate our attention in determining the elastic constants. The lattice distortions employed here are those given by Fast et al. [66]. To calculate five independent elastic constants we have to require five different strains. The distortions applied in the present elastic property study of MgB_2 and the corresponding energies are as follows [66, 32]:

(a) Distortion that changes the size of the basal plane, keeping z-axis constant (symmetry of the strained lattice is still hexagonal):

$$D_1 = \begin{pmatrix} 1+\delta & 0 & 0 \\ 0 & 1+\delta & 0 \\ 0 & 0 & 1 \end{pmatrix} \qquad (4.32)$$

$$E(V,\delta) = E(V_0,0) + V_0\left[(\tau_1 + \tau_2)\delta + (C_{11} + C_{12})\delta^2\right] \qquad (4.33)$$

(b) Distortion in which z-axis is kept constant, x axis increases and y axis decreases by equal amount (symmetry of the strained lattice is monoclinic):

$$D_2 = \begin{pmatrix} 1+\delta & 0 & 0 \\ 0 & 1-\delta & 0 \\ 0 & 0 & 1 \end{pmatrix} \qquad (4.34)$$

$$E(V,\delta) = E(V_0,0) + V_0\left[(\tau_1 - \tau_2)\delta + (C_{11} - C_{12})\delta^2\right] \qquad (4.35)$$

(c) Distortion that stretches z axis, keeping other axes unchanged (shear maintains hexagonal symmetry):

$$D_3 = \begin{pmatrix} 1 & 0 & 0 \\ 0 & 1 & 0 \\ 0 & 0 & 1+\delta \end{pmatrix} \tag{4.36}$$

$$E(V,\delta) = E(V_0,0) + V_0\left[(\tau_3\delta + \tfrac{1}{2}C_{33}\delta^2\right] \tag{4.37}$$

(d) Distortion that preserves the symmetry but changes the volume:

$$D_4 = \begin{pmatrix} 1+\delta & 0 & 0 \\ 0 & 1+\delta & 0 \\ 0 & 0 & 1+\delta \end{pmatrix} \tag{4.38}$$

$$E(V,\delta) = E(V_0,0) + V_0\left[(\tau_1 + \tau_2 + \tau_3)\delta + \tfrac{1}{2}(2C_{11} + 2C_{12} + 4C_{13} + C_{33})\delta^2\right] \tag{4.39}$$

(e) Volume conserving triclinic distortion:

$$D_5 = \begin{pmatrix} 1 & 0 & \delta \\ 0 & 1 & 0 \\ \delta & 0 & 1 \end{pmatrix} \tag{4.40}$$

$$E(V,\delta) = E(V_0,0) + V_0\left[(\tau_5\delta + 2C_{44})\delta^2\right] \tag{4.41}$$

The improvements in accuracy and speed of the program due to the availability of high-speed computers allow us to evaluate the elastic constants of simple highly symmetric systems by computing numerically the second derivatives of the energy. Thus imposing the above-mentioned distortions we have calculated the total energy by means of *ab initio* DFT method. The corresponding energy expressions of the applied distortions have been used to evaluate the elastic constants. To evaluate the elastic constants third-order polynomials were fitted to the data.

4.7.3 Electronic Band Structure Calculation

We already mentioned that DFT method has been used to calculate the band structure of MgB_2. A byproduct of DFT eigenvalues for periodic system is the associated band structure. In other words, the spectrum of the energy eigenvalues of a periodic system is the band structure. So, the lattice periodicity of a crystal has important consequences for the dynamics of the electrons. Each level of the isolated atom spreads out to form a band of allowed electron energies. The electronic band structure determines the electronic properties of the crystal. In the present calculation, seven lines have been explored in the reciprocal space for evaluating the electronic band structure of MgB_2. Eight bands have been evaluated starting from the initial band 8 to the final band 15. Total number of equal spaced 133 k-points has been used along each of these lines by introducing the value of the shrinking factor 12.. The calculations are done at equilibrium (P = 0) and under pressures of P = - 24 GPa and P = 38 GPa while all the conditions are kept undisturbed. A similar band structure calculation was done for fewer symmetry directions and shorter energy ranges in order to get a broader vision of the bands, which would help us to make comments on electronic structure. In the later case, 9 to 14 bands have been considered by exploring five lines. We have also been done the same calculations for the band of MgB_2.

4.7.4 Density of States (DOS) Evaluation

The electronic density of states (DOS) is treated as a qualitative instrument for understanding the electronic structure of any material. Especially it is very useful in the point of view of the projected density of states (PDOS). Projected density of states are a useful means for characterizing in a

synthetic way the crystalline orbitals (COs) associated with the various energy levels and for analyzing the ground state wave function from a physical point of view [50]. According to PDOS, the states are attributed to the basis functions and then to the atoms of the unit cell. The total DOS is then written as a sum over atomic contributions. The DOS is calculated by using the expression [46],

$$n(\varepsilon) = 2\sum_{n,\kappa}\delta\left(\varepsilon - \varepsilon_n^{\kappa}\right) = \left(2/V_{BZ}\right)\sum_{n}\int\delta\left(\varepsilon - \varepsilon_n^{\kappa}\right)d\kappa \qquad (4.42)$$

and the number of electron in the unit cell is given by, $\int_{-\infty}^{\varepsilon_F} n(\varepsilon)\,d(\varepsilon)$.

In the present study, 8 to 15 bands have been considered for the corresponding density of states (DOS) calculation and fourteen Legendre polynomials have been used to expand the DOS.

4.7.5 Electron Charge Density (ECD)

To examine the effects of volume (and hence pressure) on the electronic band structure near the Fermi level (E_F) we chose the maximum change in V_n in such a way that pressure P lies in the range -25 to 40 GPa. At each volume within the range the structural parameters have been optimized and the energy bands and density of states were calculated. The full BZ are spanned in such a way that Γ-M-K-Γ-A-L-H-A directions are covered. The Γ-M-K-Γ lines are in the basal plane, while A-L-H-A lines are on the top of the plane at k_Z.

4.7.6 Electric Field Gradient (EFG)

The theoretical measurement of the electric field gradient (EFG) is very important for a better understanding of the experimental results. We determined EFG from the first principles i.e. using *ab initio* technique. The general expression for the principal component of the EFG tensor, arising from a charge density, $\rho(\mathbf{r})$, is defined as [46],

$$V_{zz} = \int \rho(\mathbf{r}) \frac{2P_2(\cos(\theta))}{r^3} d\mathbf{r} \qquad (4.43)$$

where P_2 is the second order Legendre polynomial. Thus once the charge density of a system is known accurately, the EFG can be obtained.

The EFG tensor was calculated directly from the SCF-HF-DFT electron density. The coordinate axes are chosen in such a manner that V_{zz} is the EFG component along the crystallographic c-axis. Then the tensor is completely characterized by two parameters: the largest component V_{zz} and the axial asymmetry parameter η defined by $\eta = |V_{xx} - V_{yy}| / |V_{zz}|$.

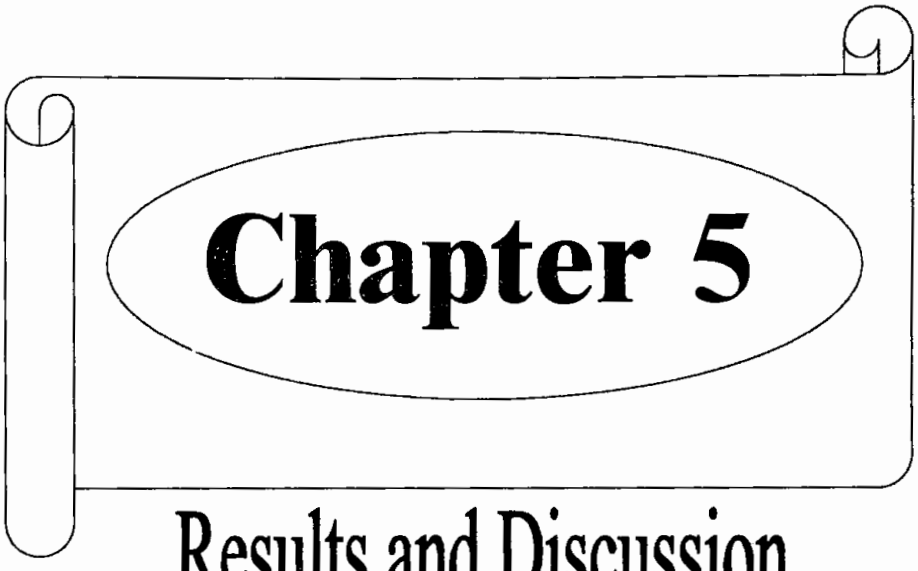

Results and Discussion

CHAPTER 5

RESULTS AND DISCUSSION

5.1 Introduction

The results of our investigations on the newly discovered magnesium diboride, MgB_2 superconductor are organized in the present chapter. The ground states total energy and the structural properties of magnesium diboride are reported. The relations among various parameters and their pressure dependence are demonstrated by suitable figures. In the present study we have determined five elastic constants, bulk modulus and the pressure derivatives of bulk modulus for MgB_2. The foremost interest of the investigations was to calculate the electronic bands and to focus it in the light of superconductivity in MgB_2. The structure and behaviour of the bands are studied with a pressure range of ~ -25 GPa to ~ 40 GPa. The corresponding partial and total density of states (DOS) are then evaluated and analyzed. In addition, we present here the charge density of MgB_2 for (110) plane. Finally, a short discussion is made on the electric field gradient (EFG) evaluation.

5.2 Structural and Mechanical Properties of MgB_2

The ground state properties of MgB_2 have been obtained by minimization of the total energy with respect to the unit cell volume. A uniform compression and expansion of the lattice were used to make isotropical variation of the unit cell volume [67]. Our calculated total energy of MgB_2 is shown as a function of the cell volume in figure 5.1. Figures 5.1(a) and 5.1(b) show the

energy versus volume data for two different *ab initio* calculations - HF and DFT, respectively. It was necessary to perform 20 independent calculations over a range of volumes and c/a ratio. The energy was minimized as a function of the c/a ratio for selected values of volume. The calculated c/a ratio has been plotted as a function of normalized volume and is shown in figure 5.2(a) along with the result (open square) from [68]. The energies ΔE (= $E-E_0$, where E_0 is the minimum or equilibrium energy) of MgB_2 calculated at different primitive cell volume (V) have been shown in figures 5.2(b) and 5.2(c) as a function of the normalized volume V_n (=V/V_0, where V_0 is the equilibrium volume) respectively for HF and DFT methods. The data points of figures 5.2(b) and 5.2(c) are fitted by the Murnaghan equation of state (4.28) to obtain the lattice parameters of the equilibrium structure and then to determine the bulk modulus by analyzing the fitting parameters. The optimized lattice parameters of MgB_2 are: a = 3.0889 Å and c = 3.5337 Å. We observed that these values are in excellent agreement with the experimentally measured values: a = 3.086 Å and c = 3.524 Å [1]. We have used these calculated values of the lattice parameters all through our investigations for a variety of properties of MgB_2.

The pressure dependence of volume (V) of MgB_2 is obtained through the thermodynamic relationship (4.29). The resulting pressure dependence of volume (V) as well as normalized primitive cell volume (V_n) of MgB_2 is shown in figure 5.3. It is obvious from figure 5.3(b) that the pressure dependence of normalized volume is almost independent of HF or DFT approach. On the other hand, the volume gradually decreases with the increase of pressure. Figure 5.4 shows the pressure dependence of the normalized lattice constants of MgB_2. The results (open circle) of ref. [68] over a pressure range of P = 0-12 GPa have been plotted along with our

calculated data in figure 5.4. The figure shows evidence of a very good harmony between these two sets of data. The variation of lattice parameters with pressure is illustrated in figure 5.5 as well. Our calculated results for lattice parameters, equilibrium volume and bond distance (nearest neighbour distance) of Mg atoms and B atoms are presented along with some other available experimental and theoretical data in Table 5.1.

For solids with isotropic compression, the mode Grüneisen parameter γ of zone-centre phonons are ~1. Loa *et al.* [29] assumed this to be 1 while estimating $d\ln T_c/dP$ using McMillan's formula for T_c. In doing so they had to choose an exceptionally small $\mu^*= 0.04$ in order to reproduce the measured T_c. In fact the expression for $d\ln T_c/dP$ contains λ (electron-phonon coupling), pressure dependence of density of state $d\ln N(0)/dP$ and $\gamma = B_0 d\ln\omega/dP$. Apart from other reasons smaller γ would require small μ^*. Recently Goncharov *et al.* [68] determined γ to be 2.9±0.3. Utilizing $\lambda = 0.9$ [17], $d\ln N(0)/dP = - 0.004$ GPa^{-1} [11], $\mu^* = 0.1$, and the experimental value of $dT_c/dP = -1.9$ K/GPa [7], we estimate $\gamma \sim 1.88 - 2.35$ with $B_0 = 120 - 150$ GPa. If we ignore pressure dependence of density of states then these values become 2.21 and 2.77, respectively. Thus we find γ to be substantially larger than 1, which is expected for phonon in a compound with covalent bonding like graphite. For iron with partial metallic bonding $\gamma = 1.7$ [69]. Thus for MgB_2 we should not expect γ to be ~1 as has been assumed in ref. [29]. It is to be noted that larger γ is usually associated with enhanced anharmonicity of the particular normal mode of vibration, and is broadly consistent with theoretical prediction for the E_{2g} in-plane B stretching mode [68].

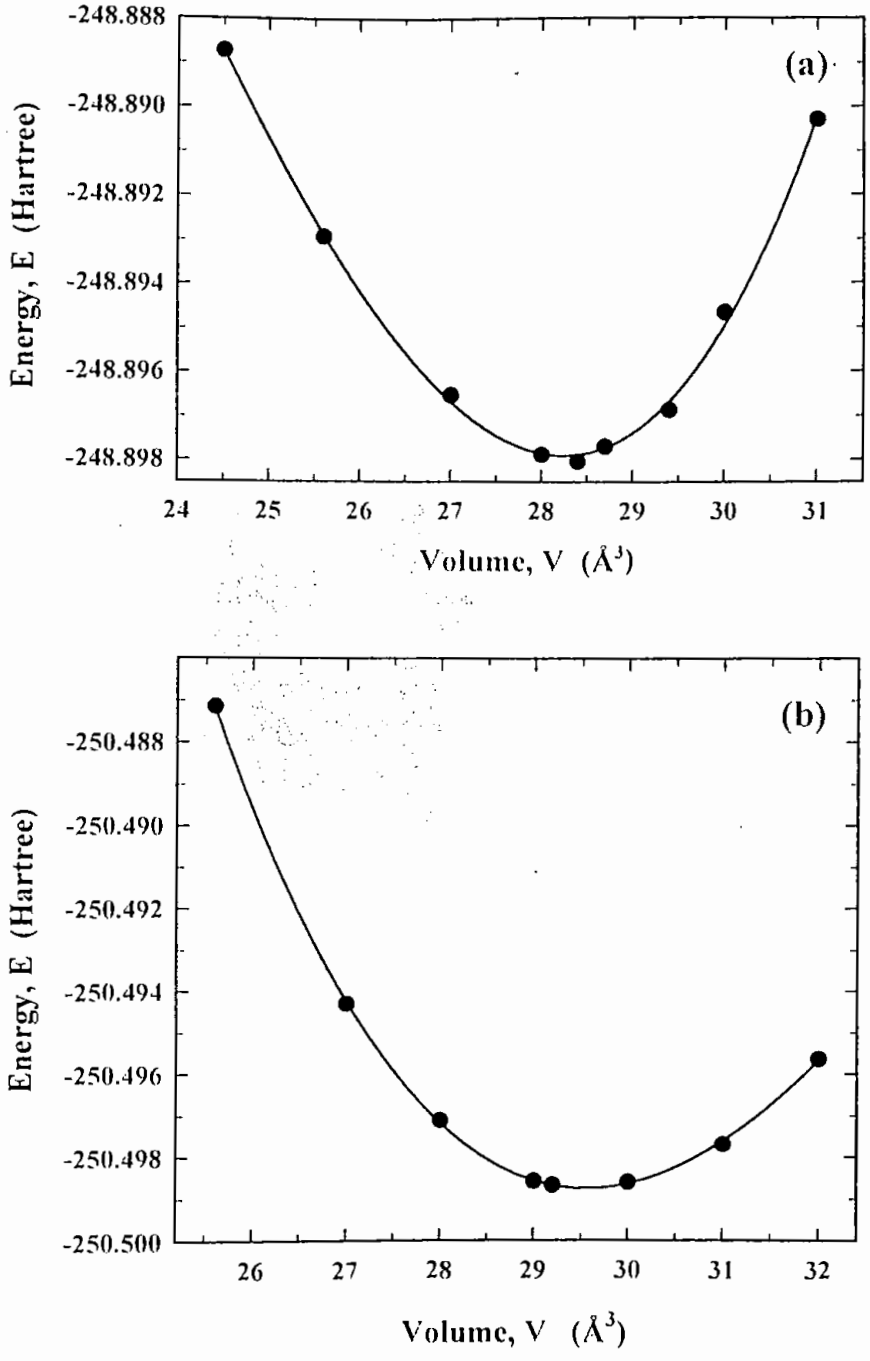

Figure 5.1. The energy of MgB_2 as a function of the primitive cell volume calculated by (a) HF method and (b) DFT method. The solid lines through the data points are the resulting fits of Murnaghan equation of state.

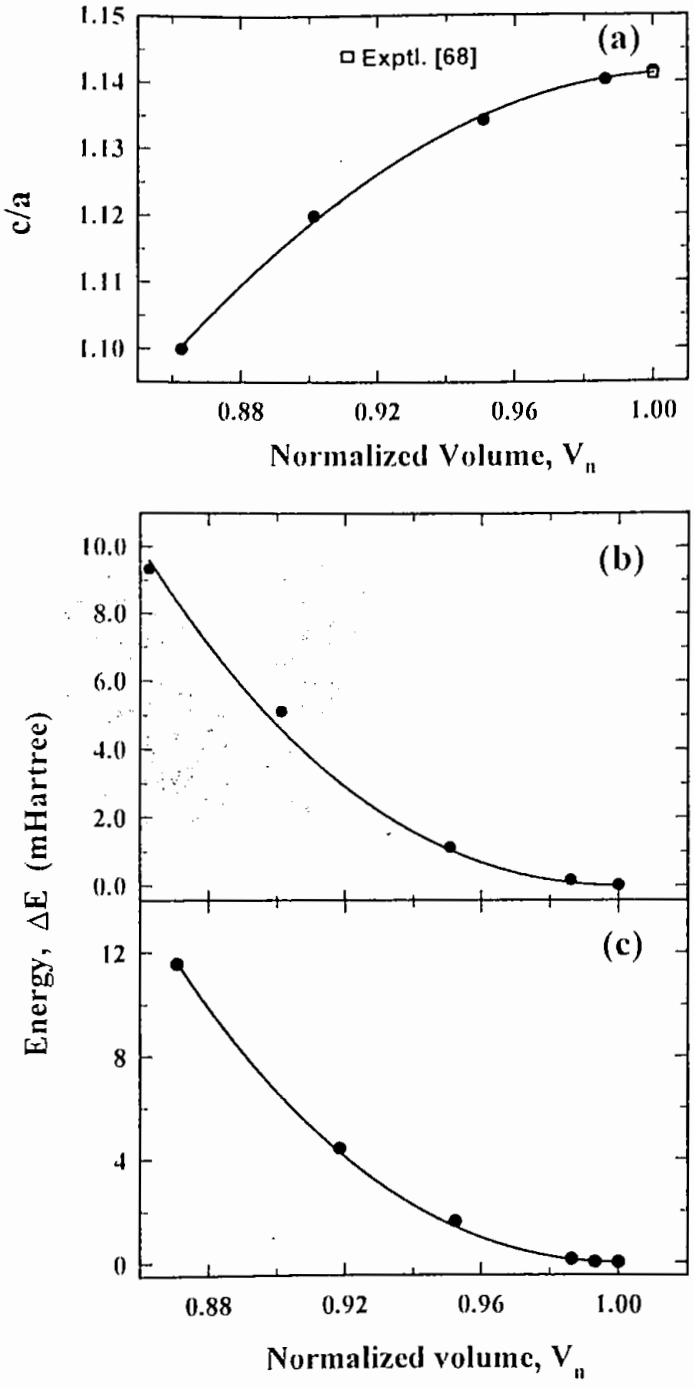

Figure 5.2. (a) Lattice parameter ratio, c/a as a function of normalized cell volume, V_n. (b) Energy ΔE ($E-E_0$) as a function of V_n for HF calculation. (c) Energy ΔE as a function of V_n for DFT method.

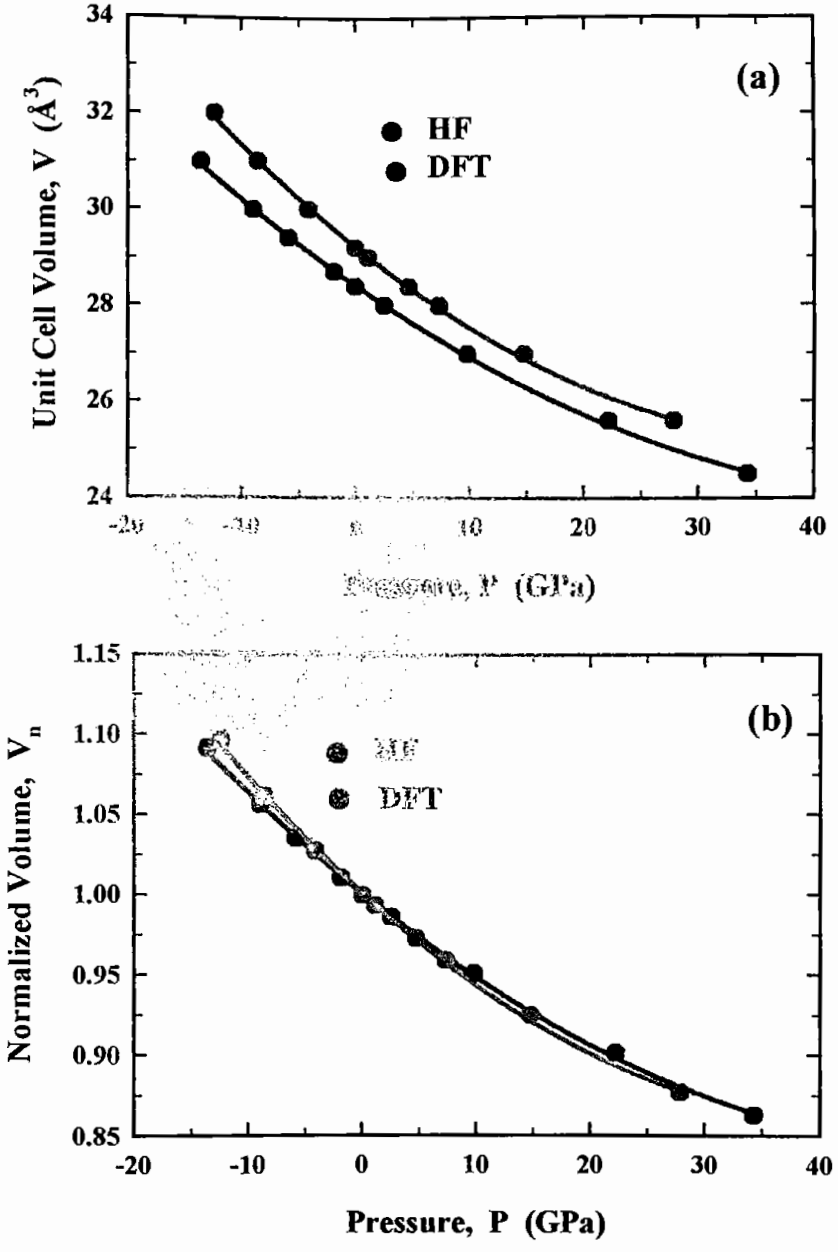

Figure 5.3. (a) Pressure dependence of unit cell volume of MgB2- a comparison between two *ab initio* calculations. (b) Pressure dependence of normalized volume - a comparison between two *ab initio* calculations.

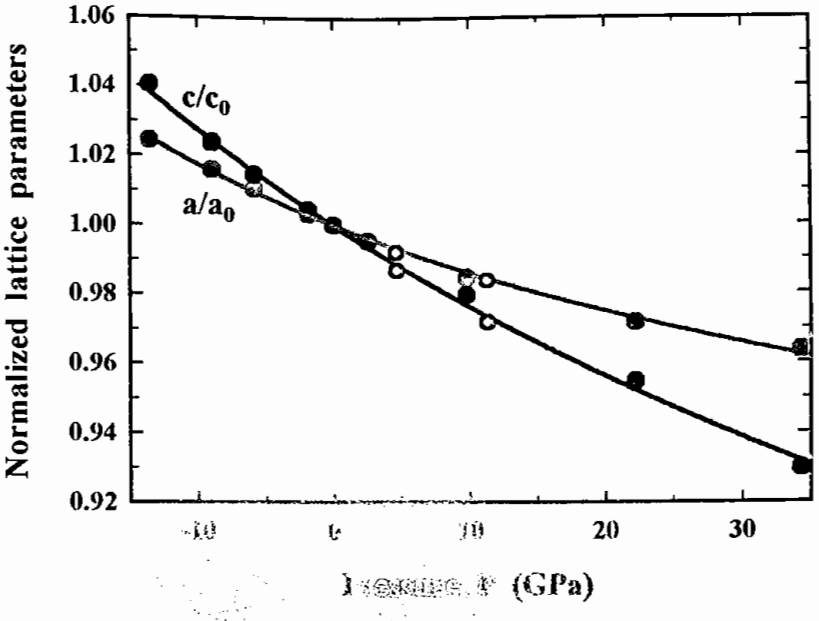

Figure 5.4. Pressure dependence of the normalized lattice parameter of the MgB_2. The curves through the data points are the fits to the Murnaghan equation of state. The open circles correspond to measured values [68] for P=0-12 GPa.

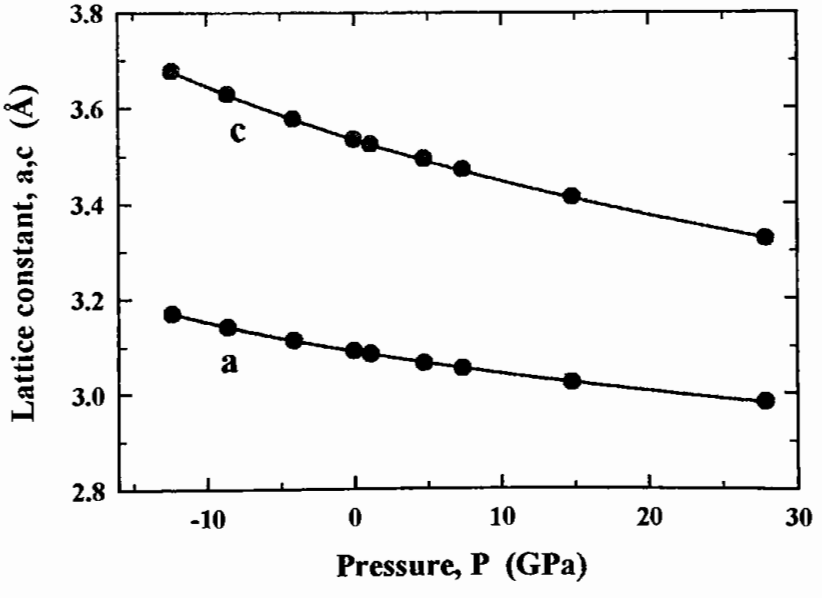

Figure 5.5. Lattice constants (a, c) as a function of pressure of MgB_2.

Table 5.1. Experimental and theoretical information on structural parameters of MgB_2 at equilibrium condition.

	Calc.	a(Å)	c(Å)	c/a	V(Å^3)	Mg-B	B-B	Ref.
Theoretical	LCAO-DFT	3.089	3.534	1.144	29.199	2.510	1.783	Present
	LCAO-HF	3.064	3.493	1.140	28.399	2.486	1.769	Present
	FP-LAPW	3.075	3.527	1.147	28.882	-	-	[10]
	DFT	3.065	3.519	1.148	28.629	-	-	[30]
	FP-LMTO	3.084	3.522	1.142	29.010	2.504	1.781	[36]
	LMTO-TB	3.071	3.528	1.149	28.815	-	-	[23]
	FLAPW	3.089	3.548	1.149	29.319	-	-	[70]
Experimental	SQUID & X-ray Diffrac.	3.086	3.5224	1.141	29.051	-	-	[1]
	TDPAC	3.075	3.519	1.142	28.816	-	-	[10]
	Magneto-Transport	3.140	3.520	1.121	30.056	-	-	[3]
	X-ray powder diffrac.	3.086	3.521	1.141	29.039	-	-	[70]
	Neutron Powder Diffrac.	3.085	3.521	1.141	29.021	-	-	[4]

]

5.2.1 Elastic Constants, C_{ij}

There are five independent components of the elasticity tensor for MgB_2, instead of three as in the cubic case. With these five distinct lattice deformations, we have calculated the energy using the appropriate expressions (equations (4.30) to (4.41) in chapter 4). The dependence of calculated strain energy, ΔE $[E(V,\delta) - E(V_0,\delta)]$ on deformation δ is shown in figures 5.6 and 5.7. It is important to discuss the positions of boron used in the calculation particularly in distortions of figures 5.6(b) and figure 5.7(c). We illustrate at this time the case of figure 5.6(b). Here the positions of atoms (in Å) for δ = 0.01 are Mg (0, 0, 0), B (-3.404, 0, -3.305), B (-1.702, -2.889, -3.305). These may be compared with the positions before deformation: Mg(0,0,0), B(-3.305,0,-3.305), B(-1.685,-2.919,-3.305). This corresponds to changes in the crystallographic cell edges and angles in the range $\leq$0.05 Å and $\leq$0.51°, respectively. The case of figure 5.7(c) is not much different from this scenario. The coordinates of Mg and B atoms were not optimized each time the lattice was deformed. This should not affect the results for $C_{11}+C_{12}$ (Equation 4.33) and C_{13} (Equation 4.39), as the site symmetries and the Bravais lattice remain unchanged in these cases. The maximum deformation was kept under $\pm$1% of the equilibrium lattice parameters in order to reduce the influence of the higher order terms in the expansion of the strain energy. The deviation from zero deformation of the minimum in the strain energy curve for cases figure 5.6(a) and figure 5.7(c) is due to the fact that the algorithm used to search for the structure of minimum energy was not exhaustively iterated. Similar effect was observed by Perottoni et al. [71] for TiB_2, where corrections for the lattice parameters were less than 0.5%. Third order polynomials were fitted to the data in

figures 5.6 and 5.7 from which five elastic constants of MgB_2 were calculated according to appropriate expressions given in chapter 4. It is to be noted at this point that the third order component of the fit which affects the total energy by an amount which is less than an order of magnitude compared with the second order term. The results of the calculated elastic constants are given in Table 5.2 along with those from the full potential LMTO calculations of Ravindran et al. [32] for MgB_2. Experimental values of elastic constants are not yet available for comparison. Thus for the purpose of comparison the room-temperature experimental values of a similar type material TiB_2 due to Spoor et al. [72] have been shown in the table. Our values are found to be comparable with those due to Ravindran et al. [32]. The largest discrepancy is observed for C_{12} (Figure 5.6).

At this point it is not possible to distinguish clearly the advantage or disadvantage of the present method over FPLMTO. The two methods use different approaches to the problems, but both of these allow total energy calculations to be done for arbitrary crystal structures. The energy is evaluated directly with inclusion of exchange and correlation effects in both the methods. To improve our Fock matrix at the self-consistent-field cycle j was made equal to $F_j^{new} = (1-m)F_j + mF_{j-1}$, where m is a mixing parameter equal to 0.3 [45, 50]. The present DFT technique has been shown [16, 71] to yield better estimates of energy despite approximate treatment of correlation effects. This, however, may not be always true for properties that depend on energy derivatives.

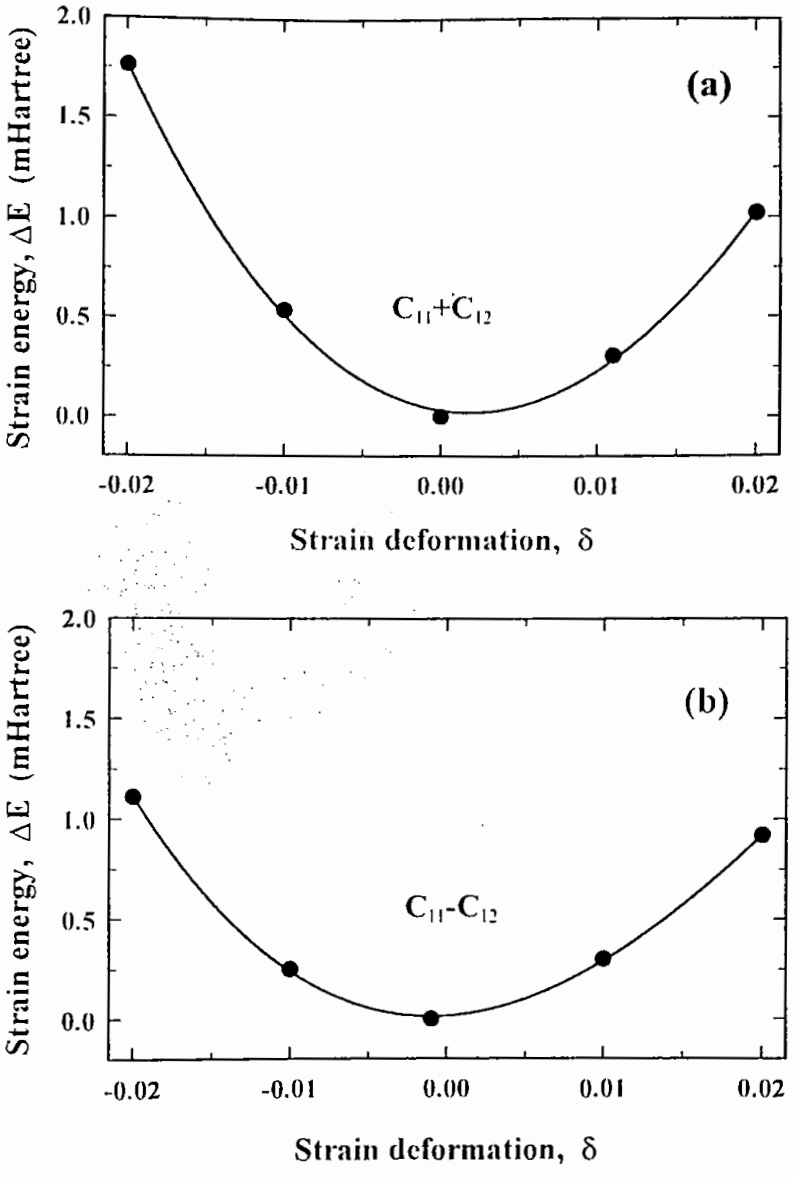

Figure 5.6. Strain energy ΔE as a function of the lattice deformation δ for elastic constants (a) $C_{11} + C_{12}$ and (b) $C_{11} - C_{12}$. The solid curves represent the third order polynomials fitting of the data.

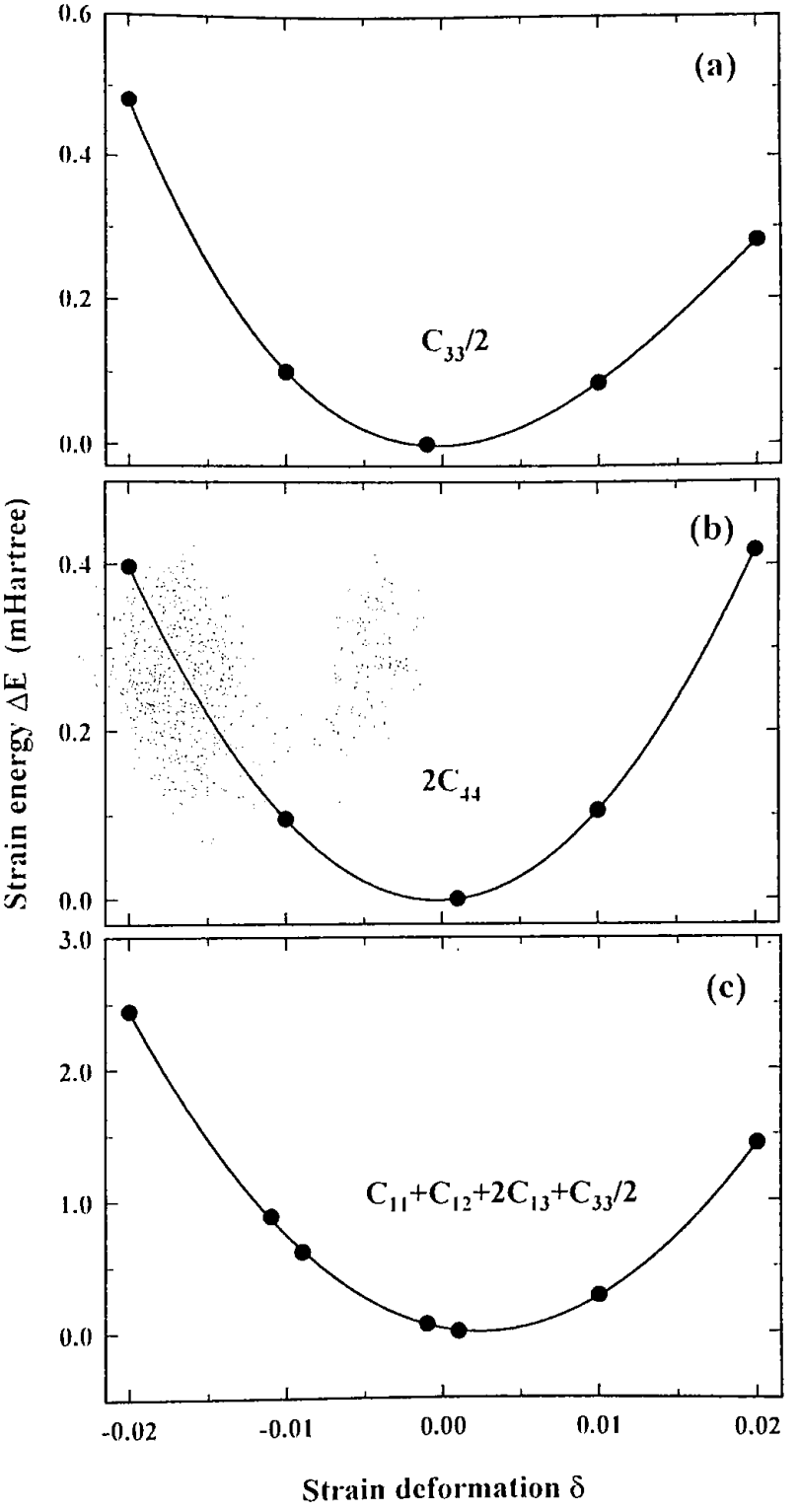

Figure 5.7. Strain energy ΔE as a function of the lattice deformation δ for elastic constants (a) C_{33}, (b) C_{44} and (c) C_{13}. The solid curves represent the third order polynomials fitting of the data.

The tendency of the type of calculations presented here to overestimate some elastic constants including C_{12} has been pointed out by several authors (see Ref. [71]). Moreover the values for the combinations $C_{11}+C_{12}$ and $C_{11}-C_{12}$ are found to vary depending upon the particular functionals used for the exchange-correlation.

Table 5.2. Elastic constants C_{ij} and bulk modulus B (calculated from the elastic constants) of MgB_2 and TiB_2 (in GPa).

Ref.	C_{11}	C_{12}	C_{13}	C_{33}	C_{44}	B_{iso}
Present	446	68	39	284	77	158
[32]	438	43	33	264	80	150
[72]*	660	48	93	432	260	244

* Experimental value for TiB_2.

5.2.2 Bulk Modulus and its Pressure Derivative

We calculated the isotropic bulk modulus B_{iso} (given in table 5.2), obtained under the assumption that the c/a ratio remains unchanged when the lattice is subjected to an isotropic stress [66],

$$B_{iso} = \frac{2}{9}(C_{11} + C_{12} + 2C_{13} + \frac{1}{2}C_{33}) \quad (5.1)$$

The set of calculated elastic constants gives B_{iso} = 163 GPa. This may be compared with the bulk modulus obtained through the analysis of the data from figure 5.2(c). The solid curve in figure 5.2(c) is the resulting fit of Murnaghan equation of state [16, 65]. The fit yielded B = 163 GPa and 167 GPa with dB/dP = 4 and 3.5, respectively. Thus the value is in very good agreement with that obtained from our calculated elastic constants.

The linear bulk modulus at P = 0 along the crystallographic axes a and c (B_{a0} and B_{c0}) and their pressure derivatives are also obtained by fitting equation (4.29) to data of figures 5.4 and 5.5. The linear bulk moduli B_{a0} and B_{c0} and their pressure derivatives are shown in Table 5.3. The anisotropy in bonding of MgB_2 is illustrated in figure 5.4. As the pressure increases from 0 to 10 GPa, the c/a ratio decreases by 0.51%. Compression along the c-axis is larger than along the a-axis, consistent with the comparatively weaker Mg-B bonds that determine the c-axis length. The result is in line with the measurements at room temperature [73], but of a larger magnitude. A similar but smaller anisotropy has been seen for TiB_2 [71]. The layered cuprates show much larger (~a factor of 2) compression anisotropy [4]. The fitted values for B_{a0}, B'_{a0}, B_{c0}, B'_{c0} clearly reveal the diversity in bonding interactions present. MgB_2 is less compressible in the basal plane, in which the covalent B-B bonds lie. The interlayer linear

compressibility, d*l*nc/dP = 0.00204 GPa^{-1} is ~1.4 times larger than the in-plane value (d*l*na/dP = 0.0015 GPa^{-1}). It is worth noting that the structurally related alkali-metal intercalated graphite is strongly anisotropic (see [74]) with interlayer compressibility about ten times larger than the corresponding value in MgB_2.

We furthermore estimated the zero-pressure bulk modulus B for a single crystal with hexagonal symmetry, when there is no constraint on the c/a dependence on lattice strain. The expression for this is given below [66, 75],

$$B = \frac{C_{33}(C_{11}+C_{12})-2C_{13}^2}{C_{11}+C_{12}-4C_{13}+2C_{33}} \qquad (5.2)$$

Our calculated data in Table 5.2 yields B = 158 GPa. The isotropic bulk modulus B_{iso} is about 3.4% above the value obtained when there is relaxation of c/a ratio, equation (5.2). The corresponding value is ~2.3% for TiB_2 [71], indicating a similar but smaller anisotropy for this compound TiB_2. The layered cuprates show much larger (a factor ~2) compression anisotropy [4]. Equation (5.2) cannot be used for this strong anisotropic case due to lack of elastic constant data. We may further compare the degree of anisotropy in the linear compressibilities of the two diborides. The values of the linear bulk modulus along the a-axis and the c-axis for MgB_2 are 793 GPa and 446 GPa, respectively. We obtain these using appropriate expressions for hexagonal crystals given in Ref. [32]. The corresponding values for these linear bulk moduli are 1031 GPa and 675 GPa, respectively, for TiB_2. MgB2 is less compressible in the basal plane, in which the covalent B-B bonds lie. Further the interlayer linear compressibility d*l*nc/dp is ~1.4 times larger than the in-plane value [16]. It is to be noted that the structurally related alkali-metal intercalated graphite is strongly

anisotropic with interlayer compressibility ~ 10 times larger than the corresponding value in MgB_2 [74].

The comparison between the isotropic and fully relaxed bulk moduli may suggest that MgB_2 is less anisotropic than one would think on the basis of its 'planar' crystal structure. The same observation was made earlier for TiB_2 [71], which was further corroborated by a study of the directional dependence of Young and bulk moduli. It is, therefore, likely that in MgB_2 also the interaction between B planes are not negligible and should be taken into account for a better understanding of the origin of the mechanical behaviour.

Table 5.3. Bulk modulus, pressure derivative of bulk modulus and their in- and out-of-plane linear values for MgB_2 superconductor.

Method of calc.	B_0 (GPa)	B_0'	B_{a0} (GPa)	B_{a0}'	B_{c0} GPa)	B_{c0}'	Ref.
HF	122	3. 4	653	15.0	397	5.5	This work[#]
DFT	163 167	4.0 3.5	580	16.0	362	7.7	This work[#]
Synchrotron X-ray diffrac.	155	4.0	625	-	333	-	[68]
Synchrotron X-ray diffrac.	120	3.6	410	13.0	292	8.5	[74]
FPLAPW	143	3.46	-	-	-	-	[10]
FPLAPW	140	3.93	-	-	-	-	[29]
FLAPW	139	-	-	-	-	-	[11]
X-ray power diffrac.	151±5[a]						

[#] For entire pressure range.
[a] Experimental value

5.3 Electronic Properties of MgB_2

5.3.1 Band Structure and Pressure

The calculations of electronic band structure of MgB_2 superconductor have been performed by all-electron *ab initio* self-consistent-field HF-LCAO method, as described in the previous chapter, using DFT approach with generalized Gaussian Approximation. The basis-sets used in this band evaluation are explained in chapter 3 and presented in table 3.1 and 3.2.

To examine the effects of volume (and hence pressure) on the electronic band structure near the Fermi level (E_F) we chose the maximum change in V_n in such a way that pressure P lies in the range -25 to 40 GPa. At each volume within the range the structural parameters have been optimized and the energy bands and density of states were calculated. The full BZ are spanned in such a way that Γ-M-K-Γ-A-L-H-A directions are covered. The Γ-M-K-Γ lines are in the basal plane, while A-L-H-A lines are on the top of the plane at k_Z. Figure 5.8 shows the band structure of MgB_2 at the equilibrium volume (P = 0). Band structure at an extended volume (P = -24 GPa) is shown in figure 5.9(a) while figure 5.9(b) shows the band structure under a pressure of 38 GPa. The result for the same band structure calculation but with a wider energy range and along some additional symmetry directions, e.g., L-H-A are also illustrated in figures 5.10(a) and 5.10(b) for the applied pressure of –24 GPa and 38 GPa, respectively.

There are two distinct types of bands, both of which are contributed by boron. The upper part of the valence band is composed of B 2p-states which form two sets of bands with $\sigma(2p_{x,y})$ and $\pi(p_z)$ character. The general

features of the bands obtained in the present study are in very good agreement with results from other studies [23, 24, 26, 30, 35]. The $\sigma(2p_{x,y})$ band along Γ–A is double degenerate, quasi two-dimensional and makes a considerable contribution to DOS at Fermi energy, E_F for MgB_2. The existence of degenerate $p_{x,y}$-states above E_F at the Γ point in BZ has been shown to be crucial for superconductivity in MgB_2 [23]. The weaker ppπ-interactions result from B $2p_z$-bands. These 3D-like bands possess maximum dispersion along the Γ-A direction.

The band structure away from the equilibrium is shown in figure 5.9 and 5.10. The character of σ band is unchanged even after application of pressure as because the symmetry is not broken. The weak dispersion of the σ band along Γ–A reflects their particular quasi-two-dimensionality. The dispersion increases slightly with increase of pressure. The σ band crosses the Fermi surface at Γ point at a pressure of ~38 GPa (V_n= 0.85). When the σ band is below the Fermi surface, the σ bonding state is completely filled. Thus compression decreases the holes in the σ band. Neaton et al. [30] observed that the σ bands of MgB_2 are nearly free electron-like: their dispersion is parabolic near the Γ point, and their overall bandwidth is comparable to the free electron value (~15.5 eV). We find the same features and confirm their observation that the bandwidth (~15 eV) increases as pressure increases in line with that expected for free electrons.

A redistribution of carriers between σ and π bands occurs with the increase of pressure, and the number of holes in the σ band decreases, i.e., the top of the band moves down towards E_F and below. The strongly electron-phonon coupling results in splitting the σ band into two sub-bands [26]. With

application of pressure of 38 GPa the lower sub-band crosses E_F, thereby changing the Fermi surface topology. Tissen et al. [12] assumed that the Fermi level crosses the van Hove singularity in the DOS at $P \sim 9$ GPa, thereby causing the anomaly in $T_c(P)$ due to the electronic transition.

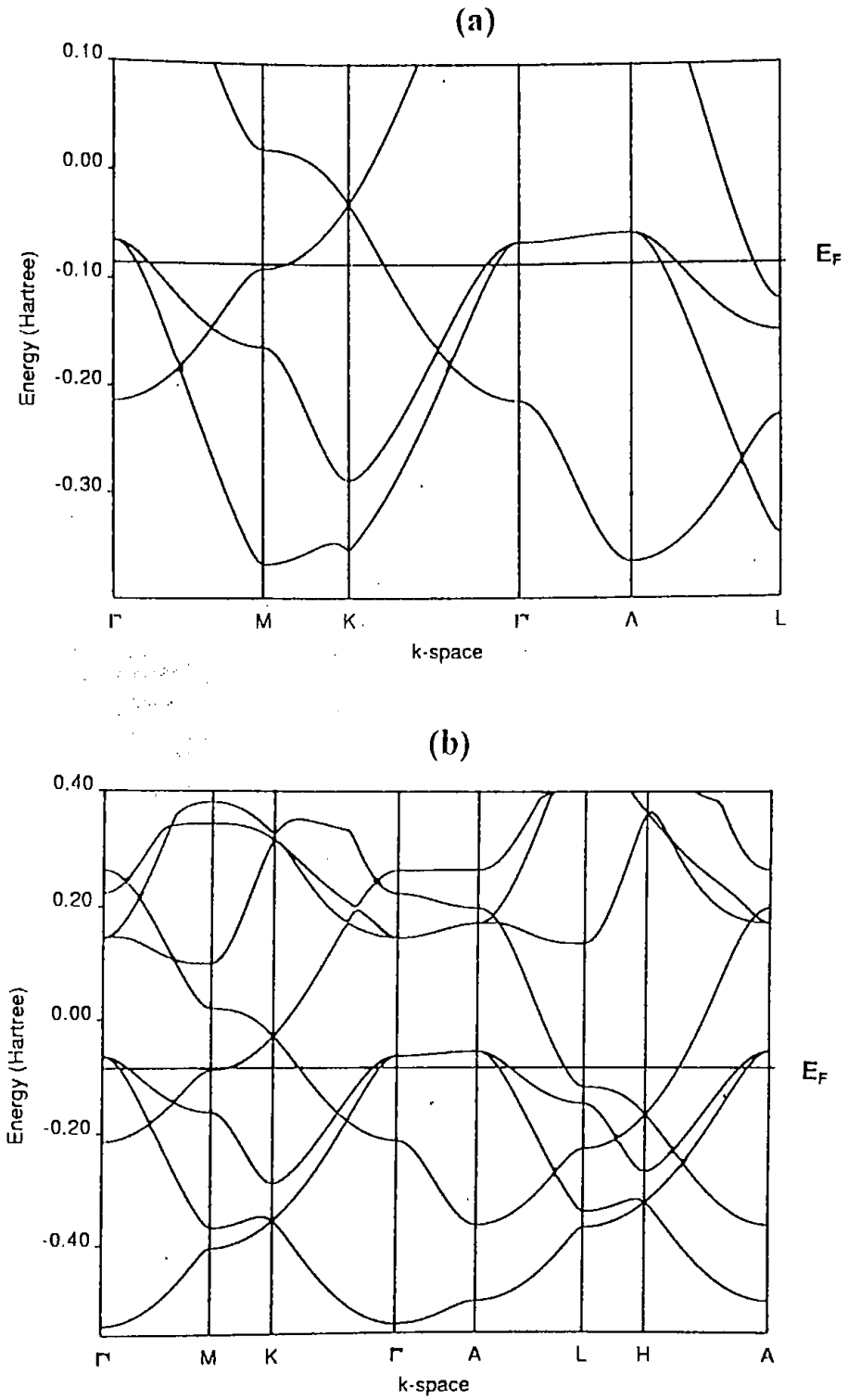

Figure 5.8. Band structure of MgB_2 at equilibrium i.e. P = 0; (a) enlarged view of the bands near Fermi energy and (b) bands along some additional symmetry directions and with a wider energy range.

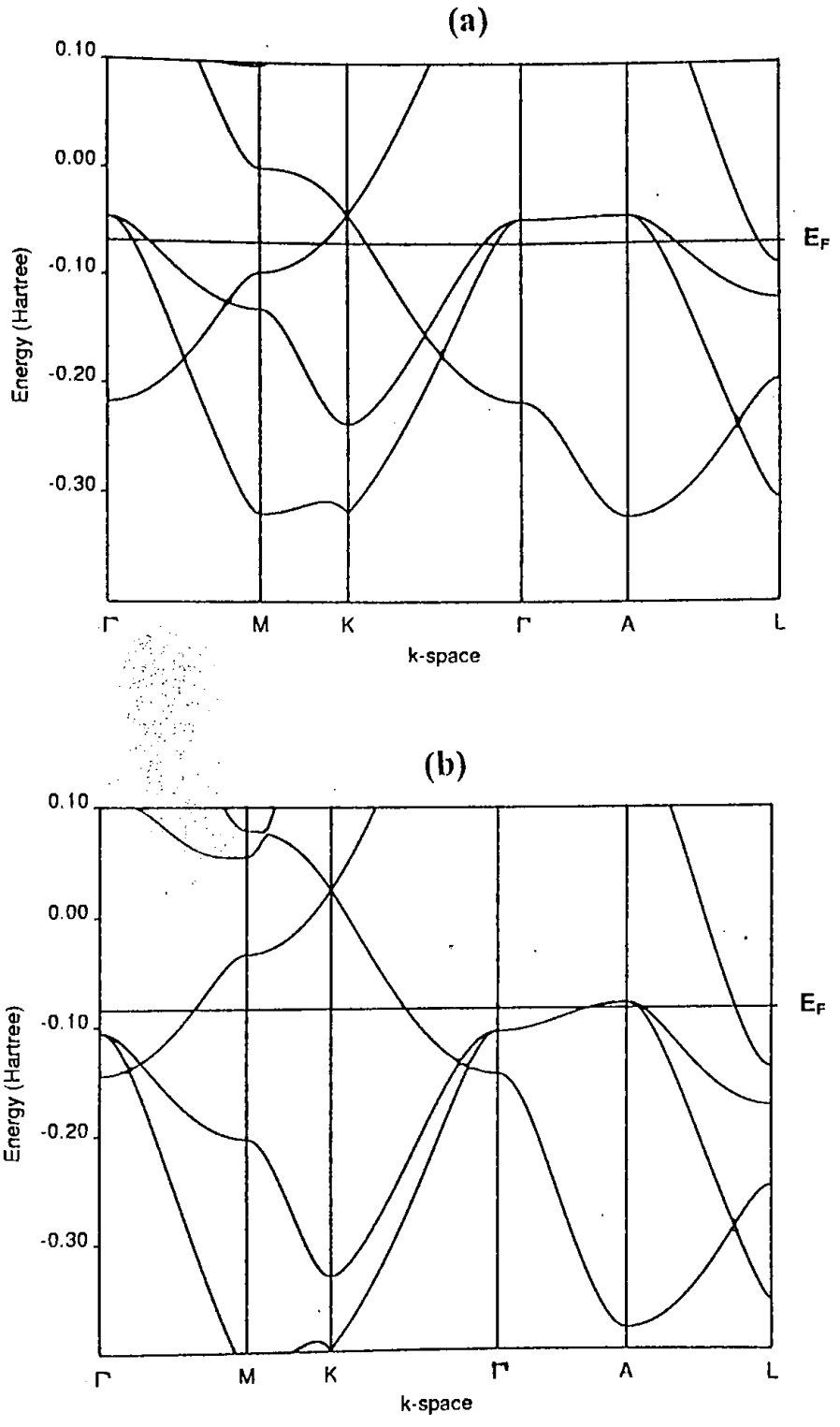

Figure 5.9. Band structure of MgB_2 (a) after expansion (V_n = 1.096, P = -24 GPa) and (b) under pressure (V_n= 0.85, P = 38 GPa).

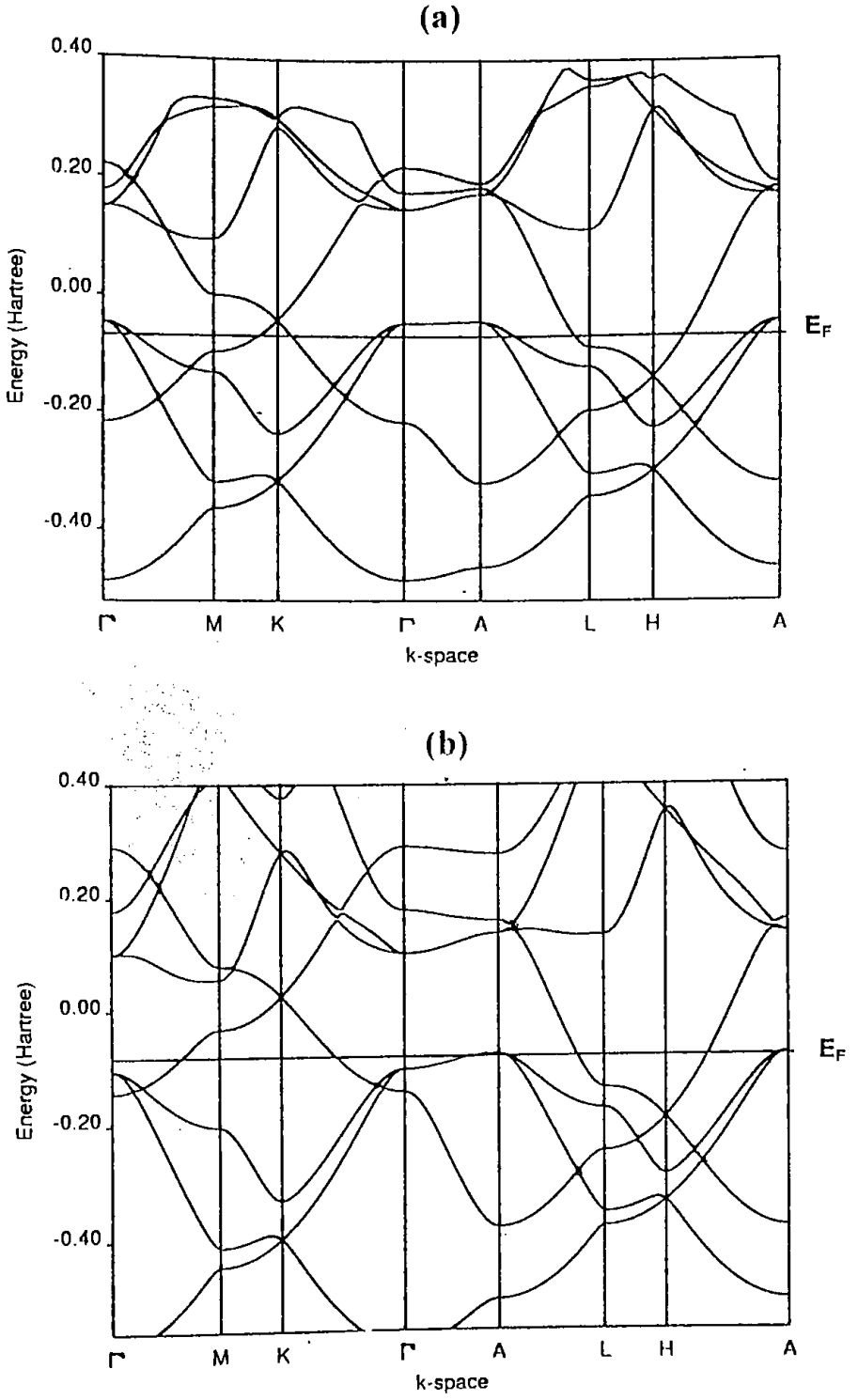

Figure 5.10. Band structure of MgB_2 over a wider energy range and along some additional symmetry directions; (a) after expansion (V_n = 1.096, P = -24 GPa) and (b) under pressure (V_n = 0.85, P = 38 GPa).

Our calculations do not indicate this to happen at a pressure as low as ~9 GPa. The results of Deemyad et al. [15] also support our findings. They measured the dependence of T_c on nearly hydrostatic pressure for an isotopically pure (^{11}B) MgB_2 sample. The analysis of $T_c(P)$ data to 20 GPa demonstrates that the monotonic decrease of T_c with pressure arises predominantly from the decrease in the coupling constant λ due to lattice stiffening, and not from electronic effects.

5.4 Density of States (DOS)

5.4.1 Density of States at Equilibrium and under Pressure

In figure 5.11, we have shown the total and partial electronic density of states near the Fermi level as a function of pressure. The figure 5.12 shows the total DOS over a wider energy range. The shape and locations of the bands shown in figures 5.8(b) and 5.10 are reflected in the density of states. The density of states $N(E_F)$ at equilibrium (P = 0) is 17.5 states/hartree. The value reduces to 12.5 states/hartree at P=38 GPa. Thus the DOS decreases by as much as 29% over this pressure increase. That the $N(E_F)$ increases as the lattice is expanded is contrary to expectation for a nearly-free electron metal. The result is in agreement with that of other workers [30, 31, 34]. This observation, via BCS equation, shows that T_c should decrease with the increase of pressure, a result in agreement with experiment for MgB_2 [12]. Neaton et al. [30] remarked that the dependence of the DOS on pressure is almost entirely due to the changes in the width and position of a considerable van Hove peak (~2 eV below the Fermi level). This originates from a saddle point in the highest occupied σ band at the M point. Further the decrease in bandwidth with decreasing pressure reduces the separation

between the peak and the Fermi level, enhancing DOS. The singularity is further enhanced by an increase in two-dimensionality.

5.5 Electronic Charge Density (ECD) at Different Pressures

The total charge densities of MgB_2 at different pressures for (1 1 0) plane are shown in figure 5.13 while the corresponding difference (crystal minus ionic superposition) charge density maps for the same plane are illustrated in figure 5.14. The nature of bonding in MgB_2 can be understood from the density plots of figures 5.13 and 5.14. Mg nuclei are located at the corners of the charge density map and B nuclei are at the (1/3, 1/2) and (2/3,1/2) positions. The density profile at zero pressure figure 5.13(a) and 5.14(a) show similar feature to that in ref. [29]. A low electron accumulation between Mg and B is indicated. Further the electron population in the Mg site is much lower than that for a neutral Mg atom. These indicate an ionic bonding between Mg and B. On the other hand, there is a strong covalent bonding between B-B atoms. This is evident by the maximum charge density (with a strongly aspherical character) at the bond middle. A somewhat homogeneous charge distribution between the Mg atoms indicates an appreciable degree of metallic bonding between them. Hence the charge density study provides the bonding behaviour in MgB_2 as a combination of covalent, ionic and metallic nature i.e. MgB_2 is a mixed bonded solid. The band structure also shows features similar to sp metals. The effect of application of pressure on charge density is evident from figure 5.13(b, c) and 5.14(b, c). There is a moderate transfer of charge from the region between the B ions into the adjacent interstitial region. This is regarded as a transfer from σ to π type bonds [29]. The main features at P = 38 GPa are not too different from those at ambient pressure.

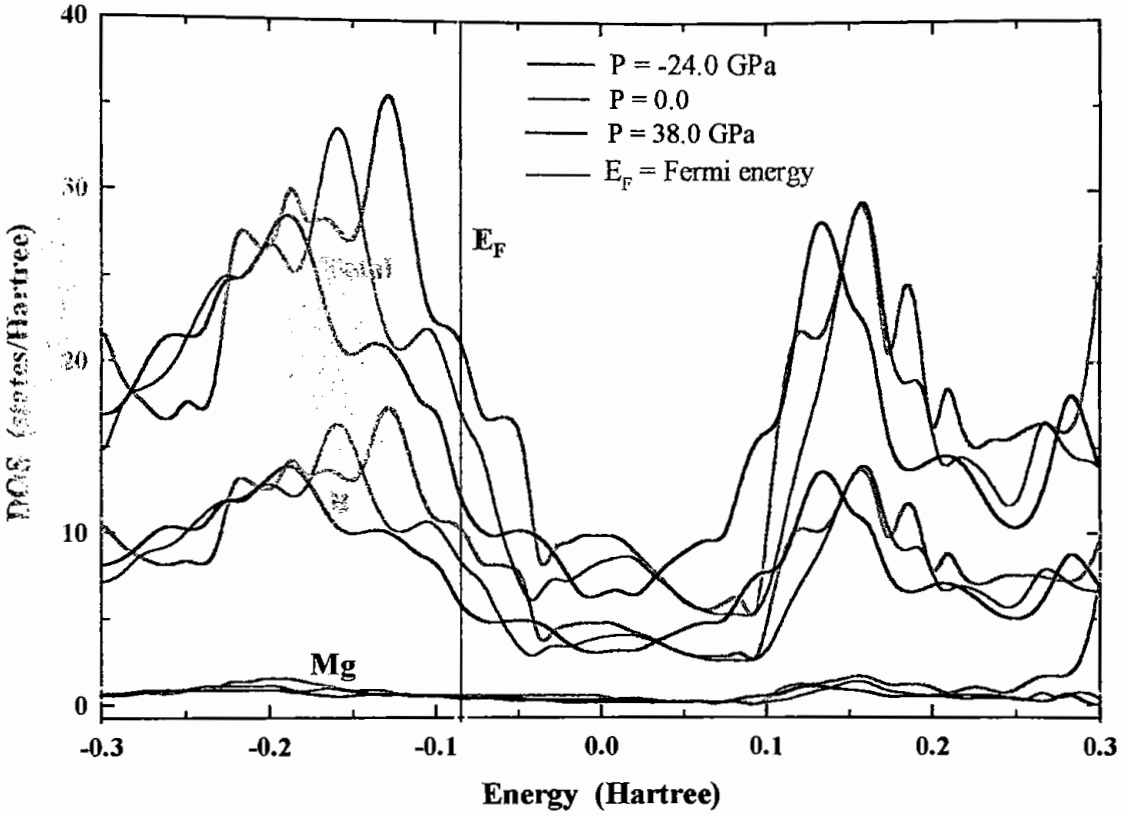

Figure 5.11. Total and partial electronic density of states (DOS) of MgB_2 as a function of pressure.

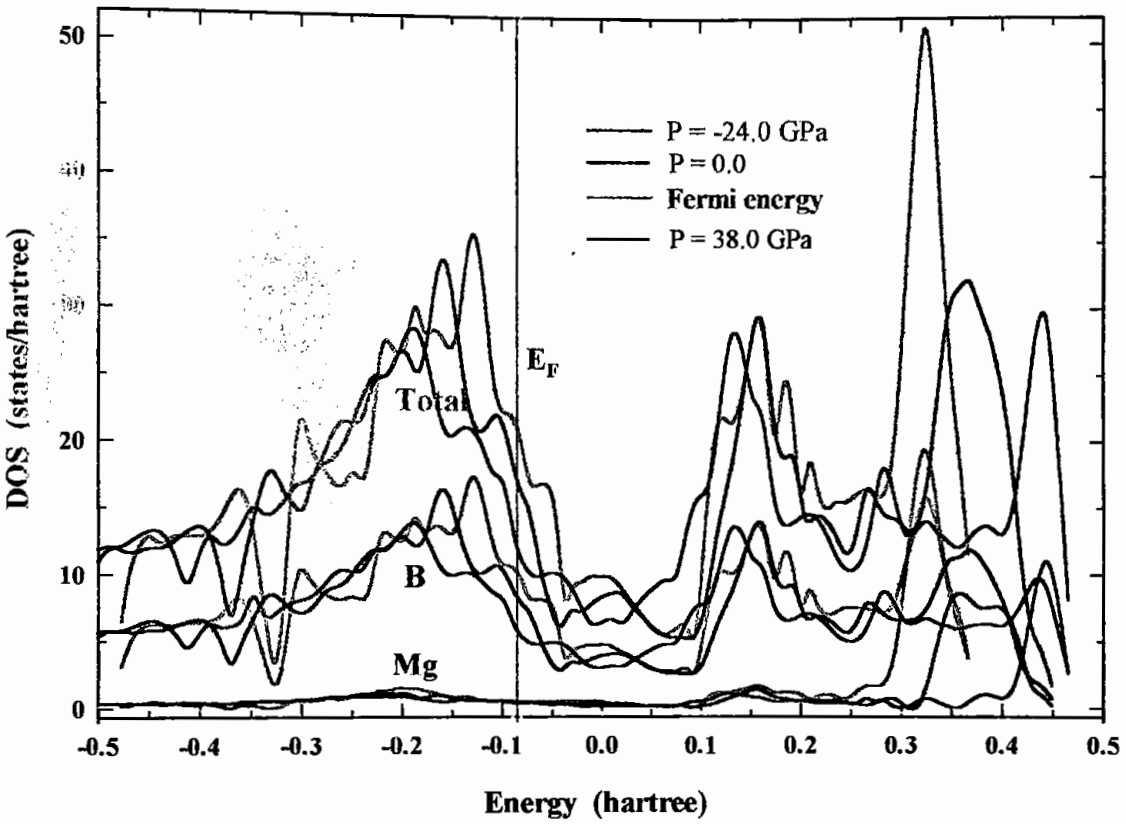

Figure 5.12. Total and partial electronic density of states (DOS) of MgB_2 as a function of pressure over a wider energy range.

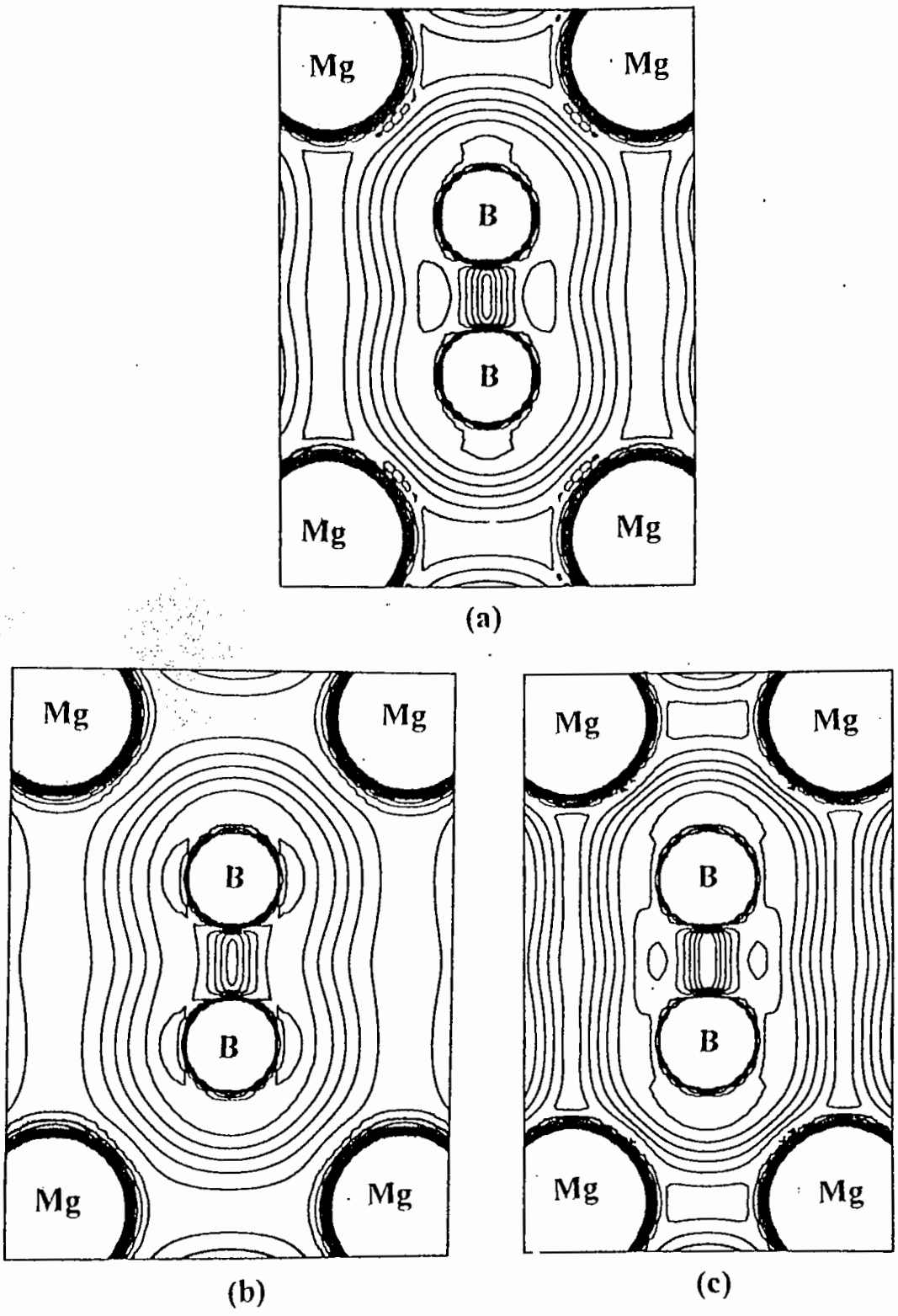

Figure 5.13. Total electron charge density map on the (110) plane through Mg and B atoms at (a) equilibrium i.e. P = 0, (b) P = -24 GPa and (c) P = 38 GPa. The isodensity curves are separated by 0.01 e/Å^3.

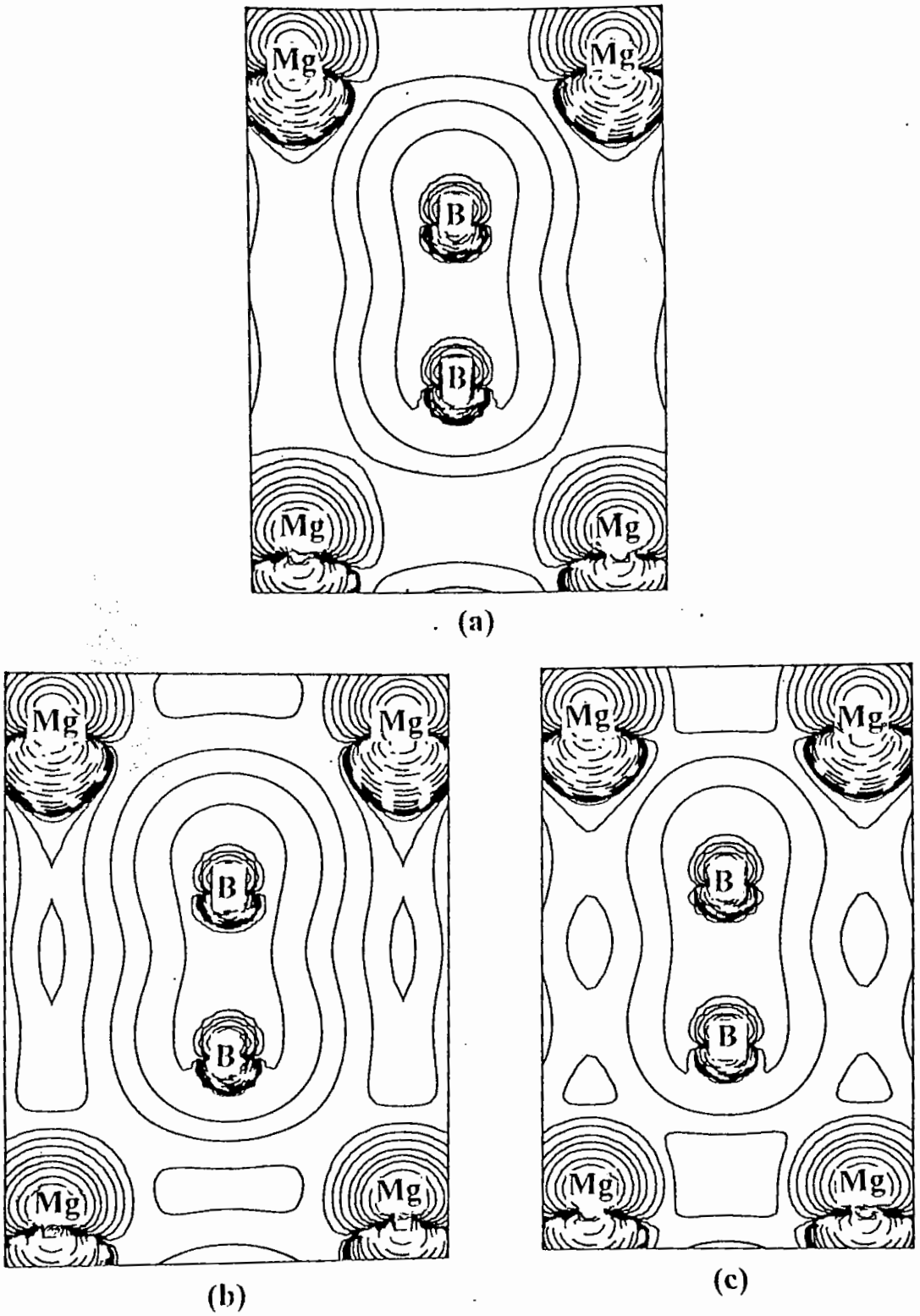

Figure 5.14. Difference electron charge density map on the (110) plane through Mg and B atoms at (a) equilibrium i.e. P = 0, (b) P = -24 GPa and (c) P = 38 GPa. The isodensity curves are separated by 0.001 e/Å^3.

5.6 Electric Field Gradient (EFG)

The EFG tensor was estimated directly from the SCF-DFT electron density. The principal component of the EFG tensor at boron site and Mg site are shown together with other available data. The calculated values of EFG at B site agree well with the available experimental data and theoretical results obtained using different methods [9, 10, 14, 33, 36]. The axial asymmetry parameter, $\eta = |V_{xx} - V_{yy}| / |V_{zz}|$ was found to zero as expected.

Table 5.4. V_{zz}^{B} in 10^{21} volt/m^2 for MgB_2 at equilibrium.

Calculation	V_{zz}^{B}	Reference
Theoretical	1.50	This work [19]
	1.85	[10]
	1.88	[33]
Experimental	1.68	[9]
	1.7±0.01	[36]
	1.7±0.1	[14]

The calculated values of EFG at B site is of the same order of magnitude as V_{zz} at the Mg site and is of opposite sign. No conclusion can be drawn regarding the value of V_{zz} at the Mg site as no experimental value is available. Figure 5.15 shows the changes of EFG in MgB_2 as a function of pressure. The B EFG is nearly constant up to ~40 GPa, and that of Mg increases rapidly (34% change over the pressure range considered) but at a slower rate compared to that obtained in [33]. The large value of EFG at the B site can be explained by the existence of boron $2p_{x,y}$ hole states as was done in ref. [33]. Since the EFG is a sensitive characteristic of the electronic charge distribution, we conclude that there are no large changes in the partial charges of the B 2p states and boron electronic structure under pressure. This confirms the observation made by Medvedeva et al. [33] but disagrees with that of Vogt et al. [11].

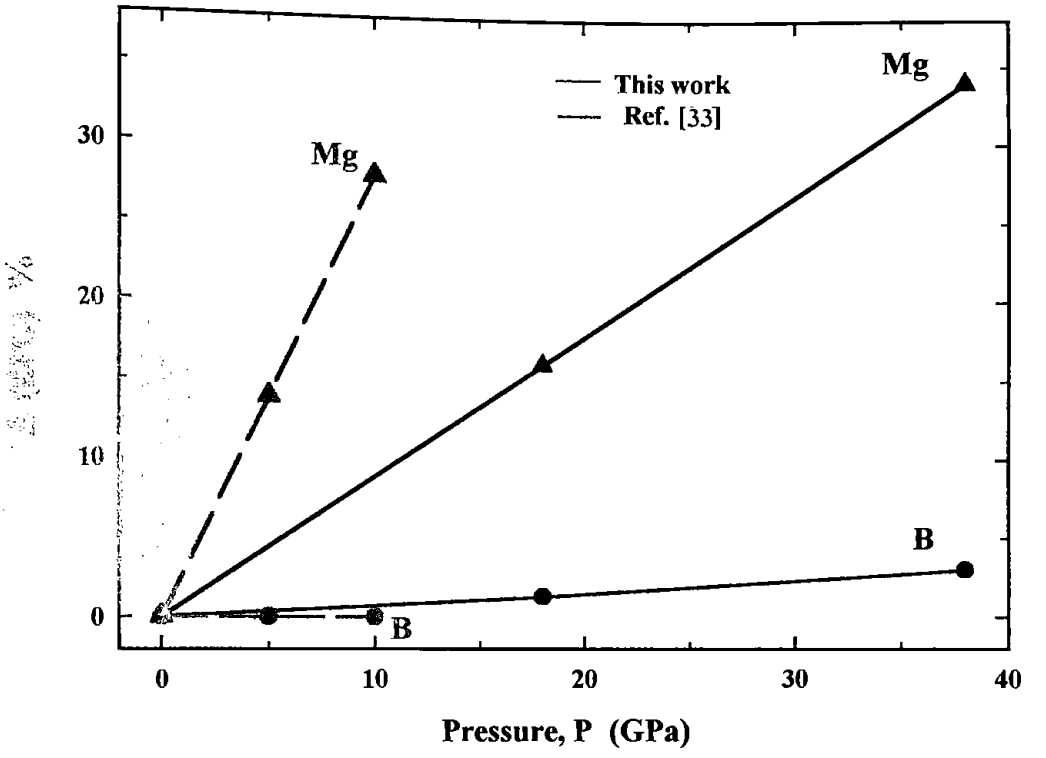

Figure 5.15. Percentage change of the values of EFG at B and Mg sites as a function of pressure.

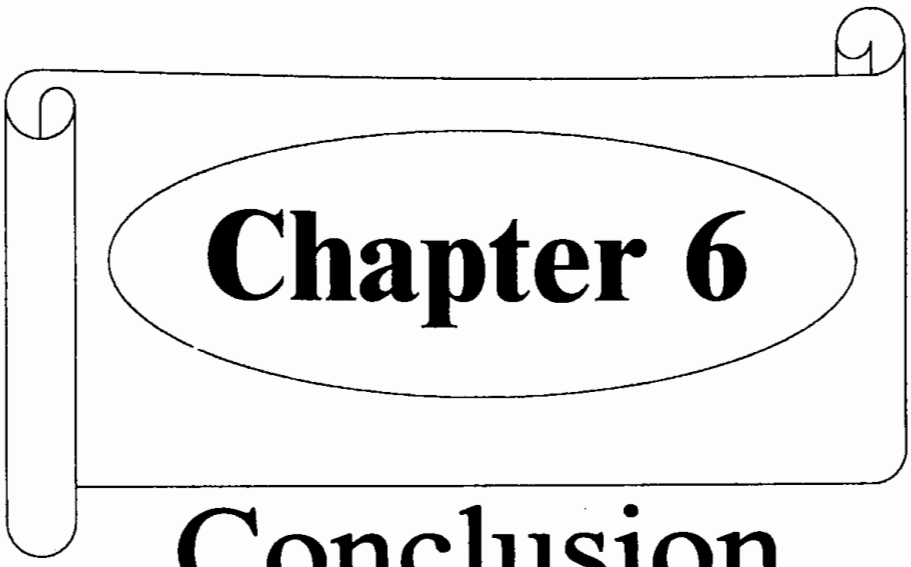

Conclusion

CHAPTER 6

CONCLUSION

In the present investigations, we have performed detailed *ab initio* Hartree-Fock and density functional studies for the ground state properties of MgB_2, a new superconductor discovered in January 2001.

MgB_2 has been found to be less compressible in the basal plane. The interlayer compressibility of MgB_2 at equilibrium is ~1.4 times larger than the in-plane value indicating the anisotropic nature of the crystal structure. It is worth noting that the structurally related alkali-metal intercalated graphite is strongly anisotropic [74] with interlayer compressibility about ten times larger than the corresponding value in MgB_2. The volume coefficient of the transition temperature T_c is an important parameter that implies the sensitivity of superconducting properties to the interatomic distances. Its value for MgB_2 is found to be significantly larger than those found in fulleride superconductors.

The analysis of the calculated zero pressure bulk modulus and pressure derivative of bulk modulus reveal the diversity in bonding interactions. The present study also suggests that the interaction between B planes has also a significant contribution to the superconducting behaviour of MgB_2. The markedly anisotropic compression behaviour of MgB_2 may induce different pressure effects on different phonon modes and is also more likely to influence the electronic structure at the Fermi energy than when compression is isotropic because B-B and Mg-B distances change at

different rates. In other words the pressure can influence the electronic band in different direction of the BZ in an unusually different manner and hence the physical properties.

The band, DOS and charge density have been studied at equilibrium and under a pressure of ~ –14 GPa to ~ 40 GPa. A fortunate combination of strong bonding, dominant phonon frequency and reasonable density of state at the Fermi level is now believed to lead to the observed T_c of MgB_2. Our calculated band structure shows that the superconductivity in MgB_2 is related to and dominated by the existence of boron σ $p_{x,y}$-band holes at the Γ-point, with negligible contribution from the Mg ions. We identified two degenerate flat bands near Fermi energy, E_F in the Γ-A direction of the Brillouin zone. From the band structure scenario it can be inferred that the degenerate B $p_{x,y}$ bands would be the key factor in the realization of the high temperature superconductivity of MgB_2. The character of the σ band is unchanged even after application of pressure, although there is a shift of position and an increase of dispersion. The calculated density of states decreases with pressure, which in conjunction with the Bardeen-Cooper-Schrieffer (BCS) theory, agrees with the trend of the experimental T_c versus pressure data. The broad bump in $T_c(P)$ data observed by Tissen et al. [12] near 9 GPa is not indicated in the present band structure study.

The analysis of the total and difference charge density establishes a mixed bonding behaviour of MgB_2. These indicate an ionic bonding between Mg and B. On the other hand there is a strong covalent bonding between B-B atoms. This is evident by the maximum charge density (with a strongly aspherical character) at the bond middle. The more or less homogeneous charge distribution between the Mg atoms indicates an appreciable degree

of metallic bonding between them. The role of Mg in MgB_2 is to donate electrons to B atoms and hence to shift E_F such that it lies very closer to the flat band, the feature that we believe very important for superconductivity. The observed bonding anisotropy and moderately anisotropic elastic properties carry important information that would be valuable in testing the predictions of competing models for the mechanism of superconductivity.

Finally, we feel the necessity for more theoretical and experimental investigations on MgB_2 superconductor and similar other binary compounds using latest available techniques in order to obtain more precise results and other unrevealed properties.

REFERENCE

[1] J Nagamatsu, N Nakagawa, T Muranaka, Y Zenitani and J Akimitsu, *Nature* **410** (2001) 63

[2] J Akimitsu, 2001 Symposium on Transition Metal Oxides, 10 January 2001, Sendai, Japan

[3] S L Bud'ko, G Lapertot, C Petrovic, C E Cunningham, N Anderson, and P C Canfield, *Phys. Rev. Lett.* **86** (2001) 1877

[4] J D Jorgensen, S Pei, P Lightfoot, D G Hinks, B W Veal, B Dabrowski, A P Paulikas and R Kleb, *Physica C* **171** (1990) 93

[5] Y Takano, H Takeya, H Fujii, H Kumakura, T Hatano, K Togano, H Kito and H Ihara, *Appl. Phys. Lett.* **78** (2001) 2914

[6] B Lorenz, R L Meng and C W Chu, *Phys. Rev. B* **64** (2001) 012507

[7] E Saito, T Takenobu, T Ito, Y Iwasa, K Prassides and T Arima, *J. Phys.: Condens. Matter* **13** (2001) L267

[8] T Tomito, J J Hamlin, J S Schilling, D J Hinks and D Jorgensen, *Phys. Rev. B* **64** (2001) 092505

[9] Gerashenko, K Mikhalev and Verkhovskii, *Preprint* (2001) cond-mat/0102421.

[10] A V Tsvyashchenko, L N Fomicheva, M V Magnitskaya, E N Shirani, V B Brudanin, Filossofov, O I Kochetov, N A Lebedev, A F Novgorodov, A V Salamatin, N A Korolev, A I Velichkov, V V Timkin, A P Menushenkov, A V Kuznetsov, V M Shabanov and Z Z Akselrod, *Preprint* (2001) cond-mat/0104560.

[11] T Vogt, G Schneider, J A Hriljac, G Yang and J S Abell, *Phys. Rev. B* **63** (2001) 220505

[12] V. G Tissen, M V Nfedova, N N Kolesnikov and M P Kulakov, *Physica C* **363** (2001) 194

[13] J K Jung, S H Baek, F Borsa, S L Bud'ko, G Lapertot and P C Canfield, *Phys. Rev. B* **64** (2001) 012514

[14] H Tou, H Ikejiri, Y Maniwa, T Ito, T Takenobu, K Prassides and Y Iwasa, *Preprint* (2001) cond-mat/0103484.

[15] S Deemyad, J S Schilling, J D Jorgensen and D G Hinks, *Physica C* **361** (2001) 227

[16] A K M A Islam, F N Islam and S Kabir, *J. Phys: Condens. Matter* **13** (2001) L641.

[17] A K M A Islam, F N Islam and M N Islam, *Phys. Lett. A* **286** (2001) 357.

[18] A K M A Islam and F N Islam, *Physica C* **363** (2001) 189.

[19] F N Islam, A K M A Islam and M N Islam, *J. Phys.: Condens. Matter* **13** (2001) 11661.

[20] A K M A Islam and F N Islam, *Physica B* xxx (2002) *in press.*

[21] J.E. Hirsch, *Phys. Lett. A* **282** (2001) 392

[22] G. Baskaran, *Preprint* (2001) cond-mat/0103308.

[23] J Kortus, I I Mazin, K D Belashchenko, V P Antropov and L L Boyer, *Phys. Rev. Lett.* **86** (2001) 4656.

[24] K D Belashchenko, M V Schilfgaarde, V P Antropov, *Phys. Rev. B* **64** (2001) 92503

[25] Y Kong, O V Dolgov, O Jepsen and O K Anderson, *Phys. Rev. B* **64** (2001) 020501®

[26] J M An and W E Pickett *Phys. Rev. Lett.* **86** (2001) 4366

[27] S Suzuki, S Higai and K J Nakao, *J. Phys. Soc. Jpn* **70** (2001) 1206

[28] A Reyes-Serrato and H Galván, *Preprint* (2001) cond-mat/0103477

[29] I Loa and K Syassen, *Solid State Commun.* **118** (2001) 279

[30] J B Neaton and A Perali *Preprint* (2001) cond-mat/0104098

[31] X Wan, J Dong, H Weng and D Y Xing, *Phys. Rev. B* **65** (2001) 012502

[32] P Ravindran, P Vajeeston, R Vidya, A Kjekshus and H Fjellvag, *Phys. Rev. B* **64** (2001) 224509

[33] N I Medvedeva, Ivanovskii, J E Medvedeva, A J Freeman and D L Novikov, *Phys. Rev. B* **65** (2001) 052501

[34] K Kunc, I Loa, K Syassen, R K Kremer and K Ahn, *J. Phys.: Condens. Matter* **13** (2001) 9945

[35] G Satta, G Profeta, F Bernardini, A Continenza and S Massidda, *Phys. Rev. B* **64** (2001) 104507

[36] I R Shein, N I Medvedeva and A L Ivanovskii, *Physics of the Solid State,* **43** (2001) 2213

[37] H Goldschmidth, *Interstitial Alloys,* Butterworths, London (1967)

[38] G V Samsonov, T I Serebryakova and V A Neronov, *Borides,* Atomizdat, Moscow (1975)

[39] G V Samsonov, I M Vinitskii, *Refractory Compounds: Handbook (Metallurgiya)* Moscow (1976)

[40] Yu B Kuz'ma, *Crystal Chemistry of Borides,* Vishcha Shkola, Lvov (1983)

[41] T I Serebryakova, V A Neronov and P D Peshev, *High-Temperature Borides (Metallurgiya),* Moscow (1991)

[42] P Bordet et al., *Phys. Rev. B* **64** (2001) 172502

[43] Ulrich Muller, *Inorganic Structural Chemistry*, John Wiley & Sons Ltd., West Sussex PO19 1UD, England, Reprinted (1997)

[44] P Vajeeston, P Ravindran, C Ravi, R Asokamani, *Phys. Rev. B* **63** (2001) 045115

[45] V R Saunders, R Dovesi, C Roetti, M Causa`, N M Harrison, R Orlando and C M Zicovich-Wilson, CRYSTAL98, *User's Manual, University of Torino, Torino* (1998)

[46] C Pisani (Ed.), *Lecture Notes in Chemistry* (Quantum-Mechanical Ab-initio Calculation of the Properties of Crystalline Materials) Springer-Verlag, Heidelberg, Vol. **67** (1996)

[47] S Baroni, G Pastori Parravicini and G Pezzica, *Phys. Rev. B* **32** (1985) 4077

[48] M causa et al., *Phys. Rev. B* **33** (1986) 1308

[49] R Orlando, R Dovesi, C Roetti, *J. Phys.: Condens. Matter,* **2** (1990) 7769

[50] C Pisani, R Dovesi and C Roetti, *Lecture Notes in Chemistry* (Hartree-Fock *Ab Initio* Treatment of Crystalline Systems) Springer-Verlag, Heidelberg, Vol. **48** (1988)

[51] P Hohenberg and W Kohn, *Phys. Rev. B* **136** (1964) 864

[52] W Kohn and L J Sham, *Phys. Rev. A* **140** (1965) 1133

[53] R Dovesi, C Pisani, C Roetti and V R Saunders, *Phys. Rev. B* **28** (1983) 5781

[54] V R Saunders, C Freyria-Fava, R Dovesi, L Salasco and C Roetti, *Mol. Phys.* 77 (1992) 629

[55] M Causà, R Dovesi, R Orlando, C Pisani, and V R Saunders, *Phys. Chem.* **92** (1988) 909

[56] R Dovesi, *Int. J. Quantum Chem.* **29** (1986) 1755

[57] FORTRAN90, ISO 1539-1991. *Technical report, ANSI,* 1430, Broadway, New York, N.Y. 10018

[58] FORTRAN77, ISO 1539-1980(E). *Technical report, ANSI,* 1430, Broadway, New York, N.Y. 10018

[59] J P Perdew, *Electronic Structure of Solids*, Akademic Verlag, Berlin, 1991

[60] J P Perdew and Y Wang, *Phys.Rev. B* **33** (1986) 8800

[61] J P Perdew and Y Wang, *Phys.Rev. B* **45** (1992) 13244

[62] A D Becke, *J. Chem. Phys.* **98** (1993) 5648

[63] H J Monkhorst and J D Pack, *Phys. Rev. B* **13** (1976) 5188

[64] G Gilat and J L Raubenheimer, *Phys. Rev.* **144** (1966) 390

[65] F D Murnaghan, *Proc. Natl. Acad. Sci. USA,* **20** (1944) 244

[66] L Fast, J M Wills, B Johansson and O Eriksson, *Phys. Rev. B* **51** (1995) 17431

[67] A Reyes-Serrato and M A Borja, *Phys. Rev. B* **62** (2000) 4890

[68] A F Goncharov, V V Struzhkin, E Gregoryanz, J Hu, R J Hemley, H Mao, G Lepertot, S L Bud'ko, P C Canfield, *Phys. Rev. B* **64** (2001) 100509

[69] S Markel, A F Goncharov, H K Mao, P Gillet and R J Hemley, *Science*, **288** (2000) 1626

[70] T Vogt, G Schneider, J A Hriljac, G Hriljac and J S Abell, *Preprint* (2001) cond-mat/0102334

[71] C A Perottoni, A S Pereira and J A H da Jornada, *J. Phys.: Condens. Matter* **12** (2000) 7205

[72] P S Spoor, J D Maynard, M J Pan, D J Green, J R Hellman and T Tanaka, *Appl. Phys. Lett.*, **70** (1997) 1959

[73] Jorgensen J D, Hinks D G, Short S, *Phys. Rev. B* **63** (2001) 224522

[74] K Prassides, Y Iwasa, T Ito, D H Chi, K Uehara, E Nishibori, M Takata, S Sakata, Y Ohishi, O Shimomura, Y Muranaka and J Akimitsu, *Phys. Rev. B* **64** (2001) 012509

[75] J F Nye, *Physical Properties of Crystals,* Oxford University Press, London (1967) Chapter 8.

APPENDIX – A

LIST OF ACRONYMS

a.u.	Atomic Unit
ab initio	'From the beginning'
AO	Atomic Orbital
APW	Augmented Plane Wave
BCS	Bardeen, Cooper and Schrieffer
BF	Bloch Functions
BS	Basis-Sets
BZ	Brillouin zone (first)
CO	Crystalline Orbital
CPU	Central Processing Unit
DFT	Density Functional Theory
DM	Density Matrix
DOS	Density of States
EFG	Electric Field Gradient
FLAPW	Full-potential Linearised Augmented Plane Wave
FPLMTO	Full Potential Linear Muffin-tin Orbitals
GGA	Generalized Gradient Approximation
GSES	Ground State Electronic Structure
GTF	Gaussian Type Functions
GTO	Gaussian Type Orbitals
GTP	Gaussian Type Primitives
HF	Hartree-Fock
HF-LCAO	Hartree-Fock – Linear Combination of Atomic Orbitals

IDOS	Integrated Density of States
IR	Irreducible Representation
KS	Kohn and Sham
LAPW	Linearised Augmented Plane Wave
LCAO	Linear Combination of Atomic Orbitals
LDA	Local Density Approximation
MO	Molecular Orbital
PDOS	Projected Density of States
PP	Pseudo-potential
PW	Plane Wave
QM	Quantum Mechanics
RHF	Restricted Hartree-Fock
ROHF	Restricted Open Shell Hartree-Fock
SCF	Self-Consistent-Field
SE	Schrödinger Equation
STO	Slater Type Orbitals
UHF	Unrestricted Hartree-Fock

APPENDIX – B

Published research articles in different International Journals from the present Ph.D. work

INSTITUTE OF PHYSICS PUBLISHING
J. Phys.: Condens. Matter 13 (2001) 11661–11667
JOURNAL OF PHYSICS: CONDENSED MATTER
PII: S0953-8984(01)27745-5

Electronic structure and electric field gradient in MgB_2 under pressure: an *ab initio* study

F N Islam, A K M A Islam and M N Islam

Department of Physics, Rajshahi University, Rajshahi-6205, Bangladesh

Received 9 August 2001, in final form 28 September 2001
Published 30 November 2001
Online at stacks.iop.org/JPhysCM/13/11661

Abstract

We report here *ab initio* density functional theory study of the electronic band structure and electric field gradient (EFG) in MgB_2 under pressure. The band structure calculations are in agreement with other recent calculations. The superconductivity in MgB_2 is related to and dominated by the existence of boron σ $p_{x,y}$-band holes at the Γ point, with negligible contribution from the Mg ions. The character of the σ band is unchanged even after application of pressure, although there is a shift of position and an increase of dispersion. The calculated density of states decreases with pressure which, in conjunction with the Bardeen–Cooper–Schrieffer theory, agrees with the trend of the experimental T_c versus pressure data. The broad bump in $T_c(P)$ data observed by Tissen *et al* near 9 GPa is not indicated in the present band structure study. The EFG at the B site is nearly constant as a function of pressure and that of Mg changes by ~34% over the pressure range considered. The present result indicates that the B electronic system does not change much under pressure up to ~38 GPa, which confirms one reported study but disagrees with the other.

1. Introduction

Recent discovery of superconductivity in the non-cuprate intermetallic MgB_2 at 39 K [1] has aroused much interest in the scientific community. A variety of experimental [2–13] and theoretical [14–30] research has been carried out to find out its structural, elastic, electronic and other properties. A few of these works involve both theoretical and experimental studies. Some discussions of electronic band structure have already been made in a number of these works that reveal that there are two distinct types of band contributed by boron. Among these the two-dimensional holelike B σ bands arise from intraplanar $p_{x,y}$-like orbitals and give a flat DOS with a prominent van Hove spike. A weaker three-dimensional p_z-like band also contributes to the DOS.

High-pressure studies show that the transition temperature T_c decreases with increasing pressure [4, 5, 10, 28]. Compression decreases both lattice constants a and c. This would indicate a possible way of searching for higher T_c material. The lattice parameters are expected

to have considerable effect on the B σ band. The study of Wan *et al* [25] has indicated that increasing the lattice constant along the c axis would increase the density of states (DOS) at the Fermi level. This causes an upward shift of the σ band and thereby increases the hole number in the band, which leads to an increase of T_c. This can be done by making MgB_2 have a larger c axis and shorter a (or b) axis by doping.

The peculiarities of electronic structure and chemical bonding are connected with the electric field gradient (EFG). This is directly related to the quadrupole charge distribution of the electron density around the probe nucleus. The measured quadrupole interaction can be interpreted on the basis of EFG [27]. Thus theoretical study of EFG of MgB_2 constitutes an important exercise that can lead to reliable interpretation of the observed data and to relate this with the specific features of the electronic structure and bonding.

Very recently Tissen *et al* [10] observed an interesting feature in the pressure dependence of T_c. They reported a broad bump near 9 GPa, which they speculated to arise from a pressure-induced electronic Lifshitz transition. These authors also indicated that existing band structure calculations of MgB_2 lend some support for such an explanation. On the other hand Deemyad *et al* [13] reported a monotonic decrease of T_c with pressure right up to 20 GPa. Further there are two conflicting points of view regarding the change of B $p_{x,y}$ occupancy under pressure. Vogt *et al* [9] conclude that B $p_{x,y}$ occupancy is altered by pressure, in contrast to the B p_z states. On the other hand Medvedeva *et al* [27] disagree with this conclusion. They found small changes in the dispersion and location of the B $p_{x,y}$ bands of MgB_2 under pressure. They conclude that no large changes take place under pressure in (i) the partial B p occupations, (ii) boron EFG and hence (iii) boron electronic structure. A further investigation on the observation made by Tissen *et al* [10] and also the important question with opposing viewpoints by Vogt *et al* [9] and Medvedeva *et al* [27], respectively, is desirable. Although theoretical investigations of the band structure of MgB_2 have been carried out by several authors [15,17,19,21,25,26,29] only two groups [8, 27] reported results on both the electron band structure and EFG. Neither of these two papers, however, discussed both the above-mentioned issues together. Medvedeva *et al* [27] used the full-potential linear muffin-tin orbital generalized gradient approximation (FLMTO–GGA) only to study band structure and EFG but they did not discuss the bump structure in $T_c(P)$. It would thus be interesting to utilize a different *ab initio* approach to examine and shed further light on the issues in question.

2. Method of calculations

We use the self-consistent-field Hartree–Fock linear combination of atomic orbital (SCF-HF-LCAO) computer program CRYSTAL98 [31]. *A posteriori* density functional (DFT) correlations to the HF results for the total energy are included, with the correlation and exchange functions proposed by Perdew and Zunger [32] and Becke [33], respectively. The basis sets used are 6-21G* and 8-61G for B and Mg, respectively. The exponents of the most diffuse sp and d shells for each atom have been optimized by searching for the minimum crystalline energy. The quality of the calculation depends on the density of points with which the Brillouin zone (BZ) is sampled. The integrations over the BZ were performed using the Monkhorst–Pack scheme [34]. To ensure convergence for the BZ integration with accuracy very tight tolerances were utilized in the evaluation of the infinite Coulomb and exchange series. A dense Gilat net [35] was defined with a total of 793 k-points in the reciprocal space, corresponding to a shrinkage factor of 24.

The total energy E of MgB_2 has been calculated at different primitive cell volume (V). The energy was minimized as a function of c/a ratio for selected values of volume. The zero pressure bulk modulus B_0 and its pressure derivative B_0' were determined by fitting the Murnaghan equation of state as detailed elsewhere [22]. The pressure was then obtained from

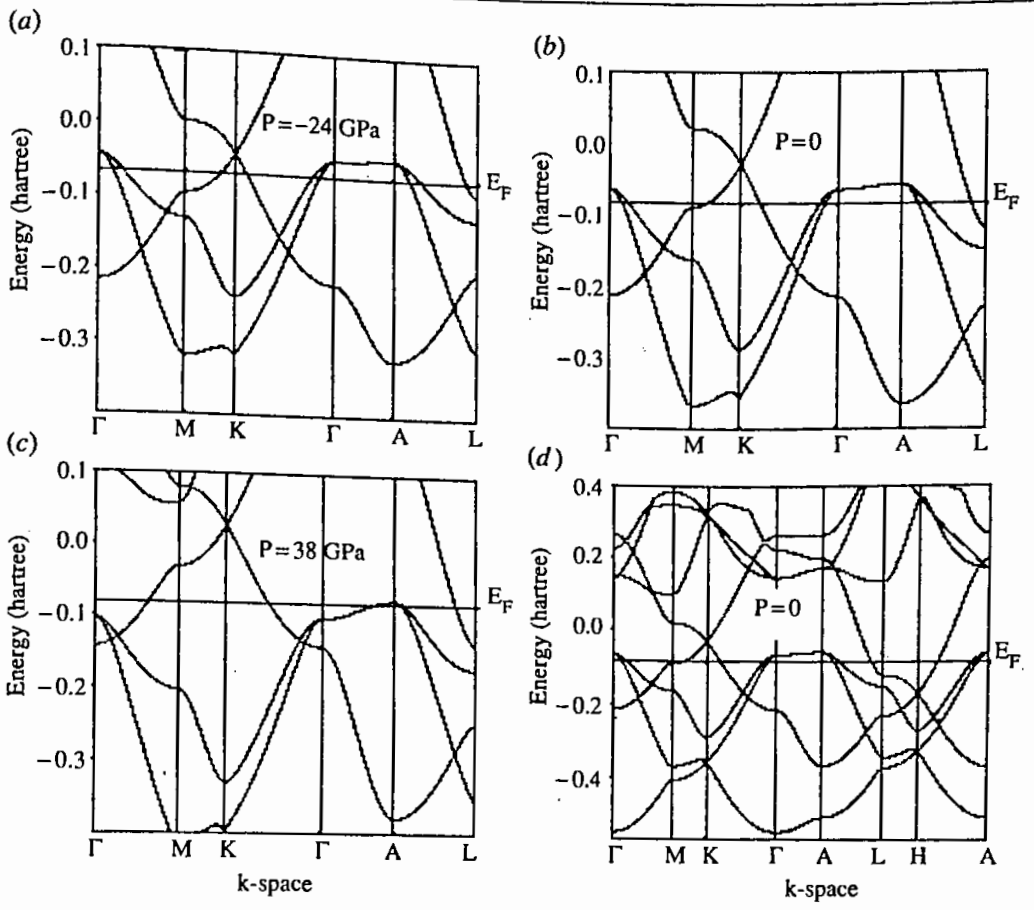

Figure 1. Band strucutre of MgB_2 (*a*) after expansion ($V_n = 1.096$, $P = -24$ GPa); (*b*) at equilibrium ($P = 0$); (*c*) under pressure ($V_n = 0.85$, $P = 38$ GPa) and (*d*) at equilibrium but over a wider energy range and along additional symmetry directions.

the normalized primitive-cell volume, $V_n (= V/V_0$, V_0 being the equilibrium volume) through the thermodynamic relationship $P = B_0(V_n^{-B_0} - 1)/B_0$.

The EFG tensor was calculated directly from the SCF-HF-DFT electron density. The coordinate axes are chosen in such a manner that V_{zz} is the EFG component along the crystallographic c axis. Then the tensor is completely characterized by two parameters: the largest component V_{zz} and the axial asymmetry parameter η defined by $\eta = |V_{xx} - V_{yy}|/|V_{zz}|$.

3. Result and discussion

We first performed detailed SCF-HF-LCAO (DFT) calculations for MgB_2 in its ground state, varying c and a, thus determining the equilibrium volume. It was necessary to perform 20 independent calculations over a range of volumes and c/a ratio. The optimized lattice parameters of MgB_2 are as follows: $a = 3.0889$ Å, $c = 3.5337$ Å. These values are in very good agreement with the measured values: $a = 3.084$ Å and $c = 3.523$ Å [1,21]. The calculated bulk modulus and elastic constants are reported elsewhere [22,24]. To examine the effects of volume (and hence pressure) on the electronic band structure near the Fermi level (E_F) we chose the maximum change in V_n in such a way that pressure P lies in the range −25 to 40 GPa. At each volume within the range the structural parameters have been optimized and the energy bands and density of states calculated. The full BZ is spanned in such a way that Γ–M–K–Γ–A–L–H–A directions are covered. The Γ–M–K–Γ lines are in the basal plane, while A–L–H–A lines are on the top of the plane at k_Z. The band structure at the equilibrium volume ($P = 0$) is shown in figure 1(*b*). Figure 1(*d*) shows the result for the band structure calculation

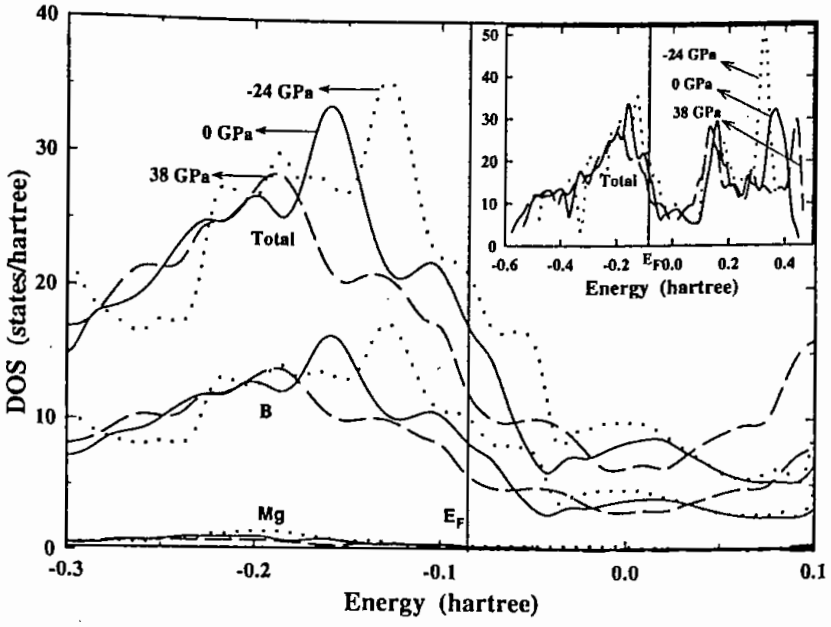

Figure 2. Total and partial electronic density of states (DOS) of MgB_2 as a function of pressure. The inset shows the toal DOS over a wider energy range.

but with a wider energy range and along additional symmetry directions, e.g., L–H–A. There are two distinct types of band, both of which are contributed by boron. The upper part of the valence band is composed of B 2p states which form two sets of bands with $\sigma(2p_{x,y})$ and $\pi(p_z)$ character. The general features of the bands obtained in this paper are in very good agreement with results from other studies [14, 15, 17, 21, 29]. The $\sigma(2p_{x,y})$ band along Γ–A is doubly degenerate, quasi-two-dimensional and makes a considerable contribution to the DOS at E_F for MgB_2. The existence of degenerate $p_{x,y}$ states above E_F at the Γ point in the BZ has been shown to be crucial for superconductivity in MgB_2 [14]. The weaker ppπ-interactions result from B $2p_z$ bands. These 3D-like bands possess maximum dispersion along the Γ–A direction.

The band structure away from equilibrium is shown in figures 1(*a*) and (*c*). The character of the σ band is unchanged even after application of pressure, because the symmetry is not broken. The weak dispersion of the σ band along Γ–A reflects the particular quasi-two-dimensionality. The dispersion increases slightly with increase of pressure. The σ band crosses the Fermi surface at the Γ point at a pressure of ~38 GPa ($V_n = 0.85$). When the σ band is below the Fermi surface, the σ bonding state is completely filled. Thus compression decreases the holes in the σ band. Neaton and Perali [21] observed that the σ bands of MgB_2 are nearly free-electron-like: their dispersion is parabolic near the Γ point, and their overall bandwidth is comparable to the free electron value (~15.5 eV). We find the same features and confirm their observation that the bandwidth (~15 eV) increases as pressure increases in line with that expected for free electrons.

In figure 2 we show the total and partial electronic density of states near the Fermi level as a function of pressure. The inset shows the total DOS over a wider energy range. The shape and locations of the bands shown in figure 1 are reflected in the density of states. The density of states $N(E_F)$ at equilibrium ($P = 0$) is 17.5 states/hartree. The value reduces to 12.5 states/hartree at $P = 38$ GPa. Thus the DOS decreases by as much as 29% over this pressure increase. That the $N(E_F)$ increases as the lattice is expanded is contrary to expectation for a nearly-free-electron metal. The result is in agreement with that of other workers [20, 21, 25]. This observation, via the BCS equation, shows that T_c should decrease

Table 1. V_{zz}^B in 10^{21} V m^{-2} for MgB_2 at equilibrium.

Ref.	V_{zz}^B
Theory	
This	1.50
[8]	1.85
[27]	1.88
Expt	
[7]	1.68
[11]	1.7 ± 0.01
[12]	1.7 ± 0.1

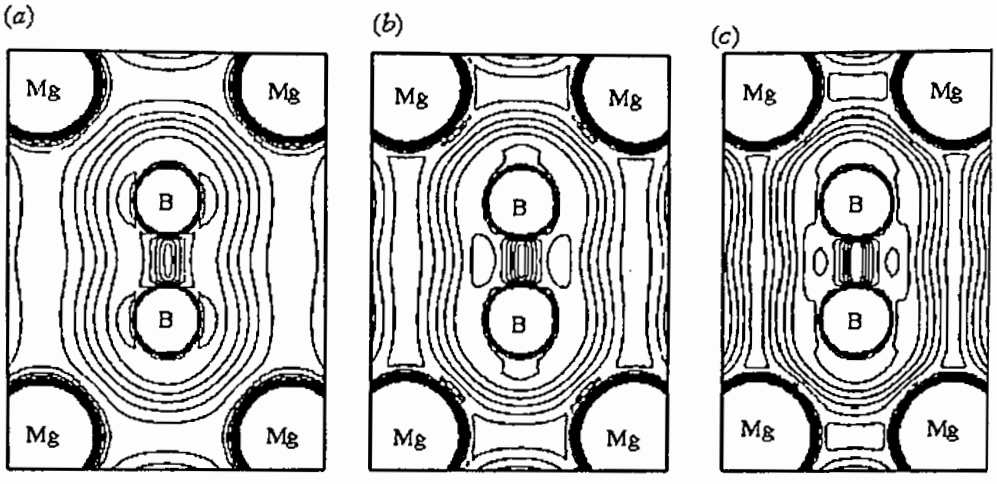

Figure 3. Total electron charge density map on the (110) plane through Mg and B atoms at (*a*) $P = -24$ GPa, (*b*) $P = 0$ and (*c*) $P = 38$ GPa. Isodensity curves are separated by 0.01 Å^{-3}.

with the increase of pressure, a result in agreement with experiment for MgB_2 [10]. Neaton and Perali [21] remarked that the dependence of the DOS on pressure is almost entirely due to the changes in the width and position of a considerable van Hove peak (~2 eV below the Fermi level). This originates from a saddle point in the highest occupied σ band at the M point. Further the decrease in bandwidth with decreasing pressure reduces the separation between the peak and the Fermi level, enhancing the DOS. The singularity is further enhanced by an increase in two-dimensionality.

A redistribution of carriers between σ and π bands occurs with the increase of pressure, and the number of holes in the σ band decreases, i.e., the top of the band moves down towards E_F and below. The strong electron–phonon coupling results in splitting the σ band into two sub-bands [17]. With application of pressure of 38 GPa the lower sub-band crosses E_F, thereby changing the Fermi surface topology. Tissen *et al* [10] assumed that the Fermi level crosses the van Hove singularity in the DOS at $P \sim 9$ GPa, thereby causing the anomaly in $T_c(P)$ due to the electronic transition. Our calculations do not indicate this to happen at a pressure as low as ~9 GPa. The results of Deemyad *et al* [13] also support our findings. They measured the dependence of T_c on nearly hydrostatic pressure for an isotopically pure (^{11}B) MgB_2 sample. The analysis of $T_c(P)$ data to 20 GPa demonstrates that the monotonic decrease of T_c with pressure arises predominantly from the decrease in the coupling constant λ due to lattice stiffening, and not from electronic effects.

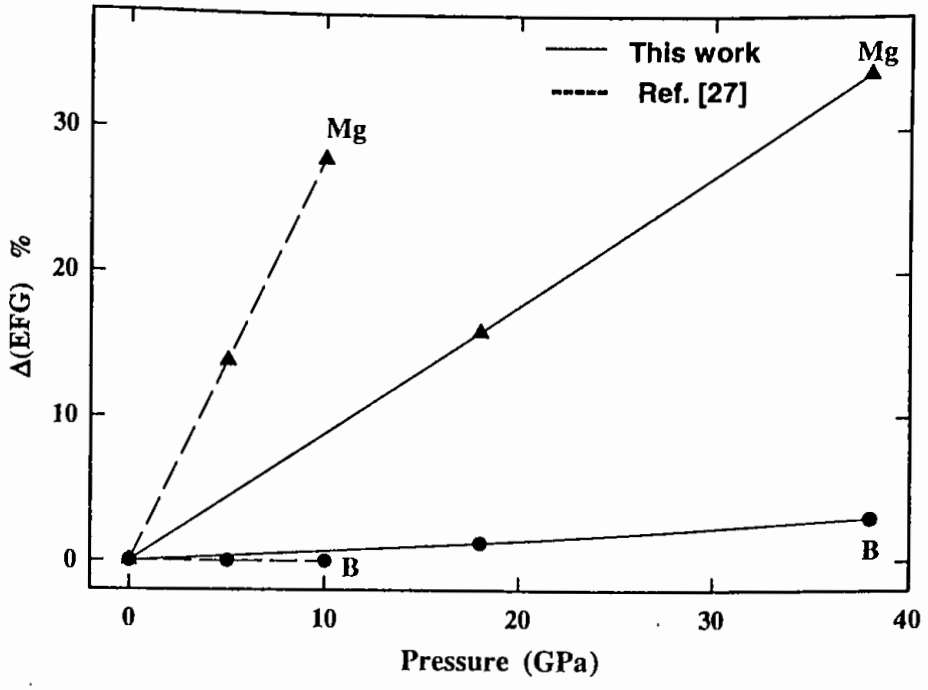

Figure 4. Percentage change of the values of EFG at B and Mg sites as a function of pressure.

The total charge densities of MgB_2 at different pressures for the (110) plane are shown in figure 3. Mg nuclei are located at the corners of the charge density map and B nuclei are at the (1/3, 1/2) and (2/3, 1/2) positions. The density profile at zero pressure (figure 3(*b*)) shows similar features to that in [20]. A low electron accumulation between Mg and B is indicated. Further the electron population in the Mg site is much lower than that for a neutral Mg atom. These indicate an ionic bonding between Mg and B. On the other hand there is a strong covalent bonding between B–B atoms. This is evident from the maximum charge density (with a strongly aspherical character) at the bond middle. A somewhat homogeneous charge distribution between the Mg atoms indicates an appreciable degree of metallic bonding between them. MgB_2 is a mixed bonded solid and the band structure shows features similar to sp metals. The effect of application of pressure on charge density is evident from figure 3(*c*). There is a moderate transfer of charge from the region between the B ions into the adjacent interstitial region. This is regarded as a transfer from σ to π type bonds [20]. The main features at $P = 38$ GPa are not too different from those at ambient pressure.

The EFG tensor was estimated directly from the SCF-DFT electron density. The principal component of the EFG tensor at the boron site and the Mg site are shown in table 1 together with other available data. The calculated values of EFG at the B site agree well with the available experimental data and theoretical results obtained using different methods [7, 8, 11, 12, 27]. The axial asymmetry parameter η was found to be zero as expected.

The calculated value of EFG at the B site is of the same order of magnitude as V_{zz} at the Mg site and is of opposite sign. No conclusion can be drawn regarding the value of V_{zz} at the Mg site as no experimental value is available. Figure 4 shows the changes of EFG in MgB_2 as a function of pressure. The B EFG is nearly constant up to ~40 GPa, and that of Mg increases rapidly (34% change over the pressure range considered) but at a slower rate compared to that obtained in [27]. The large value of EFG at the B site can be explained by the existence of boron $2p_{x,y}$ hole states as done in [27]. Since the EFG is a sensitive characteristic of the electronic charge distribution, we conclude that there are no large changes in the partial

charges of the B 2p states and boron electronic structure under pressure. This confirms the observation made by Medvedeva *et al* [27] but disagrees with that of Vogt *et al* [9].

Acknowledgments

The authors would like to thank the Ministry of Science and Technology, Government of Bangladesh for financial support. FNI acknowledges the grant of a Scholarship under the Prime Minister's Fund for Research and Higher Studies.

References

[1] Nagamatsu J, Nakagawa N, Muranaka T, Zenitani Y and Akimitsu J 2001 *Nature* **410** 63
[2] Bud'ko S L, Lapertot G, Petrovic C, Cunningham C E, Anderson N and Canfield P C 2001 *Phys. Rev. Lett.* **86** 1877
[3] Takano Y, Takeya H, Fujii H, Kumakura H, Hatano T, Togano K, Kito H and Ihara H 2001 *Preprint* cond-mat/0102167
[4] Lorenz B, Meng R L and Chu C W 2001 *Preprint* cond-mat/0102264 v2
[5] Saito E, Takenobu T, Ito T, Iwasa Y, Prassides K and Arima T 2001 *J. Phys.: Condens. Matter* **13** L267
[6] Tomito T, Hamlin J J, Schilling J S, Hinks D J and Jorgensen D 2001 *Preprint* cond-mat/0103538
[7] Gerashenko, Mikhalev K and Verkhovskii 2001 *Preprint* cond-mat/0102421
[8] Tsvyashchenko A V *et al* 2001 *Preprint* cond-mat/0104560
[9] Vogt T, Schneider G, Hriljac J A, Yang G and Abell J S 2001 *Preprint* cond-mat/0102480 v1
[10] Tissen V G, Nfedova M V, Kolesnikov N N and Kulakov M P 2001 *Preprint* cond-mat/0105475
[11] Jung J K, Seung H B, Borsa F, Bud'ko S L, Lapertot G and Canfield P C 2001 *Preprint* cond-mat/0103040
[12] Tou H, Ikejiri H, Maniwa Y, Ito T, Takenobu T, Prassides K and Iwasa Y 2001 *Preprint* cond-mat/0103484
[13] Deemyad S, Schilling J S, Jorgensen J D and Hinks D G 2001 *Preprint* cond-mat/0106057
[14] Kortus J, Mazin I I, Belashchenko K D, Antropov V P and Boyer L L 2001 *Phys. Rev. Lett.* **86** 4656
[15] Belashchenko K D, Schilfgaarde M V and Antropov V P 2001 *Preprint* cond-mat/0102290
[16] Kong Y, Dolgov O V, Jepsen O and Anderson O K 2001 *Preprint* cond-mat/0102499
[17] An J M and Pickett W E 2001 *Phys. Rev. Lett.* **86** 4366
[18] Suzuki S, Higai S and Nakao K J 2001 *J. Phys. Soc. Japan* **70** 1206
[19] Reyes-Serrato A and Galván H 2001 *Preprint* cond-mat/0103477
[20] Loa I and Syassen K 2001 *Solid State Commun.* **118** 279
[21] Neaton J B and Perali A 2001 *Preprint* cond-mat/0104098
[22] Islam A K M A, Islam F N and Kabir S 2001 *J. Phys.: Condens. Matter* **13** L641
[23] Islam A K M A, Islam F N and Islam M N 2001 *Phys. Lett.* A **286** 357
[24] Islam A K M A and Islam F N 2001 *Physica* C **363** 189
[25] Wan X, Dong J, Weng H and Xing D Y 2001 *Preprint* cond-mat/0104216
[26] Ravindran P, Vajeeston P, Vidy R, Kjekshus A and Fjellvag H 2001 *Preprint* cond-mat/0104253
[27] Medvedeva N I, Ivanovskii, Medvedeva J E, Freeman A J and Novikov D L 2001 *Preprint* cond-mat/0104346
[28] Kunc K, Loa I, Syassen K, Kremer R K and Ahn K 2001 *Preprint* cond-mat/0105402
[29] Satta G, Profeta G, Bernardini F, Continenza A and Massidda S 2001 *Preprint* cond-mat/0106239
[30] See also website http://www.iitap.iastate.edu/htcu/htcu.html
[31] Saunders V R, Dovesi R, Roetti C, Causa' M, Harrison N M, Orlando R and Zicovich-Wilson C M 1998 *CRYSTAL98 User's Manual* University of Torino
Pisani C, Dovesi R and Roetti C 1988 *Hartree–Fock Ab-initio Treatment of Crystalline Systems (Lecture Notes in Chemistry vol 48)* (Heidelberg: Springer)
[32] Perdew J P and Zunger A 1981 *Phys. Rev.* B **23** 5048
[33] Becke A D 1988 *Phys. Rev.* A **38** 3098
[34] Monkhorst H J and Pack J D 1976 *Phys. Rev.* B **13** 5188
[35] Gilat G and Raubenheimer J L 1966 *Phys. Rev.* **144** 390

ELSEVIER

Physica C 363 (2001) 189–193

PHYSICA C

www.elsevier.com/locate/physc

Ab initio investigation of elastic constants of superconducting MgB_2

A.K.M.A. Islam *, F.N. Islam

Department of Physics, Rajshahi University, Rajshahi 6205, Bangladesh

Received 22 May 2001; received in revised form 14 August 2001; accepted 14 August 2001

Abstract

The five different elastic constants of the new superconducting MgB_2 are calculated by ab initio method using a density functional theory Hamiltonian with both correlation and exchange potentials. The results are compared with those from a recent FPLMTO calculation. The fully relaxed and isotropic bulk moduli were also estimated and the implication of their comparison is made, e.g., MgB_2 is less anisotropic than one would otherwise suppose on the basis of its 'planar' crystal structure. © 2001 Elsevier Science B.V. All rights reserved.

PACS: 74; 62.20.D
Keywords: Ab initio method; Elastic constants; MgB_2

The recent discovery of superconductivity at a high $T_c \sim 40$ K in the simple intermetallic magnesium diboride [1] has triggered a flurry of research activities to study its structural, electronic and other properties [2]. MgB_2 has a very simple crystal structure where the boron atoms form graphite-like sheets separated by hexagonal layers of Mg atoms. It has AlB_2 structure with a space group P6/mmm and lattice parameters $a = 3.084$ Å and $c = 3.522$ Å [3].

There are five independent components of the elasticity tensor for MgB_2, instead of three as in the cubic case. The elastic constants are defined by means of a Taylor expansion of the total energy of the system $E(V, \delta)$, with respect to a small strain δ of the lattice of volume V. The Bravais lattice spanned by three vectors are written in a form $R = (\sqrt{3/2} - 1/2; 0\,1\,0; 0\,0\,c/a)$. We can express the energy of a strained system [4]:

$$E(V, \delta) = E(V_0, 0) + V_0 \left[\sum_i \tau_i \xi_i \delta_i + \frac{1}{2} \sum_{ij} C_{ij} \delta_i \xi_j \delta_j \right] \quad (1)$$

where $E(V_0, 0)$ is the energy of the unstrained system with volume V_0. τ_i is an element in the stress tensor, ξ_i is a factor to take care of Voigt index [4].

In this work we use a self-consistent-field Hartree–Fock linear combination of the atomic orbital computer program CRYSTAL98 [5,6] with the density functional theory (DFT) option. The DFT Hamiltonian was used where the electronic correlation and exchange potentials are chosen according to functionals proposed in the literature [7,8]. The correlation functional PWGGA due to

* Corresponding author. Fax: +880-721-750064.
E-mail address: azharislam46@yahoo.com (A.K.M.A. Islam).

0921-4534/01/$ - see front matter
PII: S0921-4534(01)00973-X

Perdew and Wang [7] uses generalized-gradient approximation. On the other hand the exchange correction is taken care of by a method due to Becke [8]. The basis sets used are as-described in Ref. [9]. The integrations over the Brillouin zone (BZ) were performed using the Monkhorst–Pack scheme [10]. To ensure convergence for the BZ integration with accuracy tight tolerances were utilized in the evaluation of the infinite Coulomb and exchange series. A Gilat net [11] was defined with a total of 150 k-points in the reciprocal space, corresponding to a shrinkage factor of 8. The total energy E of MgB_2 has been calculated at different primitive cell volume. The energy was minimized as a function of the c/a ratio for selected values of volume. Fig. 1 shows ΔE $(= E - E_0)$ as a function of normalized volume V_n $(= V/V_0)$.

Now we concentrate our attention in determining the elastic constants. The lattice distortions employed here are those given by Fast et al. [4]. The distortion and the corresponding energy are as follows [4,12]:

(a) Distortion that changes the size of the basal plane, keeping z-axis constant (symmetry of the strained lattice is still hexagonal):

$$D_1 = \begin{pmatrix} 1+\delta & 0 & 0 \\ 0 & 1+\delta & 0 \\ 0 & 0 & 1 \end{pmatrix} \tag{2}$$

$$E(V,\delta) = E(V_0,0) + V_0[(\tau_1 + \tau_2)\delta + (C_{11} + C_{12})\delta^2] \tag{3}$$

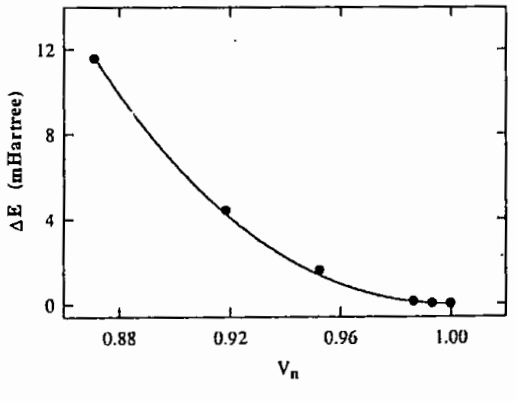

Fig. 1. Energy ΔE as a function of normalized cell volume V_n.

(b) Distortion in which z-axis is kept constant, x-axis increases and y-axis decreases by equal amount (symmetry of the strained lattice is monoclinic):

$$D_2 = \begin{pmatrix} 1+\delta & 0 & 0 \\ 0 & 1-\delta & 0 \\ 0 & 0 & 1 \end{pmatrix} \tag{4}$$

$$E(V,\delta) = E(V_0,0) + V_0[(\tau_1 - \tau_2)\delta + (C_{11} - C_{12})\delta^2] \tag{5}$$

(c) Distortion that stretches z-axis, keeping other axes unchanged (shear maintains hexagonal symmetry):

$$D_3 = \begin{pmatrix} 1 & 0 & 0 \\ 0 & 1 & 0 \\ 0 & 0 & 1+\delta \end{pmatrix} \tag{6}$$

$$E(V,\delta) = E(V_0,0) + V_0[(\tau_3\delta + \tfrac{1}{2}C_{33})\delta^2] \tag{7}$$

(d) Distortion that preserves the symmetry but changes the volume:

$$D_4 = \begin{pmatrix} 1+\delta & 0 & 0 \\ 0 & 1+\delta & 0 \\ 0 & 0 & 1+\delta \end{pmatrix} \tag{8}$$

$$E(V,\delta) = E(V_0,0) + V_0[(\tau_1 + \tau_2 + \tau_3)\delta + \tfrac{1}{2}(2C_{11} + 2C_{12} + 4C_{13} + C_{33})\delta^2] \tag{9}$$

(e) Volume conserving triclinic distortion:

$$D_5 = \begin{pmatrix} 1 & 0 & \delta \\ 0 & 1 & 0 \\ \delta & 0 & 1 \end{pmatrix} \tag{10}$$

$$E(V,\delta) = E(V_0,0) + V_0[(\tau_5\delta + 2C_{44})\delta^2] \tag{11}$$

With these five distinct lattice deformations, we calculated the energy using the appropriate expression given above. The dependence of calculated strain energy, $[E(V,\delta) - E(V_0,\delta)]$ on δ is shown in Fig. 2. It is instructive to discuss the positions of boron used in the calculation particularly in distortions like (b) and (d). We will illustrate here the case of (b). Here the positions of atoms (in Å) for $\delta = 0.01$ are: Mg(0,0,0), B(−3.404, 0, −3.305), B(−1.702, −2.889, −3.305).

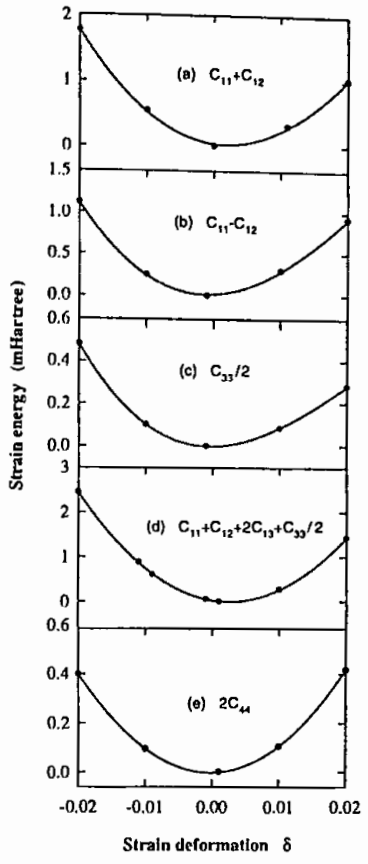

Fig. 2. Strain energy of MgB_2 as a function of the lattice distortion parameter δ, for the five different strains defined in the text.

These may be compared with the positions before deformation: Mg(0,0,0), B(−3.305, 0, −3.305), B(−1.685, −2.919, −3.305). This corresponds to changes in the crystallographic cell edges and angles in the range $\leqslant 0.05$ Å and $\leqslant 0.51°$, respectively. The case (d) is not much different from this scenario. The coordinates of Mg and B atoms were not optimized each time the lattice was deformed. This should not affect the results for $C_{11} + C_{12}$ and C_{13}, as the site symmetries and the Bravais lattice remain unchanged in these cases. The maximum deformation was kept under ±1% of the equilibrium lattice parameters in order to reduce the influence of the higher order terms in the expansion of the strain energy. The deviation from zero deformation of the minimum in the strain energy curve for cases (a) and (d) is due to the fact that the algorithm used to search for the structure of minimum energy was not exhaustively iterated. Similar effect was observed by Perottoni et al. [13] for TiB_2, where corrections for the lattice parameters were less than 0.5%. Third order polynomials were fitted to the data in Fig. 2, from which the five elastic constants of MgB_2 were calculated according to appropriate expressions given above. It is to be noted here that the third order component of the fit which affects the total energy by an amount which is less than an order of magnitude compared with the second order term. The results of the calculations are given in Table 1 along with those from the full potential LMTO calculations of Ravindran et al. [12] for MgB_2. Experimental values of elastic constants are not yet available for comparison. Thus for the purpose of comparison the room-temperature experimental values of a similar type material TiB_2 due to Spoor et al. [14] have been shown in the table. Our values are found to be comparable with those due to Ravindran et al. [12]. The largest discrepancy is for C_{12}. At this point it is not possible to distinguish clearly the advantages or disadvantages of the present method over FPLMTO. The two methods use different approaches to the problems, but both of these allow total-energy calculations to be done for arbitrary crystal structures. The energy is evaluated directly with inclusion of exchange and correlation effects in both the methods. In the FPLMTO method the effects of the exchange and correlation are treated within the generalized-gradient-corrected local density approximation using the parameterization scheme of Perdew et al. [17]. Self-consistency was achieved in both the methods by demanding the convergence of the total energy to be smaller than $\sim 10^{-5}$ Hartree. Further to

Table 1
Elastic constants C_{ij} and bulk modulus B of MgB_2 and TiB_2 (in GPa).

Reference	C_{11}	C_{12}	C_{13}	C_{33}	C_{44}	B_{iso}
Present	446	68	39	284	77	163
[9]	438	43	33	264	80	150
[11][a]	660	48	93	432	260	244

[a] Experimental value for TiB_2.

improve our Fock matrix at the self-consistent-field cycle j was made equal to $F_j^{\text{new}} = (1-m)F_j + mF_{j-1}$, where m is a mixing parameter equal to 0.3 [5,6]. The present DFT technique has been shown [9,13] to yield better estimates of energy despite approximate treatment of correlation effects. This, however, may not be always true for properties that depend on energy derivatives. The tendency of the type of calculations presented here to overestimate some elastic constants including C_{12} has been pointed out by several authors (see Ref. [13]). Moreover the values for the combinations $C_{11}+C_{12}$ and $C_{11}-C_{12}$ are found to vary depending upon the particular functionals used for the exchange–correlation. Ravindran et al. [12] has not discussed such problems while presenting their elastic data. The relative merits of our approach can only be assessed when the two methods are directly compared through the estimation of several properties involving energy derivatives. More experience is required both in terms of explored properties and types of component atoms considered in order to judge the relative merit and reliability of one method over the other.

We calculated the isotropic bulk modulus B_{iso}, obtained under the assumption that the c/a ratio remains unchanged when the lattice is subjected to an isotropic stress, from [4]

$$B_{\text{iso}} = \tfrac{2}{9}(C_{11} + C_{12} + 2C_{13} + \tfrac{1}{2}C_{33}) \qquad (12)$$

The set of calculated elastic constants gives $B_{\text{iso}} =$ 163 GPa. This may be compared with the bulk modulus obtained through the analysis of the data of energy versus primitive cell volume of MgB_2. The solid curve in Fig. 1 is the resulting fit of Murnaghan equation of state [9,15]. The fit yielded $B = 163$ and 167 GPa with $dB/dP = 4$ and 3.5, respectively. Thus the value is in very good agreement with that obtained from our calculated elastic constants. We also estimated the zero-pressure bulk modulus B for a single crystal with hexagonal symmetry, when there is no constraint on the c/a dependence on lattice strain. The expression for this is [4,16]

$$B = \frac{C_{33}(C_{11}+C_{12}) - 2C_{13}^2}{C_{11}+C_{12}-4C_{13}+2C_{33}} \qquad (13)$$

Our calculated data in Table 1 yields $B = 158$ GPa. The isotropic bulk modulus B_{iso} is about 3.4% above the value obtained when there is relaxation of c/a ratio (Eq. (13)). The corresponding value is ~2.3% for TiB_2 [13], indicating a similar but smaller anisotropy for this compound TiB_2. The layered cuprates show much larger (a factor ~2) compression anisotropy [18]. Eq. (13) cannot be used for this strong anisotropic case due to lack of elastic constant data. We may further compare the degree of anisotropy in the linear compressibilities of the two diborides. The values of the linear bulk modulus along the a-axis and the c-axis for MgB_2 are 793 and 446 GPa, respectively. We obtain these using appropriate expressions for hexagonal crystals given in Ref. [12]. The corresponding values for these linear bulk moduli are 1031 and 675 GPa, respectively, for TiB_2. MgB_2 is less compressible in the basal plane, in which the covalent B–B bonds lie. Further the interlayer linear compressibility $d \ln c/dP$ is ~1.4 times larger than the in-plane value [9]. It is to be noted that the structurally related alkali-metal intercalated graphite is strongly anisotropic with interlayer compressibility ~10 times larger than the corresponding value in MgB_2 [19].

The comparison between the isotropic and fully relaxed bulk moduli may suggest that MgB_2 is less anisotropic than one would think on the basis of its 'planar' crystal structure. The same observation was made earlier for TiB_2 [13], which was further corroborated by a study of the directional dependence of Young and bulk moduli. It is, therefore, likely that in MgB_2 also the interaction between B planes are not negligible and should be taken into account for a better understanding of the origin of the mechanical behaviour. One should, however, note here that TiB_2 is a d-band metal where the interaction between B planes is likely through d-bands on Ti.

Acknowledgements

The authors are grateful to the Ministry of Science and Technology, Government of Bangladesh for financial assistance.

References

[1] J. Nagamatsu, N. Nakagawa, T. Muranaka, Y. Zenitani, J. Akimitsu, Nature 410 (2001) 63.

[2] A.K.M.A. Islam, F.N. Islam, M.N. Islam, Phys. Lett. A 286 (2001) 357, See also the website: iitap.iastate.edu/htcu/mgb2preprints.html.

[3] M.E. Jones, R.E. Marsh, J. Am. Chem. Soc. 76 (1954) 1434.

[4] L. Fast, J.M. Wills, B. Johansson, O. Eriksson, Phys. Rev. B 51 (1995) 17431.

[5] V.R. Saunders, R. Dovesi, C. Roetti, M. Causá, N.M. Harrison, R. Orlando, C.M. Zicovich-Wilson, CRYSTAL98 User's Manual, University of Torino, Torino, 1998.

[6] C. Pisani, R. Dovesi, C. Roetti, Hartree–Fock ab initio treatment of crystalline systems, in: Springer Lecture Notes in Chemistry, vol. 48, Springer, Heidelberg, 1988.

[7] J.P. Perdew, Electronic Structure of Solids, Akademie Verlag, Berlin, 1991;
J.P. Perdew, Y. Wang, Phys. Rev. B 33 (1986) 8800;
J.P. Perdew, Y. Wang, Phys. Rev. B 45 (1992) 13244.

[8] A.D. Becke, J. Chem. Phys. 98 (1993) 5648.

[9] A.K.M.A. Islam, F.N. Islam, S. Kabir, J. Phys.: Condens. Matter 13 (2001) L641.

[10] H.J. Monkhorst, J.D. Pack, Phys. Rev. B 13 (1976) 5188.

[11] G. Gilat, J.L. Raubenheimer, Phys. Rev. B 144 (1966) 390.

[12] P. Ravindran, P. Vajeeston, R. Vidya, A. Kjekshus, H. Fjellvag, cond-mat/0104253.

[13] C.A. Perottoni, A.S. Pereira, J.A.H. da Jornada, J. Phys.: Condens. Matter 12 (2000) 7205.

[14] P.S. Spoor, J.D. Maynard, M.J. Pan, D.J. Green, J.R. Hellman, T. Tanaka, Appl. Phys. Lett. 70 (1997) 1959.

[15] F.D. Murnaghan, Proc. Natl. Acad. Sci. USA 30 (1944) 244.

[16] J.F. Nye, Physical Properties of Crystals, Oxford University Press, London, 1967, Chapter 8.

[17] J.P. Perdew, S. Burke, M. Ernzerhof, Phys. Rev. Lett. 77 (1996) 3865.

[18] J.D. Jorgensen, S. Pei, P. Lightfoot, D.G. Hinks, B.W. Veal, B. Dabrowski, A.P. Paulikas, R. Kleb, Physica C 171 (1990) 93.

[19] K. Prassides, Y. Iwasa, T. Ito, D.H. Chi, K. Uehera, E. Nishibori, M. Takata, S. Sakata, Y. Ohisi, O. Shimomura, T. Muranaka, J. Akimitsu, cond-mat/0102507.

INSTITUTE OF PHYSICS PUBLISHING JOURNAL OF PHYSICS: CONDENSED MATTER

J. Phys.: Condens. Matter 13 (2001) L641–L645 PII: S0953-8984(01)24850-4

LETTER TO THE EDITOR

Ab initio investigation of mechanical behaviour of MgB_2 superconductor under pressure

A K M A Islam, F N Islam and S Kabir

Department of Physics, Rajshahi University, Rajshahi-6205, Bangladesh

Received 9 May 2001
Published 22 June 2001
Online at stacks.iop.org/JPhysCM/13/L641

Abstract

We present *ab initio* calculations of a set of physical properties for the newly discovered MgB_2 superconductor. The zero pressure bulk modulus, the pressure derivative of the bulk modulus and their in- and out-of-plane linear values are evaluated. An analysis of the calculated parameters reveals the diversity in bonding interactions. The diboride is characterized by a moderately sizable anisotropy of compressibilites, which is smaller than for cuprates, but larger than for other related diborides. The anisotropic compression is expected to induce different pressure effects on different phonon modes and also to influence the electronic structure at the Fermi energy.

The newly discovered magnesium diboride has generated considerable interest in the scientific community and instigated vigorous research activities in order to understand the structure, properties and to determine the underlying mechanism of superconductivity in this material (see [1–11]). As a result, various theoretical ideas and experimental data are being accumulated rapidly. The magnesium diboride possesses a hexagonal crystal structure. One thus expects anisotropy in the physical properties of this material. Within the Bardeen–Cooper–Schrieffer (BCS) picture, the reduction of the density of states (DOS) at the Fermi level, due to the contraction of the B–B and Mg–B interatomic distances dominates the hardening of the B phonon frequency that should enhance T_c as external pressure is applied [10]. An and Pickett [11] found that the remarkable superconducting properties require a very specific microscopic cause. The layers of Mg^{2+} ions donate their electrons to the B layer, thus lowering the non-bonding B $\pi(p_z)$ bands relative to the bonding $\sigma(sp_xp_y)$ bands compared to graphite. This causes charge transfer from σ to π bands, which creates holes at the top of the bonding σ bands and provides a high-T_c superconductivity of MgB_2. The σ bands, due to their two dimensionality, contribute strongly to the DOS at the Fermi level. The calculated deformation potentials of Γ point phonons identify the B band stretching modes as dominating the electron–phonon coupling [11]. This deformation potential is the largest ever observed in a metal superconductivity driven by the σ band. The idea of hole superconductivity by Hirsch [2] suggests that a decrease in the B–B separation should increase T_c. Although Hirsch has also focused on the hole character of the σ bands, his emphasis is otherwise quite different from that described by An and Pickett [11]. On the other hand, Baskaran [3], based on resonating

valence bands (RVB) theory, suggests that an increase in chemical pressure along the c-axis should decrease T_c and ultimately take MgB_2 to a normal metallic state. Thus it is important to have knowledge of the anisotropy in the mechanical behaviour of this material. Rabindran *et al* [4] noted that there are contradictory experimental results regarding the anisotropy in the elastic properties of MgB_2, ranging from isotropic, moderately isotropic to highly anisotropic. They carried out detailed electronic structure studies on superconducting MgB_2 and related compounds using a full potential linearized augmented plane wave (FPLAPW) method in a scalar-relativistic version without spin–orbit coupling. They found large anisotropy in the elastic properties and polarized dielectric tensor. Loa and Syassen [5], using the FPLAPW calculation, found that MgB_2 is isotropic both electronically and mechanically under pressure. Vogt *et al* [6], based on their experiment and *ab initio* calculations, indicated a nearly isotropic mechanical behaviour under pressure. On the other hand, Jorgensen *et al* [7] observed, from their neutron diffraction measurement, large anisotropy in thermal expansion and compressibility.

We report here the results of different *ab initio* calculations, hitherto not used, for the mechanical behaviour of MgB_2 under pressure. We use a self-consistent-field (SCF) Hartree–Fock linear combination of the atomic orbital computer programme CRYSTAL98 [12], which contains a density functional theory (DFT) option that permits one to solve the Kohn–Sham (KS) equation self-consistently. The basis sets used are 6-21G* and 8-61G for B and Mg, respectively. The exponents of the most diffuse sp and d shells for each atom have been optimized by searching for the minimum crystalline energy. The exchange correction potential proposed by Becke [13] is expanded in an auxiliary basis set of symmetrized atom-centred Gaussian-type functions. The quality of the calculation depends on the density of points with which the Brillouin zone (BZ) is sampled. The integrations over the BZ were performed using the Monkhorst–Pack scheme [14]. To ensure convergence for the BZ integration with accuracy, very tight tolerances were utilized in the evaluation of the infinite Coulomb and exchange series. A dense Gilat net [15] was defined with a total of 793 k-points in the reciprocal space, corresponding to a shrinkage factor of 24.

The total energy E of MgB_2 has been calculated at different primitive cell volumes (V). The results are shown in figure 1(a) as a function of the normalized volume V_n ($=V/V_0$, where V_0 is the equilibrium volume). The energy was minimized as a function of the c/a ratio for selected values of volume. The calculated c/a ratio is plotted as a function of normalized volume in figure 1(b). The zero pressure bulk modulus B_0 and its pressure dependence, B_0' ($=\mathrm{d}B_0/\mathrm{d}P$) were determined by fitting the Murnaghan equation of state [16]:

$$\Delta E(V) = E - E_0 = B_0 V_0 \left[\frac{V_n}{B_0'} + \frac{1}{1 - B_0'} - \frac{V_n^{1-B_0'}}{B_0'(B_0' - 1)} \right] \tag{1}$$

where E_0 is the equilibrium energy. The pressure (P) versus the primitive-cell volume is obtained through the thermodynamic relationship

$$P = -\frac{\mathrm{d}E}{\mathrm{d}V} = \frac{B_0}{B_0'}[V_n^{-B_0'} - 1]. \tag{2}$$

The resulting pressure dependence of the normalized primitive-cell volume of MgB_2 is shown in figure 1(c). We then utilize equation (2) and the optimized c/a ratio at each volume to get the pressure dependence of the MgB_2 lattice parameters which are as shown in figure 2. The linear bulk modulus at $P = 0$ along the crystallographic axes a and c (B_{a0} and B_{c0}) and their pressure derivatives are then obtained by fitting equation (2) to points in figure 1(c). The results obtained are shown in table 1.

The variation of the normalized lattice parameters with pressure is shown in figure 2 along with results from [17] for $P = 0$–12 GPa. This clearly shows the anisotropy in the

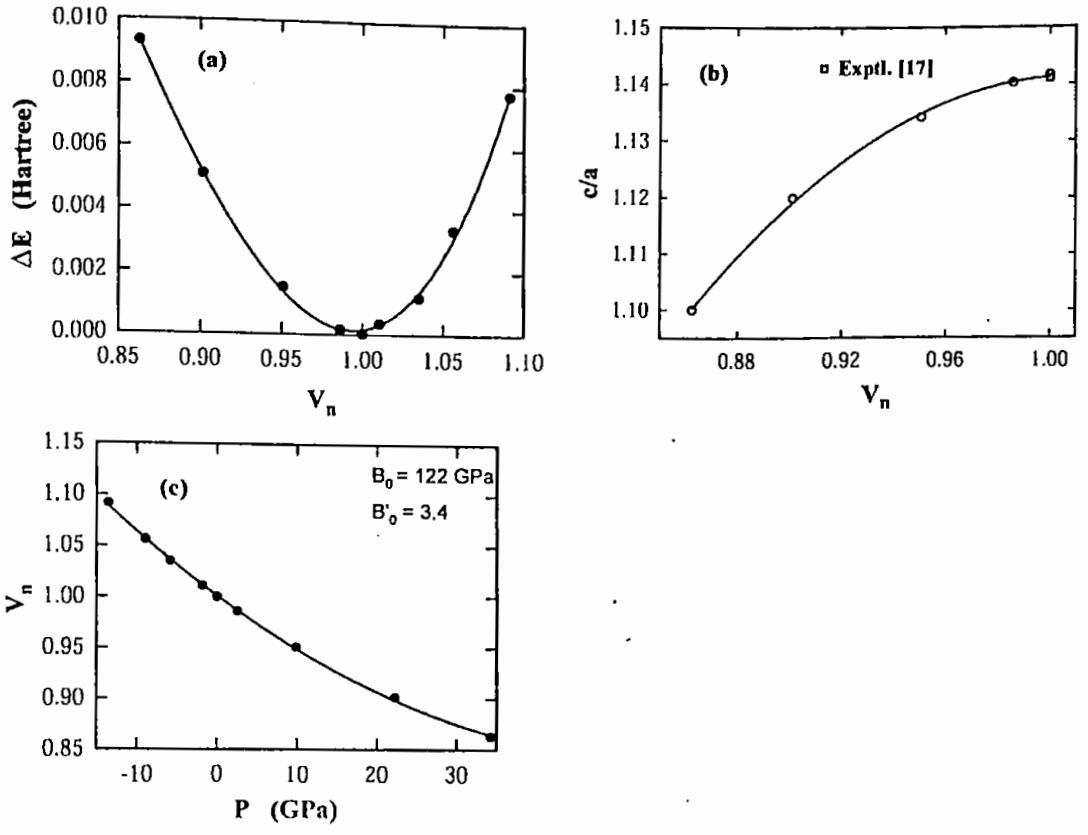

Figure 1. (a) MgB_2 energy (ΔE) as a function of the normalized primitive-cell volume V_n ($=V/V_0$). (b) Calculated c/a ratio as a function of normalized volume. The square represents experimental data [17]. (c) V_n as a function of pressure P. The curves through the data the points in (a) and (c) are the fits to the Murnaghan equation of state.

Table 1. The bulk modulus, the pressure derivative of the bulk modulus and their in- and out-of-plane linear values for MgB_2.

B_0 (GPa)	B'_0	B_{a0} (GPa)	B'_{a0}	B_{c0} (GPa)	B'_{c0}	Reference
122	3.4	653	15	397	5.5	This letter[a]
155	4.0	625	—	333	—	[17]
120	3.6	410	13	292	8.5	[18]
140	3.46	—	—	—	—	[19]
143	3.93	—	—	—	—	[5]
139; 151	—	—	—	—	—	[6]

[a] For the entire pressure range.

bonding of MgB_2. As the pressure increases from 0 to 10 GPa, the c/a ratio decreases by 0.51%. Compression along the c-axis is larger than along the a-axis, which is consistent with the comparatively weaker Mg–B bonds that determine the c-axis length. The result is in line with the measurements at room temperature [7], but has a larger magnitude. A similar but smaller anisotropy has been seen for TiB_2 [20]. The layered cuprates show much larger (~a factor of two) compression anisotropy [21]. The fitted values for B_{a0}, B'_{a0}, B_{c0}, B'_{c0} clearly reveal the diversity in the bonding interactions which are present. MgB_2 is less compressible in the basal plane, in which the covalent B–B bonds lie. The interlayer linear compressibility, $d\ln c/dP = 0.00204\ GPa^{-1}$ is ~1.4 times larger than the in-plane value ($d\ln a/dP = 0.0015\ GPa^{-1}$). It is worth noting that the structurally related alkali-metal

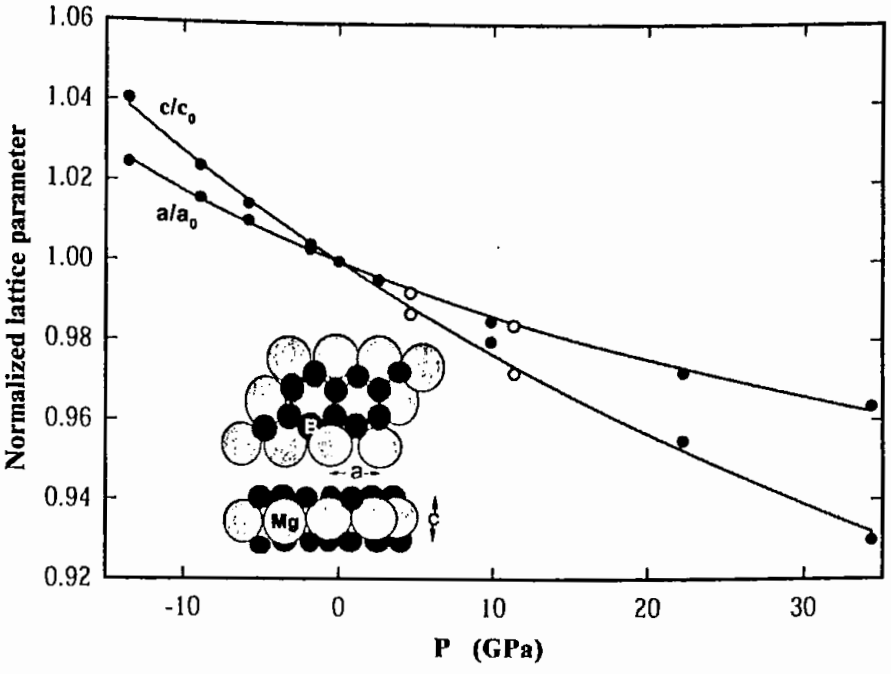

Figure 2. Pressure dependence of the normalized lattice parameters of MgB_2. The full curves through the data points are the fits to the Murnaghan equation of state. The open circles correspond to measured values [17] for $P = 0$–12 GPa. The inset shows a schematic diagram of the MgB_2 structure with lattice constants a and c.

intercalated graphite is strongly anisotropic (see [18]) with interlayer compressibility about ten times larger than the corresponding value in MgB_2.

For solids with isotropic compression, the mode Grüneisen parameter γ of zone-centre phonons is $\sim$1. Loa and Syassen [5] assumed this to be 1 while estimating $\mathrm{d}\ln T_c/\mathrm{d}P$ using McMillan's formula for T_c. In doing so they had to choose an exceptionally small $\mu^* = 0.04$ in order to reproduce the measured T_c. In fact the expression for $\mathrm{d}\ln T_c/\mathrm{d}P$ contains λ (electron–phonon coupling), the pressure dependence of the DOS $\mathrm{d}\ln N(0)/\mathrm{d}P$ and $\gamma = B_0\,\mathrm{d}\ln\omega/\mathrm{d}P$. Apart from other reasons, a smaller γ would require a smaller μ^*. Recently, Goncharov *et al* [17] determined γ to be 2.9 ± 0.3. Utilizing $\lambda = 0.9$ [9], $\mathrm{d}\ln N(0)/\mathrm{d}P = -0.004\ \mathrm{GPa}^{-1}$ [6], $\mu^* = 0.1$, and the experimental value of $\mathrm{d}T_c/\mathrm{d}P = -1.9\ \mathrm{K\ GPa}^{-1}$ [10], we estimate $\gamma \sim 1.88$–2.35 with $B_0 = 120$–150 GPa. If we ignore the pressure dependence of the DOS then these values become 2.21 and 2.77, respectively. Thus we find γ to be substantially larger than 1, which is as expected for a phonon in a compound with covalent bonding like graphite. For iron with partial metallic bonding $\gamma = 1.7$ [22]. Thus, for MgB_2 we should not expect γ to be $\sim$1 as has been assumed in [5]. It is to be noted that a larger γ is usually associated with enhanced anharmonicity of the particular normal mode of vibration, and is broadly consistent with the theoretical prediction for the E_{2g} in-plane B stretching mode [17].

The volume coefficient of T_c, $\mathrm{d}\ln T_c/\mathrm{d}V$, is an important parameter which implies the sensitivity of superconducting properties to the interatomic distances. Using our volume compressibility ($\mathrm{d}\ln V/\mathrm{d}P$), we obtain $\mathrm{d}\ln T_c/\mathrm{d}V = 0.3\ \mathrm{Å}^{-3}$ for MgB_2, a value comparable to that found by Saito *et al* [10], but significantly larger than those found in fulleride superconductors ($\sim$0.07 $\mathrm{Å}^{-3}$).

Finally, the MgB_2 is characterized by a moderately large anisotropy of compressibility. This is smaller than those of the cuprates [21] but larger than other related diborides. A fortunate combination of strong bonding, dominant phonon frequency and reasonable DOS at

the Fermi level is now believed [6, 8] to lead to the observed T_c of MgB_2. It is in this respect that the pressure effect on phonon modes is relevant in this particular diboride. The markedly anisotropic compression behaviour of MgB_2 may induce different pressure effects on different phonon modes and is also more likely to influence the electronic structure at the Fermi energy than when compression is isotropic because B–B and Mg–B distances change at different rates. In other words, the pressure can influence the electronic band in different directions of the BZ in an unusually different manner [4] and hence the physical properties.

The authors are indebted to the Ministry of Science and Technology, Government of Bangladesh for financial help.

References

[1] Nagamitsu J, Nakagawa N, Muranaka T, Zenitani Y and Akimitsu J 2001 *Nature* **410** 69
[2] Hirsch J E 2001 *Preprint* cond-mat/0102115
[3] Baskaran G 2001 *Preprint* cond-mat/0103308
[4] Rabindran P, Vajeeston P, Vidya R, Kjekshus and Fjellvag H 2001 *Preprint* cond-mat/0104253
[5] Loa I and Syassen K 2001 *Solid State Commun.* accepted for publication
[6] Vogt T, Schneider G, Hriljic J A, Yang G and Abell J S 2001 *Preprint* cond-mat/0102480
[7] Jorgensen J D, Hinks D G and Short S 2001 *Preprint* cond-mat/0103069
[8] Kortus J, Mazin I I, Belashchenko K D, Antropov V P and Boyer L L 2001 *Preprint* cond-mat/0101446
[9] Islam A K M A, Islam F N and Islam M N 2001 *Phys. Lett.* A submitted; see also the references cited therein
[10] Saito E, Taknenobu T, Ito T, Iwasaa Y, Prassides K and Arima A 2001 *J. Phys.: Condens. Matter* **13** L267
[11] An J M and Pickett W E 2001 *Preprint* cond-mat/0102391 v2
[12] Saunders V R, Dovesi R, Roetti C, Causa' M, Harrison N M, Orlando R and Zicovich-Wilson C M 1998 CRYSTAL98 *User's Manual* University of Torino, Torino and the references cited therein
[13] Becke A D 1988 *Phys. Rev.* A **38** 3098
[14] Monkhorst H J and Pack J D 1976 *Phys. Rev.* B **13** 5188
[15] Gilat G and Raubenheimer J L 1966 *Phys. Rev.* B **144** 390
[16] Murnaghan F D 1944 *Proc. Natl Acad. Sci. USA* **30** 244
[17] Goncharov A F, Struzhkin V V, Gregoryanz E, Hu J, Hemley R J, Mao H, Lepertot G, Bud'ko S L and Canfield P C 2001 *Preprint* cond-mat/ 0104042 v2
[18] Prassides K, Iwasa Y, Ito T, Chi D H, Uehara K, Nishibori E, Takata M, Sakata S, Ohishi Y, Shimomura O, Muranaka Y and Akimitsu J 2001 *Preprint* cond-mat/0102507
[19] Tsvyashchenko A V *et al* 2001 *Preprint* cond-mat/0104560
[20] Perottoni C A, Pereira A S and da Jornada J A 2000 *J. Phys.: Condens. Matter* **12** 7205
[21] Jorgensen J D, Pei S, Lightfoot P, Hinks D G, Veal B W, Dabrowski B, Paulikas A P and Kleb R 1990 *Physica* C **171** 93
[22] Markel S, Goncharov A F, Mao H K, Gillet P and Hemley R J 2000 *Science* **288** 1626

Properties of newly discovered MgB_2 superconductor under pressure

[1]A K M A Islam and F N Islam
Department of Physics, Rajshahi University, Rajshahi-6205, Bangladesh

Abstract

An *ab initio* study of the pressure dependence of various properties of the newly discovered MgB_2 superconductor is presented here. The zero pressure bulk modulus, pressure derivative of bulk modulus and their in- and out-of-plane linear values are evaluated. The diboride is found to be characterized by moderately sizable anisotropy of compressibility, which is smaller than cuprates, but larger than related diborides. The electronic band structure is also studied as a function of pressure. The superconductivity in MgB_2 is related to and dominated by the existence of $\sigma p_{x,y}$-band holes at the Γ point. The character of σ band does not change even with the application of pressure. The calculated density of states decreases with pressure. This is in agreement with the experimental T_c versus pressure data that follows the prediction of *BCS* theory.

Key words: MgB_2, *ab initio* method, compressibility, band structure, *DOS*, pressure effects

[1] Corresponding author. Fax : 00 88 0721 750064; e-mail: azharislam46@yahoo.com

1. Introduction

The recent discovery of the superconducting MgB_2 (T_c ~39 K) has triggered vigorous research activities by the scientific community to understand the structure, electronic properties and to determine the underlying mechanism of superconductivity in this simple compound (see, refs. [1-14]). The material possesses a hexagonal crystal structure. One thus expects anisotropy in its physical properties. Within the *BCS* picture, the reduction of the density of states (*DOS*) at the Fermi level, due to the contraction of the *B-B* and *Mg-B* interatomic distances dominates the hardening of *B* phonon frequency that should enhance T_c as external pressure is applied [13]. The idea of hole superconductivity by Hirsch [3] suggests that a decrease in the *B-B* separation should increase T_c. Although Hirsch has also focussed on the hole character of the σ bands, his emphasis is otherwise quite different from that described by An and Pickett [14]. They [14] maintain that the *B* σ bands play important role in the superconductivity of MgB_2. On the other hand Baskaran [4], based on *RVB* theory, suggests that an increase in chemical pressure along the c axis should decrease T_c and ultimately takes MgB_2 to a normal metallic state. Thus it is important to have knowledge of the anisotropy in the mechanical behaviour of this material. Rabindran et al [5] noted that there are contradictory experimental results regarding the anisotropy in the elastic properties of MgB_2 ranging from isotropic moderately, isotropic to highly anisotropic. They found large anisotropy in the elastic properties and polarized dielectric tensor. Loa and Syassen [6], using *FPLAPW* calculation, found that MgB_2 is isotropic both electronically and mechanically under pressure. Vogt et al [7], based on their experiment and *ab initio* calculations, indicated nearly isotropic mechanical behaviour under pressure. On the other hand Jorgensen et al [8] observed, from their neutron diffraction measurement, large anisotropy in thermal expansion and compressibility. The band structure calculations of MgB_2 at different pressures should yield important information on the superconductivity of this compound. The total and site projected *DOS* will also reflect features of the dominating atom contributing to the *DOS* at E_F. We report

here the results of a different *ab initio* calculations, hitherto not used, for various ground state properties including the mechanical behaviour and electronic band structure of MgB_2 under pressure.

2. Calculations

We perform calculations using all-electron *ab initio* self-consistent (*SCF*) Hartree-Fock linear combination of atomic orbital computer programme *CRYSTAL98* [15,16]. A *posteriori* density functional (*DFT*) correlation to the *HF* results for the total energy are included, with the correlation and exchange functions proposed by Perdew and Zunger [17] and Becke [18], respectively. The results can be quite sensitive to the choice of basis sets. The basis sets used are *6-21G** and *8-61G* for *B* and *Mg*, respectively. Other details of Brillouin zone integration and accuracy are given elsewhere [10,12] and hence will be omitted here.

3. Results and Discussions

The ground state properties of MgB_2 are obtained by minimization of the total energy E with respect to the unit-cell volume V. The energy was minimized as a function of the c/a ratio for selected values of volume. The calculated values of E and c/a ratio have been plotted as a function of volume in Figs.1a,b. The zero pressure bulk modulus B_0 and its pressure dependence, B_0' ($=dB_0/dP$) are determined by fitting the $E(V)$ curve by the Murnaghan equation-of-state [19]. The pressure versus volume curve of MgB_2 is obtained as detailed in Ref. [10] and is shown in Fig. 2. The pressure dependence of MgB_2 lattice parameters is shown in Fig. 3. The linear bulk modulus at P=0 along the crystallographic axes a and c (B_{a0} and B_{c0}) and their pressure derivatives are then obtained from Fig. 3. The obtained results are shown in Table 1, along with some recent results.

The variation of the lattice parameters with pressure clearly shows the anisotropy in bonding of MgB_2. Compression along the c-axis is larger than along the a-axis, consistent with the comparatively weaker *Mg-B* bonds that determine the c-axis length. MgB_2 is characterized by

moderately large anisotropy of compressibility. This is smaller than those of cuprates [25] but larger than other related diborides.

Fig. 4a shows the electronic structure of MgB_2 at equilibrium that reveals two distinct types of bands, both of which are contributed by boron. The upper part of the valence band is composed of *B* $2p$-states which form two sets of bands with $\sigma(2p_{x,y})$ and $\pi(p_z)$ character. The general features of the bands obtained in the present study are in very good agreement with results from other studies [9,14,27,28]. The $\sigma(2p_{x,y})$ band along Γ–A is double degenerate, quasi two-dimensional and makes a considerable contribution to *DOS* at E_F for MgB_2. The existence of degenerate $p_{x,y}$-states above E_F at the Γ point in *BZ* has been shown to be crucial for superconductivity in MgB_2 [9]. The weaker ppπ-interactions result from *B* $2p_z$-bands. These 3*D*-like bands possess maximum dispersion along Γ-A direction. The band structure of MgB_2 at P=38 GPa (Fig. 4b) shows that the character of σ band is unchanged even after application of pressure as because the symmetry is not broken. The weak dispersion of the σ band along Γ-A reflects their particular quasi-two-dimensionality. The dispersion increases slightly with increase of pressure. The σ band crosses the Fermi surface at Γ point at a pressure of ~38 GPa. When the σ band is below the Fermi surface, the σ bonding state is completely filled. Thus compression decreases the holes in σ band. Neaton et al [27] observed that the σ bands of MgB_2 are nearly free electron-like: their dispersion is parabolic near the Γ point, and their overall bandwidth is comparable to the free electron value (~15.5 eV). We find the same features and confirm their observation that the bandwidth (~15 eV) increases as pressure increases in line with that expected for free electrons.

Fig. 5 shows the total and partial electronic density of states near E_F. The density of states $N(E_F)$ decreases by as much as 29% for a pressure increase of 38 GPa. That $N(E_F)$ increases as the lattice is expanded is contrary to expectation for a nearly-free electron metal. The result is in agreement with that of other workers [6,27,29]. This observation, via *BCS* equation, shows that T_c

should decrease with the increase of pressure, a result in agreement with experiment for MgB_2 [30].

The total charge density of MgB_2 for (110) plane (Fig. 6a) shows a low electron accumulation between *Mg* and *B*. Further the electron population in the *Mg* site is much lower than that for a neutral *Mg* atom. These indicate an ionic bonding between *Mg* and *B*. On the other hand there is a strong covalent bonding between *B-B* atoms. This is evident by the maximum charge density (with a strongly aspherical character) at the bond middle. The more or less homogeneous charge distribution between the *Mg* atoms indicate an appreciable degree of metallic bonding between them. The effect of compression of MgB_2 can clearly be seen from Fig. 6b. Finally MgB_2 can be said to be mixed bonded solid and the band structure shows features similar to *sp* metals.

4. Acknowledgements

The authors acknowledge the financial support from the Ministry of Science & Technology, Government of Bangladesh.

References

[1] J. Nagamitsu et al., Nature 410 (2001) 69.

[2] S.L. Bud'ko et al., Phys. Rev. Lett., 86 (2001) 1877.

[3] J.E. Hirsch, Preprint cond-mat/0102115 (2001).

[4] G. Baskaran, Preprint cond-mat/0103308 (2001).

[5] P. Rabindran et al., Preprint cond-mat/0104253 (2001).

[6] I. Loa and K. Syassen, Solid State Commun. (2001) – in press.

[7] T. Vogt et al., Preprint cond-mat/0102480 (2001).

[8] J.D. Jorgensen and D.G. Hinks, S. Short, Preprint cond-mat/0103069 (2001).

[9] J. Kortus et al., Phys. Rev. Lett. 86 (2001) 4656.

[10] A K M A Islam et al., J. Phys.: Condens. Matter 13 (2001) L641.

[11] A K M A Islam et al., Phys. Lett. A 286 (2001) 357.

[12] A K M A Islam et al., Physica C (2001) – submitted.

[13] E. Saito et al., J. Phys.: Condens. Matter 13 (2001) L267.

[14] J.M. An and W.E. Pickett, Phys. Rev. Lett. 86 (2001) 4366.

[15] V.R. Saunders et al., CRYSTAL98 User's Manual, University of Torino, Torino (1998).

[16] C. Pisani et al., Lecture Notes in Chemistry (Springer-Verlag, Heidelberg, 1988) Vol. 48.

[17] J.P. Perdew and A. Zunger, Phys. Rev. B 23 (1981) 5048.

[18] A.D. Becke, Phys. Rev. A 38 (1988) 3098.

[19] F.D. Murnaghan, Proc. Natl. Acad. Sci. USA, 20 (1944) 244.

[20] A.F. Goncharov et al., Preprint cond-mat/ 0104042 v2 (2001).

[21] K. Prassides et al., *Preprint* cond-mat/0102507 (2001).

[22] A.V. Tsvyashchenko *et al*, Preprint cond-mat/0104560 (2001).

[23] S.I. Schlachter et al., Preprint cond-mat/0107205 (2001).

[24] C.A. Perottoni et al., J. Phys.: Condens. Matter 12 (2000) 7205.

[25] J.D. Jorgensen et al., Physica C 171 (1990) 93.

[26] S. Markel et al., Science 288 (2000) 1626.

[27] J.B. Neaton and A. Perali, Preprint cond-mat/0104098 (2001).

[28] G. Satta et al., Preprint cond-mat/0106239 (2001).

[29] X. Wan, J. Dong, H. Weng and D.Y. Xing, Preprint cond-mat/0104216 (2001).

[30] V.G. Tissen et al., Preprint cond-mat/0105475 (2001).

Table 1. Bulk modulus, pressure derivative of bulk modulus and their in-and out-of-plane linear values for MgB_2.

B_0 (GPa)	B_0'	B_{a0} (GPa)	B_0'	B_{c0} (GPa)	B_{c0}'	Ref.
161	4.0	580	16	362	7.7	This[#]
143	3.9	-	-	-	-	[6]
151	-	-	-	-	-	[7]
155	4.0	625	-	333	-	[20]
120	3.6	410	13	292	8.5	[21]
140	3.5	-	-	-	-	[22]
196	10	625	-	455	-	[23]

[#] For entire pressure range.

Figure captions

Fig. 1. (a) Total energy of MgB_2 as a function of unit-cell volume. The inset (b) shows the ratio c/a versus volume.

Fig. 2. Pressure versus unit-cell volume of MgB_2.

Fig. 3. Lattice parameters as a function of pressure of MgB_2.

Fig. 4. Electronic band structure of MgB_2 at (a) P=0 and (b) P=38 GPa.

Fig. 5. Total and partial electronic density of states of MgB_2 at (a) equilibrium (P=0) and at (b) P=38 GPa.

Fig. 6. Total electron density map on the (110) plane through Mg and B atoms at (a) equilibrium (P= 0) and (b) P= 38 GPa. Isodensity curves are separated by 0.01 e/Å^3.

Fig. 1
ST24
Islam et al.

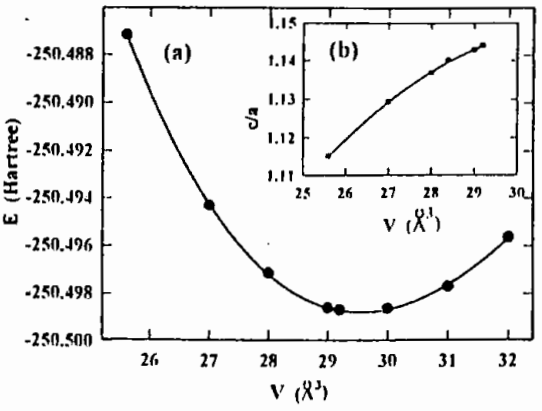

Fig. 2
ST24
Islam et al.

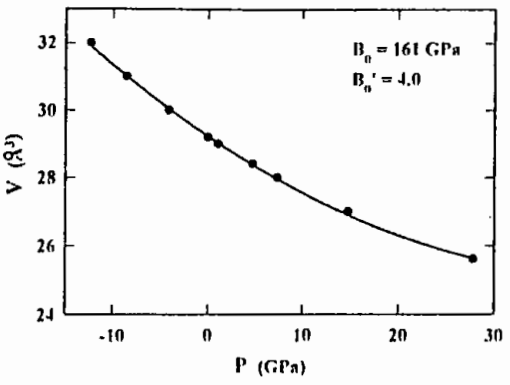

Fig. 3
ST24
Islam et al.

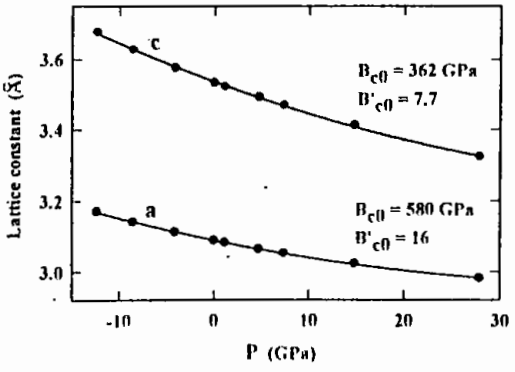

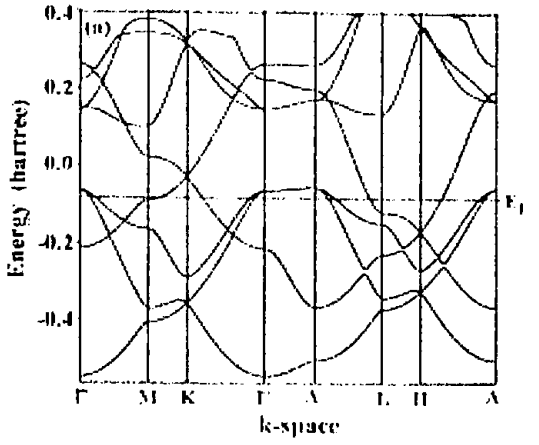

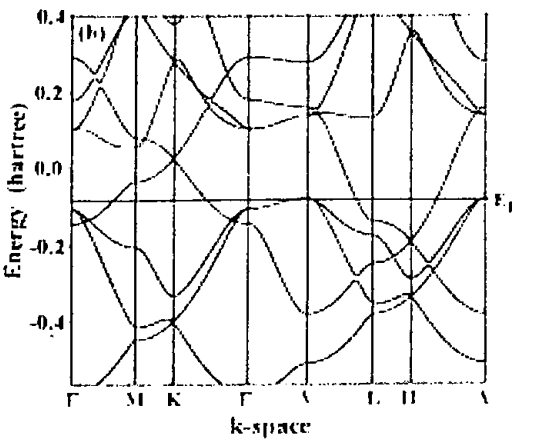

Fig. 4 a,b
ST24
Islam et al.

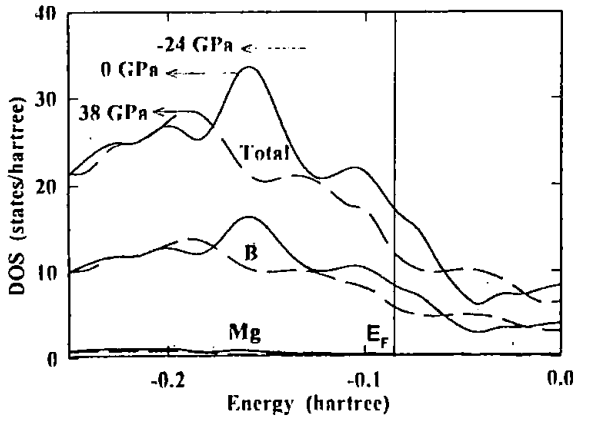

Fig. 5
ST24
Islam et al.

Fig. 6 a,b
ST24
Islam et al.